

Charged Carbon Nanomaterials: Redox Chemistries of Fullerenes, Carbon Nanotubes, and Graphenes

Adam J. Clancy,^{†,‡} Mustafa K. Bayazit,^{†,§} Stephen A. Hodge,^{†,||} Neal T. Skipper,[⊥] Christopher A. Howard,[⊥] and Milo S. P. Shaffer^{*,†,||}

[†]Department of Chemistry, Imperial College London, London SW7 2AZ, U.K.

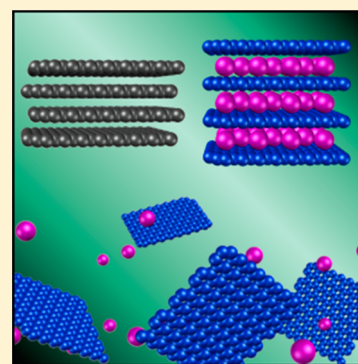
[‡]Institute for Materials Discovery, University College London, London WC1E 7JE, U.K.

[§]Department of Chemical Engineering, University College London, London WC1E 7JE, U.K.

^{||}Cambridge Graphene Centre, Engineering Department, University of Cambridge, Cambridge CB3 0FA, U.K.

[⊥]Department of Physics & Astronomy, University College London, London WC1E 6BT, U.K.

ABSTRACT: Since the discovery of buckminsterfullerene over 30 years ago, sp²-hybridised carbon nanomaterials (including fullerenes, carbon nanotubes, and graphene) have stimulated new science and technology across a huge range of fields. Despite the impressive intrinsic properties, challenges in processing and chemical modification continue to hinder applications. Charged carbon nanomaterials (CCNs), formed via the reduction or oxidation of these carbon nanomaterials, facilitate dissolution, purification, separation, chemical modification, and assembly. This approach provides a compelling alternative to traditional damaging and restrictive liquid phase exfoliation routes. The broad chemistry of CCNs not only provides a versatile and potent means to modify the properties of the parent nanomaterial but also raises interesting scientific issues. This review focuses on the fundamental structural forms: buckminsterfullerene, single-walled carbon nanotubes, and single-layer graphene, describing the generation of their respective charged nanocarbon species, their interactions with solvents, chemical reactivity, specific (opto)electronic properties, and emerging applications.



CONTENTS

1. Introduction	7364	3.4.2. GIC Dissolution	7378
2. Carbon Nanomaterials	7365	3.5. Associative Ion Charging	7378
2.1. Intrinsic Structure of Carbon Nanomaterials	7365	4. Reactivity of CCNs	7379
2.2. Electronic Properties of Neutral Carbon Nanomaterials	7366	4.1. Reactivity of Neutral Nanocarbons	7379
2.3. Utilizing Carbon Nanomaterials	7367	4.2. Reductive Functionalization	7380
2.3.1. Nanocarbon Applications	7367	4.3. Mechanism of Reductive Functionalization	7381
2.3.2. Processing Challenges	7367	4.4. Discharging CCNs	7383
2.4. Starting Materials	7369	5. Behavior of CCN Solutions	7384
3. Charged Carbon Nanomaterial Synthesis and Properties	7370	5.1. Polyelectrolyte Theory	7384
3.1. Intercalation Compounds	7370	5.2. Polyelectrolyte Theory for CCNs	7385
3.1.1. Graphite Intercalation Compounds	7370	5.3. Liquid Crystals	7386
3.1.2. SWCNT Bundle and Fullerene Intercalation	7371	6. Selectivity	7388
3.2. CCN Synthesis	7371	6.1. Electronic Selectivity	7388
3.2.1. Chemical Routes	7371	6.2. Geometric Selectivity	7388
3.2.2. Electrochemical CCN Synthesis	7373	7. Redox Chemistry of Other Nanomaterials	7389
3.3. Physical Properties of CCNs	7373	7.1. Further Carbon-Based Nanomaterials	7389
3.3.1. GIC Band Structure	7373	7.2. Non-Carbon Nanomaterials	7390
3.3.2. CCN (Super)conductivity	7374	8. Current and Emerging Applications	7391
3.3.3. CCN Optical Properties	7374	9. Conclusion	7393
3.3.4. CCN Geometric Properties	7376	Author Information	7394
3.4. CCN Solutions	7376	Corresponding Author	7394
3.4.1. Charged SWCNT Solutions	7377	ORCID	7394
		Notes	7394

Received: February 27, 2018

Published: August 15, 2018

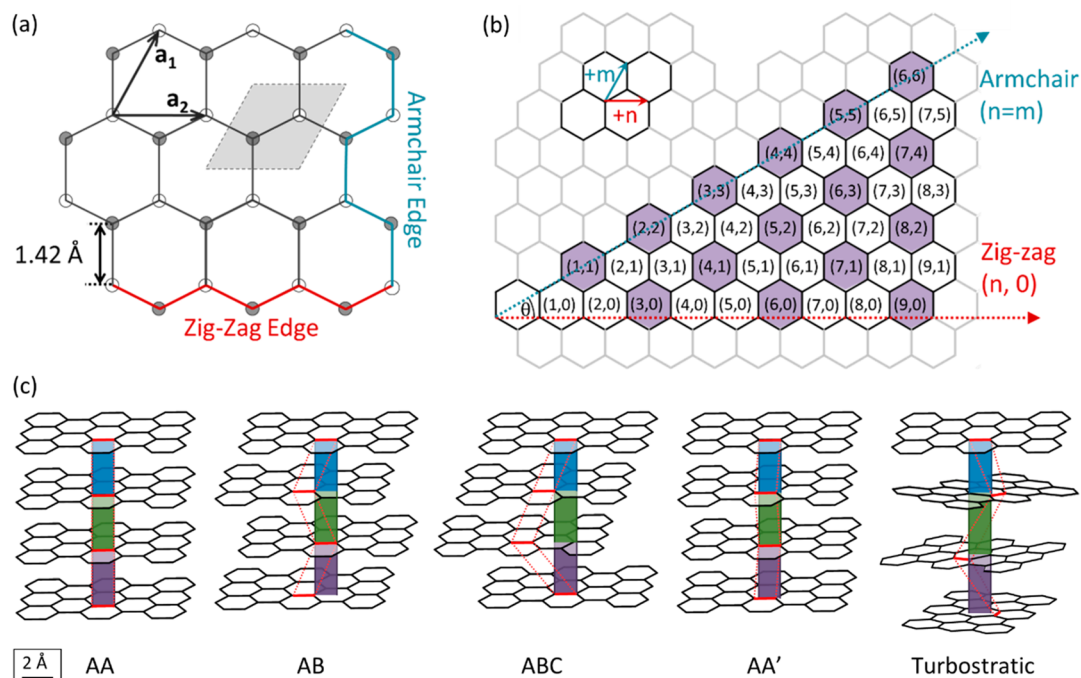


Figure 1. (a) Lattice of graphene, consisting of two offset triangular sublattices (white and gray circles), indicating basis vectors of the triangular lattice (a_1 and a_2), unit cell (gray rhombus), and structure of defined edge types. (b) SWCNT rolling vector map on a graphene sheet. SWCNT type is assigned by a characteristic lattice vector $C = m(a_1) + n(a_2)$, where m and n are integers in the graphene plane. On rolling the plane to form the tube, the vector C is mapped onto the SWCNT circumference. Metallic helicities highlighted in purple. (c) Illustration of the different stacking forms of graphite depicted to scale. An equivalent bond is highlighted within each layer (connected with dotted red line) to highlight interlayer translations. A vector is projected vertically down the c axis from the highlighted bond of the top graphene layer (with differing colors between layers for clarity) to illustrate the offset between layers.

Biographies	7394
Acknowledgments	7394
List of Abbreviations	7394
List of Symbols	7395
References	7395

1. INTRODUCTION

Historically, carbon was classified in three forms: amorphous carbon, graphite, and diamond. A new era of carbon science began with the discovery¹ of buckminsterfullerene (C_{60}) in 1985, formed via the laser ablation of graphite, quickly followed by the assignment of other fullerene analogues such as C_{70} and C_{80} formed in the same process. These developments in fullerene chemistry subsequently drew attention to the one-dimensional tubular carbon nanotubes² (CNTs), originally with the recognition of multiwall carbon nanotubes (MWCNTs),^{3,4} followed by the synthesis of single-walled carbon nanotubes^{5,6} (SWCNTs). The two-dimensional structure of graphene had long been discussed theoretically but was not isolated⁷ and fully characterized until 2004. Whereas C_{60} and SWCNTs were originally synthesized by laser ablation and arc discharge processes,⁸ graphene was originally prepared by the mechanical exfoliation of graphite using the “scotch-tape” method. Research over the last 30 years has led to a wide array of other techniques for the synthesis of these materials, notably chemical vapor deposition^{9,10} (CVD) and more recently low temperature organic synthesis.¹¹ The reader is directed to previous reviews of SWCNT and graphene synthesis for more information.^{12–16}

Highly crystalline nanocarbons demonstrate superlative electronic, optical, thermal, and mechanical properties coupled with low densities and high surface areas, making them candidates for a diverse family of applications, including (but far from limited to) multifunctional composites, catalysts, energy storage devices, drug delivery, bioimaging, nano-electronics. However, in spite of their considerable promise, large scale adoption of these nanomaterials has been hindered by several factors, notably the cost/availability of the nanocarbons, and difficulties in their processing. While synthesis costs are likely to be addressed by increasing the scale of the production infrastructure, processing the materials in their raw forms remains a fundamental issue. Bulk exfoliation of stacked graphenes (i.e., graphite) and nanotube bundles typically involves high shear fields or aggressive oxidation, both of which cause substantial, irreversible damage without necessarily providing complete exfoliation to individualized species; metastable dispersions including substantial fractions of nonexfoliated species are common.

As an alternative to these damaging processing routes, by taking advantage of their easily accessible electronic states, the nanocarbons may be electronically oxidized or reduced to give a positively or negatively charged carbon nanomaterial (CCN), respectively. The resultant materials consist of a nanocarbon “ion” imbued with an electronic charge balanced by counter-charged ions which may be intercalated within, or subsequently dissociated from, the charged frameworks. In their simplest form, these chemistries have been known since the 19th century in the form of graphite intercalation compounds (GICs).

The CCNs show dramatically improved solubilities and may exfoliate spontaneously to give thermodynamically stable solutions of individual, undamaged species at high concentrations. These solutions allow manipulation and assembly of the nanocarbons for a wide range of applications, after neutralization. On the other hand, in their charged form, the CCNs show interesting phenomenology related but distinct to polyelectrolytes, the ability to form liquid crystal mesophases, and unique properties arising from their unusual electronic structure. Moreover, the additional charge can initiate a wide range of new functionalization reactions, which can be particularly effective on individualized species.

There are six fundamental CCNs based on the sign of charge and the parent nanocarbon type: fulleride (C_{60}^{n-}), fullerenium (C_{60}^{n+}), nanotubide ($SWCNT^{n-}$), nanotubium ($SWCNT^{n+}$), graphenide (C_n^{m-}), and graphenium (C_n^{m+}). While the properties between CCNs vary substantially due to the differences in the degree and sign of charging, intrinsic nanocarbon electronic structure, and dimensionality, there are common factors between CCNs in terms of reactivity, synthetic approach, and structure in both solid and solution.

This comprehensive review of CCNs discusses their synthesis, properties before and after charging, dissolution behavior, reactivity, and applications. [Section 2](#) focuses on the constituent carbon nanomaterials, discussing their structure, optoelectronic character, and uses in the neutral state, related briefly to the diversity of raw nanocarbon feedstocks. The challenges associated with manifesting these properties on a macroscopic scale are discussed in the context of conventional processing routes, particularly liquid phase exfoliation (LPE). [Section 3](#) provides a broad background to CCNs, including the synthesis, structure, and properties of both the nanocarbon frameworks and the initial intercalation compounds. The solution behavior of the CCNs is discussed and compared to that of nanocarbons charged associatively by ion (e.g., H^+ or OH^-) adsorption. [Section 4](#) covers the new functionalization reactions facilitated by CCN formation, considering the reagents required, the mechanisms, and limitations of the reactions, as compared to the chemistry of the neutral nanomaterials. [Section 5](#) examines the physical models developed to explain the solution behaviors of CCNs, by analogy to polyelectrolyte excluded volume theory, and the opportunities for further refinement. [Section 6](#) explores the relationship between structural heterogeneity and CCN phenomenology and explores the opportunities for selective dissolution and reaction. [Section 7](#) discusses alternative low dimension materials which may show similar behaviors to the carbon-based systems and identifies the material characteristics likely to enable an analogous charge-based approach. [Section 8](#) surveys the current landscape of CCN applications compared to conventional methodologies. Finally, [section 9](#) summarizes the state of the field, highlighting key practical applications of CCNs.

2. CARBON NANOMATERIALS

2.1. Intrinsic Structure of Carbon Nanomaterials

Within the (nano)carbon community, there is considerable variation in the nomenclature used for different structures; we will attempt to use the “Carbon” definitions throughout the review.¹⁷ The parent structure of all carbon nanomaterials is usually considered to be ideal graphene: an infinite 2d crystalline sheet of sp^2 hybridized carbon ([Figure 1a](#)), with a

hexagonal lattice consisting of two triangular sublattices and a universal C–C distance of 1.42 Å. When graphene layers stack to form graphite ([Figure 1c](#)), they ideally order in an AB manner¹⁸ with an interlayer spacing of 3.35 Å; natural graphite¹⁹ typically consists of ca. 85% AB hexagonal and ca. 15% rhombohedral ABC (3.33 Å) stacking. Additional interspacing structures are possible in synthetic graphite, including AA (3.55 Å) and slight-offset AA' (3.43 Å) patterns,²⁰ in addition to the in-plane randomly rotated “turbostratic” graphite¹⁹ which contains a distribution of local interlayer spacings (ca. 3.6 Å).

SWCNTs can be envisaged as a sheet of graphene rolled along a specific 2d lattice vector ([Figure 1b](#)) which defines the chiral indices, (n,m) , and helicity, quantified as the chiral angle (θ), between the “zigzag” axis and the rolling vector. Generally, three types of SWCNT structure are recognized: armchair ($\theta = 30^\circ$, $n = m$), zigzag ($\theta = 0^\circ$, $m = 0$), and chiral ($m \neq n$, $n \neq 0$). Rolling the naturally flat graphene structure into a tube introduces strain into the bonds oriented (partly) circumferentially, which is greater for smaller diameters; as a result, for example, armchair SWCNTs are more strained than zigzag SWCNTs of similar diameter.^{21,22} As-synthesized, SWCNTs typically form small parallel bundles of tens or hundreds of individual nanotubes; if the diameters are similar they form in a uniaxial, triangular lattice [for example, with a lattice constant of 17 Å for ca. (10,10) SWCNTs²³]; due to the high curvature, the minimum internanotube distance is less than in planar graphites, typically²⁴ around ~ 3.1 Å for diameters around 1 nm, though larger SWCNTs may distort through polygonization or collapse.²⁵ Synthesized SWCNT lengths vary from the millimeter²⁶ to sub-100 nm (though individual SWCNTs on the centimeter scale have been reported²⁷), dependent on synthesis route; however, they are most commonly around 1–2 μm . Multiple nanotubes may be nested coaxially to form (usually larger) MWCNTs²⁸ with typical intertube distances of 3.2–3.5 Å.

As-synthesized, the ends of CNTs usually form “caps”, with additional curvature originating from the presence of pentagons within the otherwise hexagonal network; precisely six pentagonal rings are required to close a SWCNT cap assuming all other rings are hexagonal.²⁹ Analogously, fullerenes may be seen as two SWCNT caps with an (infinitely or very) short SWCNT between the caps. The best-known fullerene, C_{60} , has icosahedral symmetry (I_h), composed of 20 hexagons of a graphene sheet ([Figure 2](#)), folded to give 12 pentagons (to satisfy the Euler formula³⁰) with all carbons equivalent and displaying near- sp^2 hybridization.³¹ In the solid state at room temperature, C_{60} packs as face-centered-cubic³² with a unit cell parameter of 14.2 Å.

While fullerenes and SWCNTs are (typically) terminated with curvature, which arises from the presence of pentagons in the framework, graphene is not usually terminated by intramolecular C–C bonds. Instead, edges are terminated through edge functionalization, often hydrogen, although a large number of alternative functionalities are known³³ and may be deliberately introduced ([section 4](#)). The edge sites can be classified as either zigzag or armchair, depending on the carbon framework arrangement ([Figure 1a](#)) with each type showing differing local electronic character. The caps of SWCNTs may also be opened to expose graphitic edges akin to graphene edges. Deviation from the idealized nanocarbon structures may be caused by a range of defects ([Figure 3](#)), including vacancies in the carbon framework, sp^3 hybridized

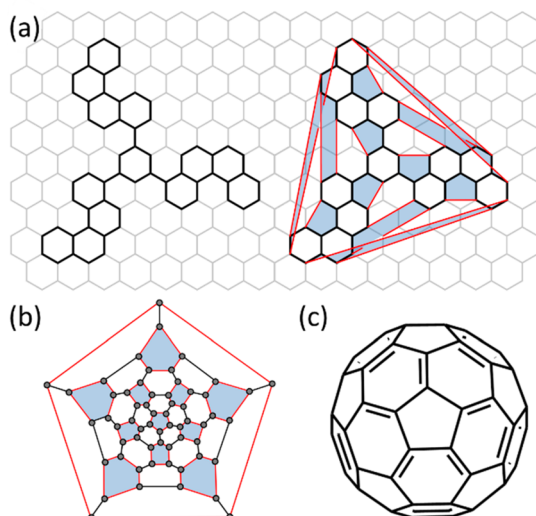


Figure 2. (a) Constituent framework of buckminsterfullerene overlaid on a graphene sheet (right) showing bonds required to form a C_{60} molecule (red) and associated pentagons (blue). (b) Truncated icosahedral graph representation of fullerene, showing pentagons (blue, n.b. outer carbons also form a nonhighlighted pentagon) and 6:5 bonds (red), adapted from the graph of a 60-fullerene (a truncated icosahedral graph) using one of the pentagons as a base (perimeter), by R. A. Nonenmacher, licensed under CC BY-SA 3.0. (c) Typical schematic representation of C_{60} molecule.

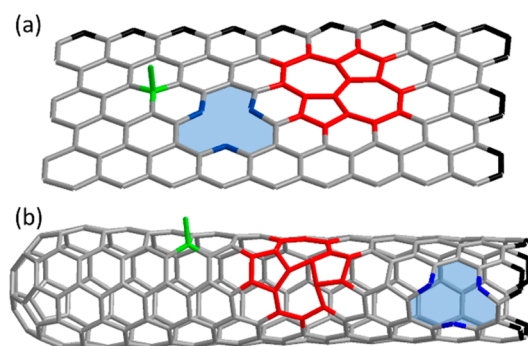


Figure 3. Typical defects on (a) graphene and (b) a (5,5) SWCNT, illustrating sp^3 defects (green), vacancies (blue), pentagon/heptagon pairs from Stone–Wales bond rotations (red) and edge/ends (black) where heteroatom terminations are expected.

carbons, and Stone–Wales bond rotations.³⁴ These defects are typically undesirable as they diminish the mechanical and optoelectronic properties.^{35,36} For example, at an average interdefect distance of ca. 50 nm, graphene tensile strength halves³⁷ and semiconducting SWCNT (sc-SWCNT, section 2.2) fluorescence is quenched.³⁸ In addition, since defects alter the electronic properties,³⁹ charge-based processes can be affected, leading to varying Fermi levels or charge densities.

2.2. Electronic Properties of Neutral Carbon Nanomaterials

Long before graphene's isolation, it was postulated to be a zero band gap semiconductor (Figure 4) with an electronic structure near the Fermi level (with a work function⁴³ of 4.66 eV) consisting of an occupied valence band (π) and an empty conduction band (π^*). These two bands just touch at the Fermi level at the K points in the Brillouin zone,⁴⁴ and the π and π^* bands are degenerate by symmetry. As such, in the

ground state, occupied and unoccupied bands lie infinitely close to each other in the electronic density of states (eDOS) but with no available states at the Fermi level. Although graphene has the highest electron mobility of any known solid⁴⁵ ($>200000 \text{ cm}^2 \text{ V}^{-1} \text{ s}^{-1}$), the low charge carrier density in ideal undoped graphene implies low conductivity; in real systems, however, electron–hole puddles arising from density fluctuations and thermal excitation supply additional charge carriers.⁴⁶ Deliberate doping or environmental effects, including interactions with the surrounding atmosphere or substrate,⁴⁷ explicitly shift the Fermi level, increasing metallic conductivity further. Many strategies have been considered to generate semiconducting character in graphene-related materials,⁴⁸ but mobility is usually significantly degraded.

The electronic properties of SWCNTs can be considered as a combination of the electronic band structure of graphene with quantum confinement of the electron momentum around the circumference (but not longitudinally). Due to symmetry, if $(n - m) = 3q$ where q is an integer (which includes all armchair SWCNTs) then the SWCNT is metallic at room temperature (m-SWCNT); otherwise, it is a sc-SWCNT with a band gap inversely related to diameter.⁴⁹ The confinement generates characteristic van Hove singularities (vHS) in the eDOS seen in all SWCNTs (Figure 4) and other 1d conductors. Optical transitions are “allowed” between levels labeled E_{ij} , where $i = 1, 2, 3$, etc., numbering the valence and conduction sub-bands; the energies E_{ij} are roughly inversely proportional to diameter and may be plotted on a Kataura plot.⁵⁰ For sc-SWCNTs, the E_{11} vHS transition is the lowest energy band gap, with values in the range of 0.3–0.8 eV for SWCNTs with diameters 3–1 nm, respectively. Overall, SWCNTs tend to have a low electronic density of states around the Fermi level on the order of 0.01 eV^{-1} per C atom for m-SWCNTs; the low density causes the average energy spacings between adjacent states to be much larger than compared to common metals. m-SWCNTs ($\epsilon > 1000$) have significantly higher dielectric constants⁵¹ than sc-SWCNTs ($\epsilon < 10$); larger diameter SWCNTs also have larger dielectric constants than small ones.⁵²

One strategy for generating a band gap in graphene also relies on 1d quantum confinement; by decreasing one lateral dimension to form a graphene nanoribbon⁵³ (GNR), the resulting electronic character depends on the orientation of the lattice and the width of the ribbon, in an analogous manner to SWCNT helicity and diameter. However, scattering from edges and the dependence on edge functionalities introduces additional complexities.^{54,55}

The eDOS of SWCNTs are relatively well-understood for any helicity (n,m) ; however, while there is universal agreement that the Fermi level of the SWCNTs is helicity dependent, there is significant disagreement not only on the absolute values but also on the trends both expected and measured.^{56–58} While research continues in the synthesis of specific (m,n) SWCNTs,^{59,60} nearly all samples contain a mixture of helicities;²² a number of postsynthetic sorting strategies have been developed, but absolute yields remain low.^{22,61,62} The mixture of electronic structures in a typical, polydispersed SWCNT sample can be simply modeled as a weight-averaged eDOS (Figure 5b) of all the helicities present.^{63,64} The bundling of even identical SWCNTs alters electronic properties, raising the work function;⁵⁷ bundles of polydispersed SWCNTs of varying helicity lose their well-defined band gaps.

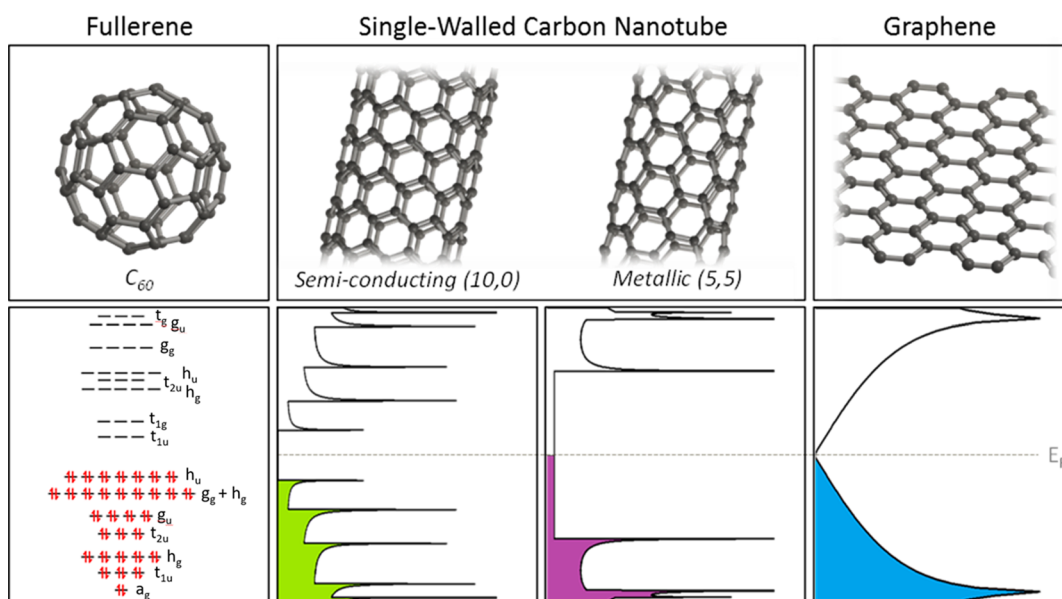


Figure 4. sp_2 -Hybridised carbon nanoform structures (top) and their undoped electronic orbitals/eDOS [bottom, Y axes represent energy (eV) over the range from -3 to $+3$ eV with the Fermi energy (E_F) positioned at 0 V in all graphs]. From left to right: fullerene (C_{60}), semiconducting (10,0), and metallic (5,5) single-walled carbon nanotubes and graphene.

The electronic properties of C_{60} are quite distinct from the eDOS continuum models of graphene/SWCNTs and are explained through molecular orbital (MO) theory. The curvature and misalignment of the π -orbitals of C_{60} molecule create significant strain and change the character of the π -orbitals, compared to flat systems.²² Haddon's Hückel MO calculations⁶⁵ of isolated fullerene revealed the highest occupied molecular orbitals (HOMO) to be a quintuplet of fully occupied degenerate h_u orbitals, while the lowest occupied molecular orbitals (LUMO) are a triply degenerate t_{1u} set of orbitals, separated by a ca. 1.8 eV gap (Figure 4). The LUMO t_{1u} density is concentrated predominantly over the 5:6 (hexagon/pentagon) bonds [i.e., between pentagons and hexagons and not the 6:6 (hexagon/hexagon) bonds]. These orbitals dominate the redox activity and their filling/emptying gives rise to fullerene's molecular ions. The reactivity of small diameter SWCNTs is sometimes interpreted in light of similar considerations about strain and rehybridization, as discussed further in section 6.2.

2.3. Utilizing Carbon Nanomaterials

2.3.1. Nanocarbon Applications. The diverse range of exceptional properties displayed by perfect carbon nanomaterials has stimulated interest in a large and varied array of applications. The redox activity of C_{60} is relevant to opportunities as diverse as organic photovoltaic devices,⁶⁶ in vitro production of singlet oxygen for cancer treatment,⁶⁷ and molecular electronics.^{68,69} As m-SWCNTs and graphene are ballistic conductors with excellent conductivity and current capacity, they are useful for transparent conducting films,^{70,71} field emission devices,⁷² and nanoelectronic circuitry.⁷³ On the other hand, the electronic properties and bandgaps of sc-SWCNTs make them useful for transistor devices,⁷⁴ solar cells,⁷⁵ and organic light-emitting diodes.⁷⁶ Graphene is a zero-gap semiconductor, so it is not as immediately useful for transistor devices, unless a band gap is introduced⁶¹ for example through the formation of GNRs⁷⁷ or covalent functionalization,⁷⁸ generally at the cost of reduced mobility. The optical properties of SWCNTs and graphene make them

attractive for a range of next generation optoelectronic and photonic devices;^{79–81} the broad optical absorption bands of graphene and helically mixed SWCNTs are well-suited to high performance saturable absorbers, while the tunability afforded from SWCNT helicity selection (and GNR width control) is inherently useful for optoelectronic components. In addition, both SWCNTs and graphene, at least ideally, have exceptional mechanical strength and high thermal/electrical conductivities that make them useful in multifunctional high performance composites.^{82–84} For composites, higher aspect ratio materials are desirable to maximize the load-bearing of the nanocarbon filler under stress, as well as increasing toughness due to pull-out, bridging, crack deflection, and realignment.^{85–87} High aspect ratios are of use in (opto)electronic applications, increasing electrical conductivity and reducing the percolation threshold;^{88,89} the intrinsic electronic effects of SWCNTs may also be diminished at short (<100 nm) length scales.⁹⁰ The high surface areas of the carbon nanomaterials (often combined with their electronic properties) make them promising candidates for gas/energy storage,^{75,91} supercapacitors,^{92,93} catalyst supports,⁹⁴ and gas sensors.^{95,96}

2.3.2. Processing Challenges. Mechanical exfoliation of graphite can generate near-perfect graphene monolayers;⁷ however, the process is inherently limited to small-scale device studies. The bottom-up synthesis of large grain-size, defect-free crystals of graphene is currently difficult to achieve⁹⁹ as generally graphene flakes of varying sizes and crystallographic domains are formed (although crystals on the millimeter scale can be grown¹⁰⁰). Typically, CVD-grown graphene is synthesized on a metal substrate (Ni, Cu) and is transferred to the end-target substrate using polymer stamps that leave behind residues that can affect final mechanical and electronic properties.¹⁰¹ So-called dry transfer approaches are beginning to facilitate high-performance CVD-derived devices;¹⁰² however, performance is still lower than those from mechanical exfoliation.

Alternatively, graphene-related materials can be synthesized by LPE of bulk graphite through either high-shear methods

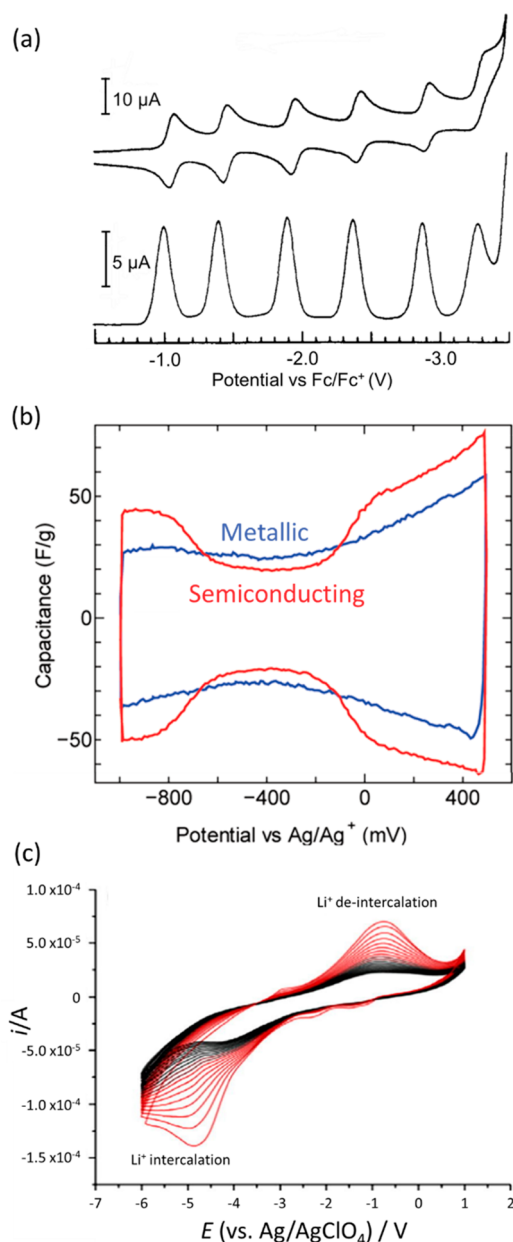


Figure 5. Voltammetric analyses of carbon nanomaterials. (a) Cyclic voltammetry (top) and differential pulse voltammetry (bottom) of C₆₀ at 10 °C in acetonitrile/toluene. Adapted from ref 40. Copyright 1992 American Chemical Society. (b) Cyclic voltammetry of (red) sc-SWCNTs and (blue) m-SWCNTs separated by density gradient ultracentrifugation. The butterfly shape of the sc-SWCNTs aligns with the first vHS transition of the (17,3) SWCNTs. vHS transitions are not seen from m-SWCNTs here as the measured potential window is insufficiently wide. Adapted from ref 41. Copyright 2012 American Chemical Society. (c) Cyclic voltammetry of graphite in LiBF₄ 0.1 M in NMP. Adapted with permission from ref 42, licensed under CC BY 3.0.

(ultrasonication, shear mixing, and microfluidization^{103,104}) or heavy acid oxidation resulting in the so-called “graphite oxide”, which is water-soluble as few/monolayer graphene oxide (GO), which must subsequently be reduced to partly recover graphene’s properties, forming reduced GO (rGO, Figure 6). Similar LPE processes were mostly developed originally for SWCNT powders¹⁰⁵ to obtain more individualized nanotubes and remain under development.¹⁰⁶ While acid oxidation of

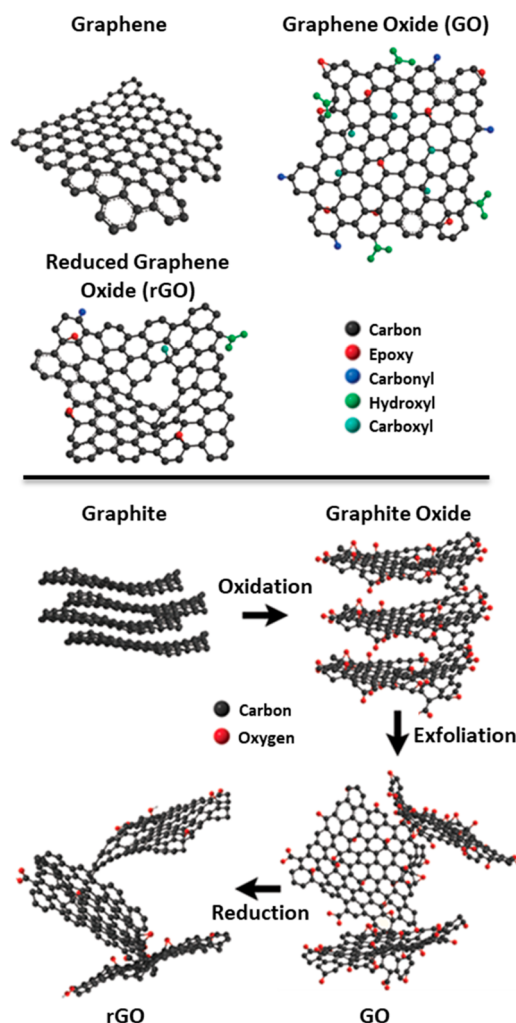


Figure 6. (Top) Schematic chemical structures of graphene, graphene oxide, and reduced graphene oxide. (Bottom) Route of graphite to reduce graphene oxide. Adapted from ref 97, licensed under CC BY 3.0.

SWCNTs does not routinely lead to a spontaneously soluble material akin to GO (although possible with extreme conditions¹⁰⁷), it is commonly applied to remove impurities, provide functionalization anchoring sites (section 4.1), and improve subsequent dispersibility.

Dispersions of carbon nanomaterials are frequently necessary for materials processing, including improved functionalization, enrichment of SWCNT helicity/electronic type, lowered size/dimension dispersity, and scalable liquid phase assembly of materials and devices. While alternative “dry” assembly routes are possible (CVD spinning of SWCNTs,¹⁰⁸ CNT-forest drawing,¹⁰⁹ mechanical forest manipulation,⁸³ etc.), they are commonly difficult to scale and are incompatible with most (typically liquid phase) purification/functionalization steps prior to assembly.

High-shear LPE is frequently used to prepare nanocarbon dispersions in pure solvents; however, the best media are typically toxic with high boiling points (e.g., *N*-methyl pyrrolidine¹¹⁰) or are based on surfactant/polymer solutions (introducing an often undesirable tertiary material). Alternatively, the feedstock can be prefunctionalized (section 4.1) to increase stability. The monolayer graphene/individualized SWCNT concentration and yield in LPE is usually low,¹¹¹ with

ultracentrifugation often used as an additional step to isolate particular species. The most significant issue of LPE processing, however, is that the necessary shear/oxidation introduces defects into the carbon framework and diminishes their aspect ratio¹¹² (Figure 7). As a result, the intrinsic

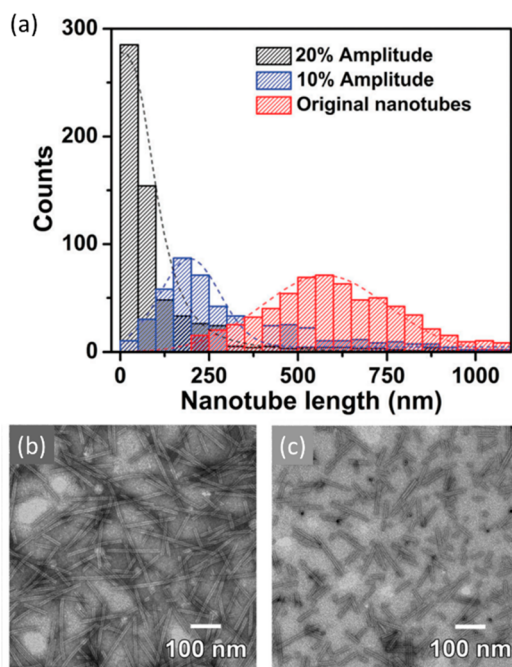


Figure 7. (a) Length distribution of CNTs as measured by atomic force microscopy (AFM) before and after ultrasonication at varying ultrasonicator power. (b and c) Transmission electron microscopy (TEM) of CNTs (b) before and (c) after sonication at 20% power. Reproduced with permission from ref 98. Copyright 2017 The Royal Society of Chemistry.

electronic,¹¹³ magnetic,¹¹⁴ and mechanical³⁷ properties of LPE-derived graphene and LPE-processed SWCNTs are diminished compared to CVD-grown/mechanically exfoliated graphene, and as-grown SWCNTs, respectively.^{83,108,109}

The processing of fullerenes is generally less challenging than that of graphene and nanotubes due to their solubility in a range of solvents, commonly toluene and carbon disulfide,¹¹⁵ and higher concentrations may be accessed using either specialist solvents (e.g., 1-halo-naphthalenes¹¹⁶) or fullerene functionalization.¹¹⁷ Solvated fullerenes may form small, loose-structured clusters¹¹⁸ due to van der Waals attractions, akin to graphite and CNT bundles but with significantly lower binding energies.

Given its utility and convenience, LPE is widely applied despite the well-known shortcomings, but there is great interest in alternative strategies. In particular, one solution is to form CCNs through (electro)chemical reduction/oxidation (not to be confused with acid oxidation). These CCNs can dissolve spontaneously to form thermodynamically stable solutions, (section 3.4), accessing the benefits of LPE but without the introduction of defects, reduction of aspect ratio, or the need to separate nonindividualized species. Additionally, the use of CCNs opens new functionalization chemistries (section 4.2), purification methodologies, and routes to hierarchical assembly.

2.4. Starting Materials

Fullerenes are typically synthesized as a mixture of sizes, however, owing to their solubility in common organic solvents¹¹⁵ (e.g., toluene, CS₂, ortho-dichlorobenzene), the separation of pure C₆₀ can be performed simply on the lab scale through chelation,¹²⁵ chromatography, or sublimation, and high yield industrial scale purifications are well-established.^{126,127} Despite considerable progress toward product control and batch repeatability, there is still significant variation in the structures, morphologies, and properties of the other carbon nanomaterials between synthesis routes (and thus nanocarbon suppliers). In addition, while commercial fullerenes and nanotubes are solely synthetic, graphite may be either synthetic or natural, providing even greater variation. It is critical to appreciate the diversity of feedstocks when selecting the materials and processes used to prepare a CCN for a particular application. The geometric polydispersity of graphenes and SWCNTs depends on the growth process and conditions; the size and shape of graphene-related materials may similarly depend on growth conditions (for CVD methods), or on the nature of the graphite used for exfoliation. In both cases, subsequent processing will continue to adjust the distribution. Deliberate sorting to reduce the dispersity typically requires individualization by ultrasonication, combined with centrifugal enrichment, or chromatographic length separation.^{62,128} While these techniques are currently small-scale, time-consuming, and involve damaging ultrasonication, these approaches simultaneously aid in the removal of impurities (vide infra) and facilitate electronic and helicity enrichment of SWCNTs. More scalable sorting methods have been proposed;^{129–131} but still require a fully individualized SWCNT feedstock, usually prepared by sonication and ultracentrifugation.

Carbon nanomaterials are typically arranged into larger structures (SWCNT bundles, graphitic crystals, or fullerites) held together by van der Waals forces which must be overcome to provide dispersions/solutions (e.g. through sonication, shear, or charging). However, since intramolecular/interlayer covalent bonds are substantially stronger and are not broken by simple charging processes, the presence of such bonds between the constituent nanotubes, layers, or fullerenes may limit individualization. Synthetic graphite, in particular, contains a high concentration^{132,133} of screw dislocations ($5 \times 10^8 \text{ cm}^{-2}$, Figure 8a), and milled graphites contain a high degree of interlayer pinning from introduced defects.¹³⁴ Adjacent graphite layers may also form from a single folded sheet leading to scroll-edges (Figure 8b) holding the layers together covalently, as well as preventing the introduction of intercalating species necessary for graphite reduction/oxidation.^{135,136}

Fullerenes are not synthesized with interspecies covalent bonds; however, exposure to ambient conditions leads to oxidized¹³⁷ (C₆₀O) and cross-linked¹³⁸ (C₁₂₀O, C₁₂₀O₂) impurities present in virtually all C₆₀ samples. As-grown SWCNTs (using current CVD/arc/laser synthetic techniques) are not reported to contain significant levels of internanotube cross-linking. If desired, such cross-linking between SWCNT bundles can be introduced through high-energy irradiation¹³⁹ (electron beam, γ rays, etc.) or ozone similarly to fullerenes.¹⁴⁰ For graphite, these internanocarbon bonds lead to intrinsically insoluble materials which must be broken to recover individualized sheets;¹⁴¹ the application of shear force can be

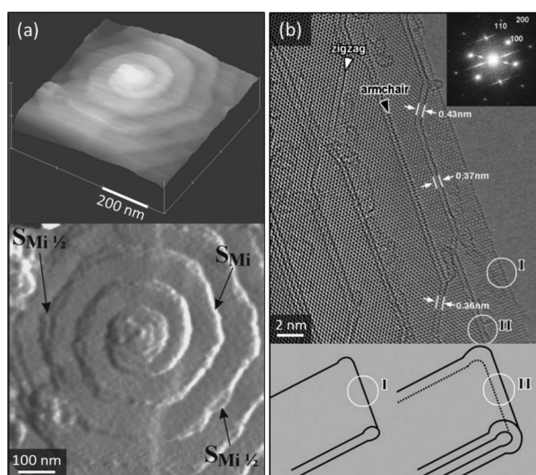


Figure 8. (a) AFM of a screw dislocation on (001) graphite face showing continuous graphene sheet spiralling about dislocation to encompass multiple layers. Adapted with permission from ref 119. Copyright 2002 The Mineralogical Society of America. (b) High-resolution-TEM image of pyrolytic graphite powders with folded (I) single- and (II) double-layer scroll edges with schematic structure below. Adapted with permission from ref 120. Copyright 2009 The American Physical Society.

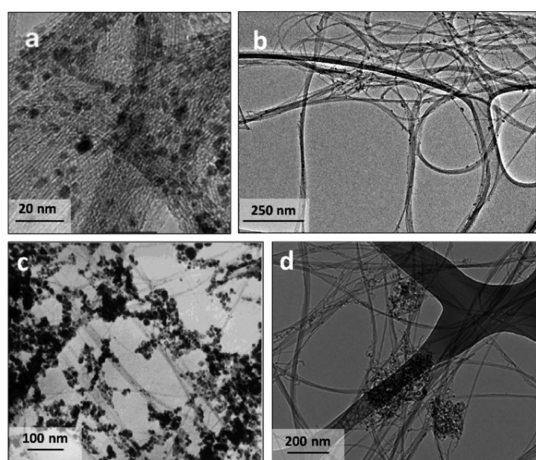


Figure 9. TEM of SWCNTs illustrating the differences in size, hierarchy, and impurity type(s)/quantity. (a) HiPco. Reproduced from ref 121. Copyright 2007 American Chemical Society. (b) Tuball. Reproduced with permission from ref 122, licensed under CC BY 4.0. (c) Hydrogen arc-discharge SWCNTs. Reproduced with permission from ref 123. Copyright 2001 Cambridge University Press. (d) CVD synthesized few-walled carbon nanotubes. Adapted with permission from ref 124. Copyright 2008 American Chemical Society.

used for exfoliation but usually leads to the recovery of smaller flakes ($<1\ \mu\text{m}$) with higher defectiveness.¹⁴²

Impurities are common in the as-received feedstocks of nanocarbon, particularly the synthetic SWCNTs and fullerenes (Figure 9). There are a variety of possible carbonaceous impurities, most commonly amorphous carbon, which consists of a disorganized network of sp^3 and sp^2 hybridized carbons, which may contain dangling bonds, as well as a variety of heteroatoms. Amorphous carbon may physically trap the desired nanocarbon species, preventing exfoliation and obscuring functionalization sites.¹⁴³ Even well-ordered carbons (fullerenes, CNTs, diamond-like carbons, nanodiamonds, graphenes, graphites, etc.) can constitute impurities, if not

the desired structure; for example, (multiwall-)fullerenes are often found in arc-grown CNT samples, or MWCNTs may contaminate SWCNT samples. Inorganic impurities, in the form of residual metal catalyst particles (often in graphitic shells) or residual catalyst substrates, can increase material density and are capable of altering the electronic,¹⁴⁴ magnetic,¹¹⁴ and physical properties of the nanocarbon. In general, impurities complicate stoichiometric control of nanocarbon charging, as the charge segregation between nanomaterial and impurities is not yet well-understood. Furthermore, the presence of particulates of differing geometry (whether due to impurity particles or simply sample heterogeneity) is known to interfere with the formation of liquid crystal phases¹⁴⁵ (section 5.3).

A high degree of nanocarbon crystallinity, minimizing associated defects (section 2.1), is required to realize the intrinsically exceptional properties. In addition, the crystallinity has a strong influence on the charging processes,¹³⁵ affecting both the stability of the charged compounds and the mechanism of intercalation. The various factors controlling the charging of graphite through ion intercalation is a broad subject, and readers are directed to the comprehensive review by Dresselhaus and Dresselhaus.¹⁴⁶ In short, ideal AB stacking of graphite along the c axis, such as that found in natural flake graphite, simplifies intercalation. Higher in-plane graphene crystallinity and larger lateral grain size also assists intercalation; domains may vary from the millimeter (e.g., kish graphite) to the submicron (e.g., highly oriented pyrolytic graphite). As noted above (section 2.1), SWCNTs are synthesized in an even wider range of lengths, although bundle diameters rarely exceed 100 nm.

The intrinsic aspect ratio of constituent SWCNTs/graphenes can thus vary over many orders of magnitude. High aspect ratios are most often preferred for applications in composites and conductive networks,⁸⁵ while lower aspect ratios may be more relevant in drug delivery or catalysis.¹⁴⁷ High aspect ratio nanocarbons are particularly challenging to prepare and manipulate via conventional methods involving ultrasound or shear, since they are more prone to buckle/break,^{148,149} but can be usefully addressed with charging methods. The charging of the nanomaterial is typically unaffected by the aspect ratio, aside from extremely short length scales where edge effects may dominate; however, the dissolution kinetics have recently been proposed to be inversely proportional to their aspect ratio.^{87,150} The aspect ratio has a significant effect on the phase behavior of the subsequent solution (section 5.3).

3. CHARGED CARBON NANOMATERIAL SYNTHESIS AND PROPERTIES

3.1. Intercalation Compounds

3.1.1. Graphite Intercalation Compounds. Graphite intercalation compounds can be viewed as the original CCNs. Graphite itself is an amphoteric layered material, with the ability to accommodate a wide range of inter gallery acceptor and donor species via preparation techniques including vapor or solvent transport and electrochemical intercalation (section 3.2). Acceptor species accept electrons from the graphite to form anions intercalated into positively graphitic sheets, while donor species reduce the graphite and have cationic intercalating ions. The first GIC was synthesized by Shaffäutl in 1840 and was an acceptor-type material formed by exposure

of graphite to sulfuric acid;¹⁵³ this acid treatment route subsequently also led to the discovery¹⁵⁴ of graphite oxide in 1859. The first donor GICs¹⁵⁵ (with alkali metal intercalants) were prepared in 1926 and were the subject of the classic compositional and structural studies of Rüdorff¹⁵⁶ and Hérold¹⁵⁷ (Figure 10). The range of known GICs is now

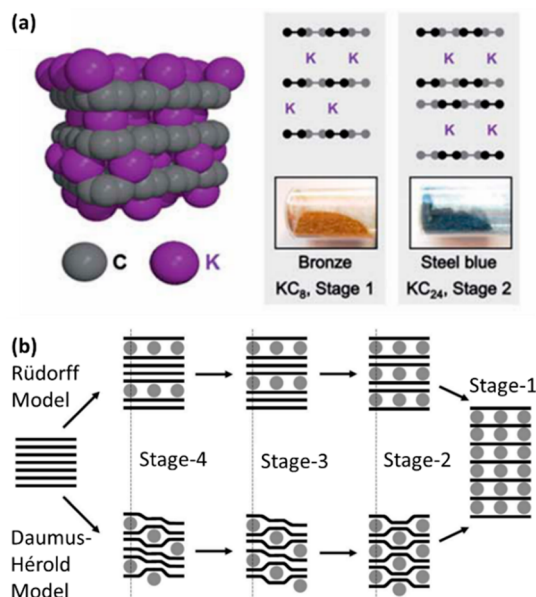


Figure 10. (a) Schematics and digital pictures of stage-1 and stage-2 potassium GICs. Reproduced with permission from ref 151. Copyright 2014 The Royal Society of Chemistry. (b) Schematics of the Rüdorff and Daumas-Hérold models of graphite intercalation. Adapted with permission from ref 152, licensed under CC BY-NC 3.0.

extremely large, including families based on electron-donating alkali, alkali earth, and rare earth metals and electron-accepting halides, metal halides, and acids.¹⁴⁶ In addition to these binary graphite-guest materials, ternary graphite-guest-guest compounds can be created (particularly for alkali metal GICs) by incorporating a third component in either elemental or molecular form such as ammonia, tetrahydrofuran (THF), or hydrogen.¹⁵⁸

Intercalation of graphite to form a GIC is always accompanied by charge (electron) transfer into the antibonding π^* -band (donor guest) or from the bonding π -band (acceptor guest). The concomitant changes in electronic structure yield materials with new physical and chemical properties, including highly conducting synthetic metals, magnetic states, and superconductivity, along with the opportunity for production of chemically active charge transfer agents. Graphite intercalates are unique among layered host-guest materials in that they yield a sequence of stoichiometric compounds with a regular c axis stacking structure. This phenomenon is called staging, with a stage- n GIC being one in which the guest species occupy every n^{th} graphite gallery. To take an archetypal example, stage-1, -2, and -3 potassium GICs have compositions KC_8 , KC_{24} , and KC_{36} , with respective out-of-plane c axis unit cell spacings of 5.35, 8.75, and 12.10 Å, consisting of a single intercalant layer and 1, 2, and 3 graphite layers, respectively. Kinetic processes surrounding staging transitions are qualitatively understood by the model proposed by Daumas and Hérold,¹⁵⁷ in which 2d diffusion of the guest within domains of stage- n leads to formation of an

intermediate phase and then domains of stage- $(n \pm 1)$. Higher stage intercalates lead to progressively weaker coupling between the guest-filled galleries, with, for example, arsenic pentafluoride and alkali metal GICs observed for $n > 6$. The in-plane intercalated structures form superlattices, which may or may not be commensurate of the underlying graphite layers, depending on the size and density of the guest species.¹⁵⁹ For many binary GICs (i.e., one intercalant type) of composition MC_n , the superlattice is $[\sqrt{(n/2)} \times \sqrt{(n/2)}]$ that of graphite; for example, stage-1 LiC_6 and KC_8 are commensurate ($\sqrt{3} \times \sqrt{3}$) and (2×2) in-plane structures, respectively, while stage-2 KC_{24} has incommensurate domains of superlattice ($\sqrt{6} \times \sqrt{6}$). However, the importance of ionization potential and ionic radius is illustrated by the difficulty in forming sodium-based GICs.¹⁶⁰

3.1.2. SWCNT Bundle and Fullerene Intercalation.

Both donors and acceptors can be intercalated into the internanotube galleries of SWCNT bundles; however, the ordering is usually less well-defined than is seen in GICs, owing to the SWCNT heterogeneity and variable carbon-carbon distances. Upon intercalation (for both reductive¹⁶⁵ and oxidative¹⁶⁶ charging), the bundle lattice expands with increasing charge ratio and counterion size.¹⁶⁷ Unlike GICs, SWCNTs have a secondary gallery type, the internal cavity of the nanotube, which may be variously filled with a range of confined continuous phases, ions, and molecules.¹⁶⁸ While the encapsulated material may be introduced during nanotube synthesis,¹⁶⁹ deliberate filling is usually performed later after end-cap removal through preferential etching. The more easily accessible internanotube galleries are typically also filled in this step, however, the SWCNT ends may be resealed through annealing and materials on the SWCNT exterior washed away.¹⁷⁰ Endohedral SWCNTs, even when filled with strong donors/acceptors, are not expected to form the nanocarbon ions described in this review, as the counterion remains trapped and thus unable to dissociate in solution. Finally, in MWCNTs, the interwall graphitic spacings may be intercalated, as described below (section 7.1).

In the presence of suitable donors/acceptors, fullerenes can form well-defined ionic crystals (Figure 11). The precise crystal lattice is dependent on the dopant, charge stoichiometry, temperature/pressure,¹⁶² initial fullerene state,⁶⁸ and cocrystallized solvent/molecules and can vary between monoclinic,^{162,171} triclinic,¹⁶³ rhombohedral,¹⁷² face centered cubic¹⁷³ (particularly for M_3C_{60}), and simple cubic¹⁶² crystals, as well as layered hexagonal¹⁶⁴ sheets, 2d-ordered chains,¹⁷⁴ and disordered¹⁷⁵ phases. Exohedral fullerene salts are typically unstable without solvent molecules; however, crystalline (monoclinic) phases may be formed when synthesized with exceptionally Lewis acidic donors¹⁷⁶ (e.g., AsF_5). As for SWCNTs, fullerenes can also be filled endohedrally, usually during the initial fullerene syntheses;¹⁷⁷ postsynthesis fillings are rare.¹⁷⁸ While the (endohedral) dopant may not dissociate from the doped fullerene, group 1 $\text{M}@\text{C}_{60}$ itself may act as a reducing agent, to give the $[\text{M}@\text{C}_{60}]^+$ ion,¹⁷⁹ which may form (monoclinic) crystals.

3.2. CCN Synthesis

3.2.1. Chemical Routes. The synthetic route to alkali metal/carbon nanomaterial salts (GIC and nanotubide) through chemical means can be broadly split into two categories: direct metal and solvated reductant. For direct metal intercalation, the metal can be added as a vapor^{180,181} or

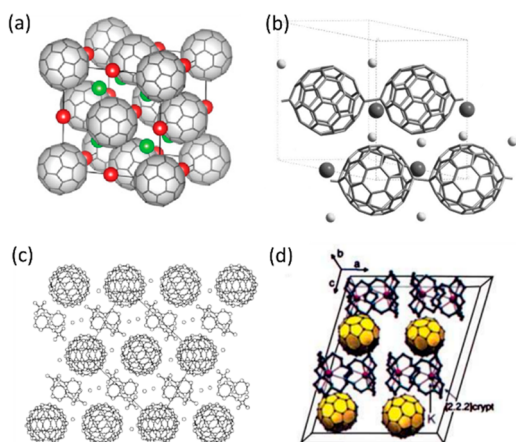


Figure 11. Fulleride crystal structures. (a) Face-centered cubic M_3C_{60} , where M is a group 1 metal in either tetrahedral (green) or octahedral (red) site. Reproduced with permission from ref 161, licensed under CC BY-NC 4.0. (b) Linear chains of fulleride “polymer-phase” with constituent orthorhombic crystal structure. Reproduced with permission from ref 162. Copyright 1999 Elsevier. (c) Layered anorthic crystal system. Reproduced with permission from ref 163. Copyright 1998 John Wiley & Sons. (d) Layered hexagonal sheet structure of $[K([2.2.2]crypt)]_2C_{60}$ crystals. Reproduced with permission from ref 164. Copyright 1997 VCH Verlagsgesellschaft mbH, Germany.

liquid,^{146,182} metal amalgam,^{183,184} eutectic alloy (GIC only to date^{185–187}), or plasma (CNTs only to date¹⁸⁸). Alternatively, solvated reductants can be used to form the CCN salts, avoiding the high temperatures or low pressures often associated with direct metal addition. The selected solvent must be dry, aprotic, and stable in the presence of the selected reductant(s) (see sections 3.2.2 and 3.4). Solvated reductant routes include Birch reductions (liquid ammonia solvating the metal cation and its valence electron(s)^{189–191}) and organic single electron transfer (SET) agents (e.g., sodium with naphthalene,^{192,193} Figure 12, or 4,4′-di-*tert*-butylbiphenyl¹⁹⁴) in coordinating solvents such as THF. In the case of solvated-reductant GICs, the resultant intercalated metal cation is typically coordinated by solvent molecules.¹⁹³ Organometallics (e.g., *n*-BuLi¹⁹⁵ and C_3H_7NHLi ¹⁹⁶) may be used to reduce carbon nanomaterials while simultaneously functionalizing with the organic group, allowing the addition of different surface moieties.^{195,197–199} While similar charging reagents have been applied in the synthesis of alkyl-fullerides,^{200,201} yield can be limited by competitive polymerization of the fullerenes.²⁰²

All stable alkali metals have been shown to be capable of forming GIC/nanotubide intercalants,^{167,203} although graphite intercalation of sodium typically leads to low stoichiometries and high-stage GICs attributed variously to the small size of the metal cations preventing intergraphitic distances reaching energy minima,²⁰⁴ the less reducing nature versus lithium, and the weakness of the subsequent ionic bond between the graphenide sheets and sodium cations.^{205,206} Pure stage-1 sodium GICs can be synthesized from decomposition of the so-called “superdense” GIC²⁰⁴ NaC_2 (formed at 40 kPa), and ternary stage-1 sodium GICs may be formed through use of a cointercalating solvent,²⁰⁷ heavy group 1 metal,²⁰⁸ or trace oxygen.²⁰⁹

The group 2 alkali earth metals calcium, strontium, and barium readily intercalate graphite,²¹⁰ while magnesium is

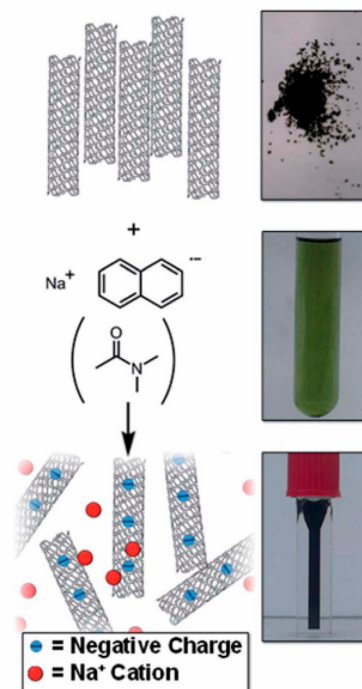


Figure 12. Schematic (left) and pictures (right) of raw SWCNT powder and sodium naphthalide/DMAc solution forming a solution of nanotubide. Reproduced with permission from ref 143. Copyright 2015 The Royal Society of Chemistry.

more challenging (analogously to sodium) but readily forms ternary intercalation compounds alongside a group 1 metal.²⁰⁸ While beryllium metal can intercalate graphite, it rapidly decomposes to give beryllium carbide.²¹¹ Of the group 2 metals, only barium has been intercalated into SWCNT bundles to date,²¹² with the electronic behavior highly dependent on the extent of charging.²¹³

For acceptor compounds, most Lewis acids can intercalate graphite and nanotube bundles, including sulfuric acid,^{153,214} a large array of metal halides,^{215–217} and bromine,^{218,219} iodine is capable of doping nanotube bundles^{166,220} (albeit with lower charge transfer versus bromine²²¹) but does not easily form a GIC, attributed to its lower electron affinity.²²² These mild dopants do not form the C_{60}^{n+} fullerene ions; compounds may form, but there is no formal electron transfer,^{223,224} as oxidation requires a redox potential greater than common oxidants.¹⁷¹ Instead, highly oxidizing, non-nucleophilic specialist acceptors must be used, notably the halocarboranes^{225,226} and arsenic pentafluoride.¹⁷⁶ While arsenic pentafluoride has also been applied to form acceptor GICs²²² (with great historical importance), it has yet to be reported as a donor for nanotubes, although its anionic analogue (AsF_6^-) is used as the counterion in nanotubium electrochemical synthesis (section 3.2.2).

The maximum charge on the CCN can be limited by one of several factors. As inferred above, GIC maximum stoichiometry is defined by the final well-defined structure of the resultant GIC, usually a stage-1 structure. For SWCNTs or individual graphene sheets, the extent of charging is not intrinsically defined by the final crystal structure (the SWCNT bundle lattice is typically not as well-defined as graphite) and instead is limited by charge saturation. During the charging process, the CCN Fermi level will shift toward the reduction/

oxidation potential of the charging species, until eventually the potentials are equal. This charge saturation is more readily reached for weak redox agents where a small degree of charge transfer is required to reach such an equilibrium. The low-lying LUMO of C_{60} facilitates the use of these milder (often organic) reducing agents, such as amines and hydrosulfite¹⁷¹ for fulleride synthesis. These organic compounds adsorb onto graphite and nanotubes, doping vacant states;²²⁷ the charge saturates at low stoichiometries, so that the final charge is small and insufficient to facilitate the dissolution/reductive functionalization seen for the alkali (earth) metal intercalated species. When charging electrochemically, there is no intrinsic charge limitation, although charging outside the electrolyte's stability window leads to degradation of the electrolyte and often also the nanocarbon (section 3.2.2).

3.2.2. Electrochemical CCN Synthesis. Electrochemistry provides an alternative route to the reduction and oxidation of carbon nanomaterials while simultaneously monitoring the redox behavior^{40,228,229} (section 3.3). Fullerenes can be electrochemically reduced or oxidized to generate isolated fulleride (C_{60}^{x-} , $x = 1-6$) and fullerenium (C_{60}^{x+} , $x = 1-3$) ions, respectively,¹⁷¹ through discrete reduction/oxidation events. Graphite intercalation is commonly performed through electrochemistry, with the GIC stage determined by the applied potential.²³⁰ Holding (solid) SWCNT powder at sufficient potential in an appropriate solvent with sufficiently low electrolyte concentration (to mitigate screening effects, section 5) leads to spontaneous dissolution of the SWCNT ions.⁶³ Electrochemistry is currently the only known route to individualized nanotubum species with well-defined cationic SWCNTs (Figure 13).²²⁸ The dissolution of CCNs is covered in greater depth later, both in terms of experimental factors (section 3.4) and theoretical considerations (section 5).

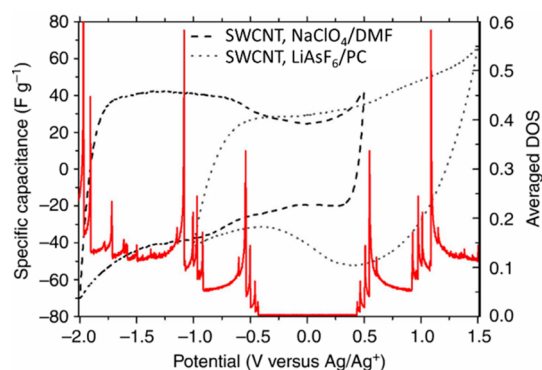


Figure 13. Reductive (dashed) and oxidative (dotted) cyclic voltammetry of (6,5) rich CoMoCat SWCNTs overlaid on averaged eDOS (red). Reproduced with permission from ref 228. Copyright 2013 Springer Nature.

Care must be taken to ensure that the potential is within the solvent's/electrolyte's electrochemical stability window to prevent solvent degradation and subsequent contamination. This requirement is particularly pertinent in oxidative syntheses that requires potentials at which few electrolyte systems are stable (e.g., LiAsF₆ in propylene carbonate^{228,231}). Due to the electrolyte window constraints, mild dissolution of graphenide or graphenium from graphite via electrochemical reduction or oxidation has yet to be demonstrated since only GIC formation occurs without appreciable dissolution. By holding graphite at reductive potentials outside this window,

exfoliation of layers occurs²³² due to extensive release of hydrogen gas (from water splitting) from between the layers; this processes typically causes substantial damage to the graphene's carbon framework. Holding graphite at an excessively oxidizing potential does not lead to gas evolution, instead leading to oxidation/functionalization of the graphite which causes damage, but may encourage exfoliation.

3.3. Physical Properties of CCNs

3.3.1. GIC Band Structure. Angle-resolved photoemission spectroscopy (ARPES) shows how charge doping affects the electronic band structure of crystalline materials. For CCNs, practical considerations limit such measurements to GICs and graphene, since the technique requires highly ordered crystal surfaces that are larger than the beam of incident photons (typically $\sim 1 \mu\text{m}$). In situ ARPES measurements of potassium-decorated graphene demonstrate the expected shift of the Dirac point to below the Fermi level as the π^* bands are occupied upon electron doping.^{233,234} These measurements also reveal a nonlinearity of the band dispersion at high doping and a trigonal warping of the now occupied π^* bands (Figure 14). Alkali metal doping can add a significantly greater number of charge carriers to graphene sheets than accessible via electrostatic gating; the Dirac energy has been found as low as -1.5 eV (compared with the maximum value of $\sim 1 \text{ eV}$ for gated graphene^{235,236}).

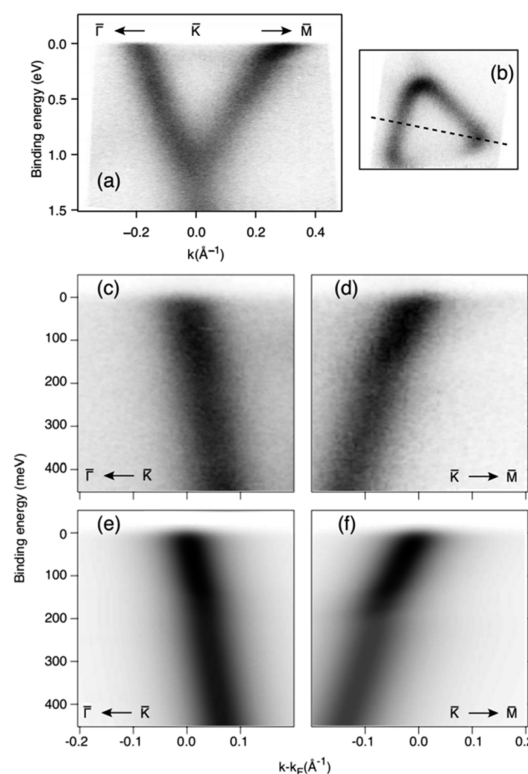


Figure 14. Angularly resolved photoemission intensity around the \bar{K} point shown as different cuts through a three-dimensional data set. (a) Large-scale dispersion through \bar{K} . (b) Fermi surface around \bar{K} with the dashed line indicating the cut shown in (a). More detailed Fermi energy crossings along the $\bar{K}-\bar{\Gamma}$ (c) and $\bar{K}-\bar{M}$ (d) directions. (e and f) show the simulated photoemission intensity corresponding to the data in (c and d, respectively). Reproduced with permission from ref 233. Copyright 2010 The American Physical Society.

For GICs, the π^* bands closely resemble those of doped graphene^{237,238} but another band, with 3d character located between the graphene sheets, is also occupied.²³⁹ This so-called interlayer (IL) band originates predominantly from the development of the alkali metal superlattice between the graphene sheets of the GIC.²⁴⁰ Although there is a full ionization of the intercalant, the relative occupation of the interlayer band is dependent on the graphene layer separation in the GIC: the closer the layers, the more the π^* band is occupied at the expense of the IL-band.²⁴¹ The lack of a clearly resolved IL band on metal-decorated graphene with ARPES could be due to choice of incident energy,²³⁹ as well as the intercalant disorder on doped graphene compared with that found for GICs. The effect of doping and superlattice formation of incrementally (potassium) doped graphene can be indirectly measured²⁴² through Raman spectroscopy (section 3.3.3): unlike GICs, for which only fixed stoichiometries with well-defined superlattices are observed (e.g., KC_8 , KC_{24}), graphene may be incrementally doped with K atoms. While at the highest levels of doping, alkali metal superlattices still form on graphene, evidenced by emergence of new phonon modes from the modified periodicity, the presence of other bands indicate that disorder remains in the saturated system. This difference in tunability of graphene compared with graphite was shown to exist for 1–4 layer graphene.²⁴²

3.3.2. CCN (Super)conductivity. The in-plane electrical conductivity of GICs increases compared to the parent graphite upon intercalation, reaching values on the order of 10^8 S m^{-1} for AsF_5 GICs, higher than metallic copper.²⁴⁴ The electrical conductivity of GICs is inherently highly anisotropic, with values for the in-plane to c axis ratio σ_a/σ_c ranging from around 15 (LiC_6) to 10^4 (FeCl_3C_8) in stage-1 compounds;²⁴⁵ the value for graphite itself is 3×10^3 . More recently, the in-plane conductivity of individual graphene monolayers has been shown to increase upon doping, without affecting band structure.²⁴⁶ Similarly, the conductivity of SWCNT bundles increases with increasing donor²⁴⁷ and acceptor²⁴⁸ intercalation.¹⁸⁰ Relatively nondoping adsorbents (e.g., aniline) may decrease conductivity,²⁴⁸ likely due to separation of adjacent SWCNTs within the bundle, or additional scattering.

Superconductivity has been observed for the alkali metal stage-1 GICs KC_8 , RbC_8 , and CsC_8 , with critical transition temperatures (T_c) all under 200 mK, while more recently divalent intercalants including YbC_6 and CaC_6 have shown superconductivity¹⁸¹ at higher T_c (6.5 and 11.5 K, respectively). In these systems, electron–phonon coupling involves both out-of-plane C and in-plane interlayer C_a phonon modes, including transitions between the IL and π^* electronic bands.²³⁹

The possibility of superconductivity in doped monolayer graphene is currently the subject of much debate; indirect measurements²⁴⁹ imply that lithium doping provides a T_c around 5 K, while other experiments rule out superconducting graphene doped with any group 1 metal with $T_c \geq 1.8 \text{ K}$, instead proposing only calcium doping to be effective.^{239,250} Fullerides can also act as organic molecular (type-II) superconductors²⁵¹ of the form M_3C_{60} where M is an alkali metal (or mix of alkali metals). $\text{RbCs}_2\text{C}_{60}$ has the highest ambient critical temperatures^{251,252} of any reported organic superconductors (33K), while Cs_3C_{60} reaches 40 K at high pressure.²⁵³ Other charged carbon structures show superconductivity (albeit with lower T_c), including doped diamond,²⁵⁴ doped Q-carbon,²⁵⁵ and reduced glassy carbon.²⁵⁶

The use of (neutral and reduced) SWCNTs as superconductors is still the subject of ongoing debate.^{257–260}

Another exotic electronic ground state found in CCNs is the so-called “charge density wave” (CDW), observed for CaC_6 by scanning tunnelling microscopy (STM).²⁴³ Here, below a critical temperature (T_{CDW}), long-range periodic stripes occur in the electron density (Figure 15), with an associated

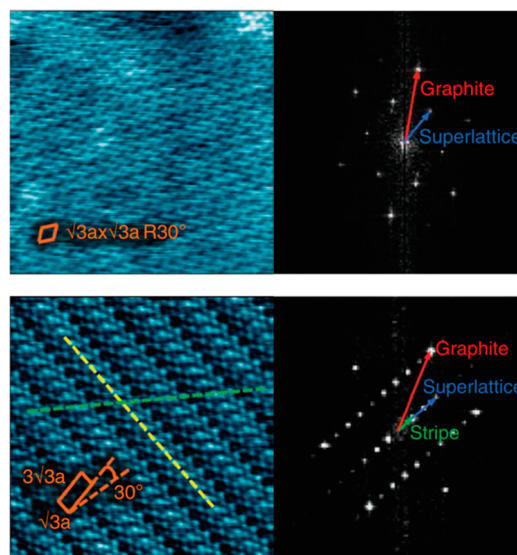


Figure 15. (Left) Constant-current STM micrographs with (right) Fourier transforms of CaC_6 structure of (top) phase surface of the standard GIC and (bottom) in the distorted CDW phase, displaying both hexagonal structures as seen for the expected phase and the stripe that shares one of the Ca symmetry directions. Adapted with permission from ref 243. Copyright 2011 Springer Nature.

distortion of the intercalated calcium superlattice (but notably not of the carbon lattice); more recently, similar electronic stripes have been observed in Ca-doped bilayer graphene.²⁶¹ A CDW state has yet to be observed in either nanotubide or fulleride crystals.

3.3.3. CCN Optical Properties. For graphitic materials, both reductive (donor) and oxidative (acceptor) charging shift the Fermi level (Figure 16a), by adding electrons to the antibonding π^* -band (conduction band) or removing them from the bonding π -band (valence band), respectively. The magnitude of the Fermi level shift is dependent on the reducing/oxidizing species,²¹⁴ the stoichiometry of the charging material,¹⁵¹ and the eDOS of the specific nanomaterial (Figure 16b). In the charged state, the filled/emtpied states may be probed spectroscopically or electrochemically. The discrete reductions of C_{60} from neutral to C_{60}^{6-} occur at regularly spaced reduction potentials (Figure 5a) as electrons are always added to the same degenerate orbital set, with some fluctuations attributable to electron–electron interactions (e.g., pairing energy) and quantum capacitance.²⁶⁴ The sequential reduction can be observed via cyclic voltammetry (CV) and differential pulse voltammetry to give clear redox events. Similar measurements can be performed on sorted SWCNTs, showing redox events at potentials matching vHSS, although the peaks are substantially less pronounced due to the continuum of states across all potentials in (polydisperse) SWCNT samples.²²⁸ The linear eDOS/potential relationship of graphene leads to a linear CV behavior.²²⁹ The doping

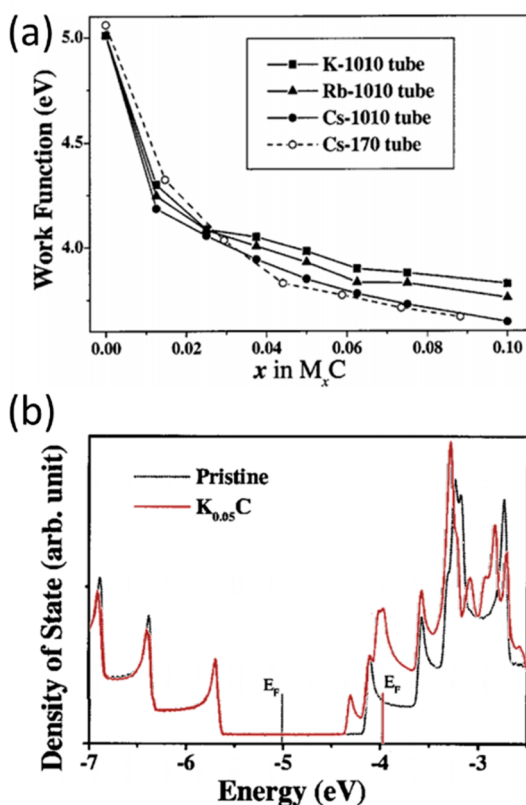


Figure 16. (a) Work function of SWCNT bundles as a function of reduction and (b) eDOS of pristine and KC_{20} (10,10) SWCNT. Reproduced with permission from ref 57. Copyright 2002 The American Physical Society.

process is easily visualized as shifting the Fermi level against the known neutral eDOS, with the new potential set by the comparing the integral of the eDOS to the number of electrons added/removed. However, at higher charge, the net electron–electron interactions increase/decrease during reduction¹⁵¹ and oxidation,²⁶⁵ respectively. As a result, the eDOS stretches (nonlinearly), increasing the magnitude of the potential for any given charge stoichiometry, relative to the neutral eDOS. While this effect has not yet been studied in detail for CCNs, quantum capacitance concepts have been used to estimate the extent of the effect for both graphenide¹⁵¹ and nanotubide,^{266,267} though the band structure may change more significantly upon heavy doping or due to dopant-related features.

The optical properties of carbon nanomaterials change upon doping due to the altered electron occupancy; recent reviews discuss the effects of charge on SWCNT spectroscopy,²¹⁷ as well as Raman scattering²⁶⁸ and optical absorption²⁶⁹ by graphene. Briefly, the optical transmission spectra of neutral SWCNTs are dominated by the allowed transitions between vHSs, giving rise to well-defined regions of (helicity dependent) absorption peaks in the UV–vis spectrum. With increasing oxidation, emptying of the valence band vHSs leads to progressive bleaching of the transitions (Figure 17a). Analogously, reductive filling of the conduction band causes bleaching due to Pauli blocking. In both cases, increasing charge leads to sequential bleaching of transitions with increasing energy (i.e., E_{11} are bleached before E_{22} etc.); these bleaching events also quench the related photo-

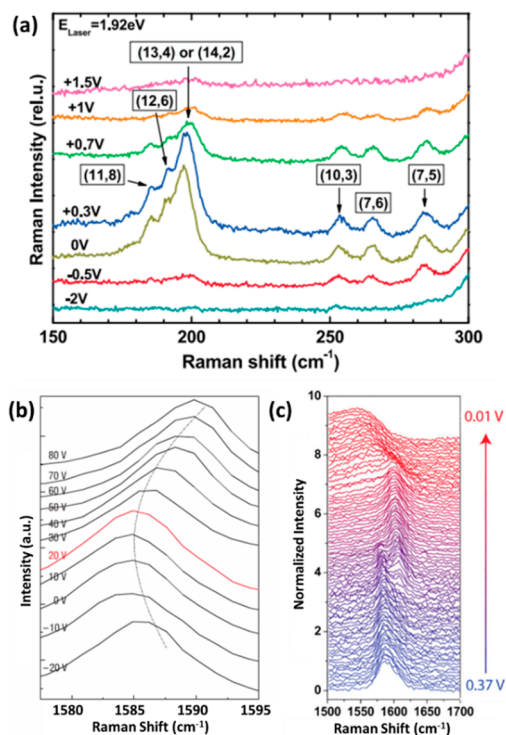


Figure 17. (a) Bleaching of SWCNT radial breathing modes upon charging from filling/emptying vHS. Reproduced from ref 262. Copyright 2011 American Chemical Society. (b) Graphene Raman G mode position as a function of gate voltage, showing upshift at increasing charge (red line at 20 V corresponds to the undoped state). Adapted with permission from ref 263. Copyright 2007 Springer Nature. (c) Graphite Raman spectra as a function of voltage. Reproduced with permission from ref 230. Copyright 2016 The Royal Society of Chemistry.

luminescence peaks of sc-SWCNTs. In principle, the bleaching events can be used to follow the redox charging behavior; however, comparisons between spectroscopic⁵⁰ and electrochemical measurements^{57,63,228} are complicated by effects of exciton binding energies which are significant in nanocarbons.²⁷⁰ While the effective eDOS may stretch due to the electron–electron interactions mentioned above, the general form of the band structure is typically not affected by the doping,^{217,271} with notable exceptions of strongly hybridizing dopants²¹² and oxidizing acids.²¹⁴ The near linear distribution of states from the Fermi level in graphene leads to an optical transmission spectrum of graphene with no features in the UV–vis range (aside from the π – π^* transition at ca. 220 nm). Upon doping, the optical absorption of graphene (at least in the 1–3 eV range) increases as a function of doping level, regardless of charging direction.^{269,272}

The optical spectrum of C_{60} varies with charge²⁷³ with both fullerides and fullereniums gaining additional peaks in the NIR–vis range, due to the reduced symmetry, and shrinkage of the HOMO–LUMO gap. Similarly, the infrared (IR) spectroscopy of fullerene changes upon reduction, with the strong t_u mode splitting; however, the final spectrum is complex and is highly dependent on the final crystal structure. The vibrational IR absorption spectrum of unfunctionalized nanotubes shows no significant peaks and does not change upon addition of a donor molecule;²⁷⁴ however, any vHS transitions present in this region²⁷⁵ (e.g., E_{11} of very large diameter SWCNTs) should be bleached upon doping.

In the Raman spectrum of the graphitic nanocarbons, the G mode upshifts to higher energies with increasing charge (Figure 17b),²⁶³ and, for graphene, the G mode also sharpens asymmetrically at low doping levels,²⁶⁸ while at higher doping levels, the G mode is found to broaden significantly and shifts to lower energies.^{242,276} In the lower doping regime, the 2D mode position is broadly inversely proportional to the electron doping level, providing a convenient estimate of charge stoichiometry.²⁷⁷ It should be noted that the position of the graphene and nanotube G mode also shifts under strain, complicating analysis;^{278–280} however, additional strain-based spectral modifications (notably G-splitting^{278,281}) may be used to differentiate doping and strain-derived G mode shifts.^{242,280}

The Raman scattering intensity of graphene as a function of doping varies for each phonon mode;²⁸² while the G mode intensity is effectively independent of Fermi level, the 2D mode intensity relies on electron–electron scattering and so scales with the number of available electrons (increasing upon reduction and falling on oxidation). Conversely, the Raman scattering intensity from SWCNTs is driven by resonance effects, with both oxidative and reductive doping causing a decrease in Raman scattering intensity,²⁸³ due to the progressive bleaching of the optical transitions, as noted above.²⁶² Additional peaks appear in the Raman spectra of intercalated nanocarbons, at energies dependent on the intercalants, for example, emergence of a C_z mode^{146,284,285} for GICs at ca. 550 cm^{-1} and Breit–Wigner–Fano interference peaks in group 1 intercalated SWCNT bundles.²²¹

3.3.4. CCN Geometric Properties. The formation of CCNs not only changes the electronic but also the geometric properties versus the neutral species. As discussed previously (section 3.1), the internanocarbon spacings (c axis spacing for GICs, lattice constants of SWCNTs/fullerenes) increase upon addition of a donor or acceptor, with the crystal system also subject to change for the fullerenes. Additionally, the intranancarbon C–C bond lengths vary as a function of charge; for example, graphene’s intralayer bonds increase in length under both reduction and oxidation²⁸⁶ (Figure 18) with a near linear charge–strain relationships for each (ca. 5% strain per carbon charge during reduction, lower for oxidation²⁸⁶). A similar, though not necessarily linear, trend has been calculated for SWCNTs but not yet determined empirically.²⁸⁸ For fullerenes, the nature of the geometric change upon reduction is more complex (Figure 19); reduction leads to a decrease in 5:6 and increase in 6:6 bond lengths,²⁸⁹ with the extent of the size change related to the magnitude of charge; in addition, fullerides with a charge of 1–5 are all degenerate, leading to Jahn–Teller distortions.^{164,171} Finally, the solubility of carbon nanomaterials is dramatically increased upon charging, as discussed later, both practically (section 3.4) and theoretically (section 5).

3.4. CCN Solutions

While neutral fullerenes are soluble in several solvents (comprehensive lists have been compiled^{115,116}), reduction to fulleride can further increase the solubility,^{40,68} and remove any clustering/agglomeration, instead solely forming individualized species with a well-ordered solvation shell. The solvent molecules in inner shells are well-ordered to maximize dipole–fulleride interactions while preserving intrinsic solvent–solvent interactions such as hydrogen-bonding motifs.^{293,294} Additionally, previously insoluble endohedral fullerenes become spontaneously soluble upon reduction to their respective

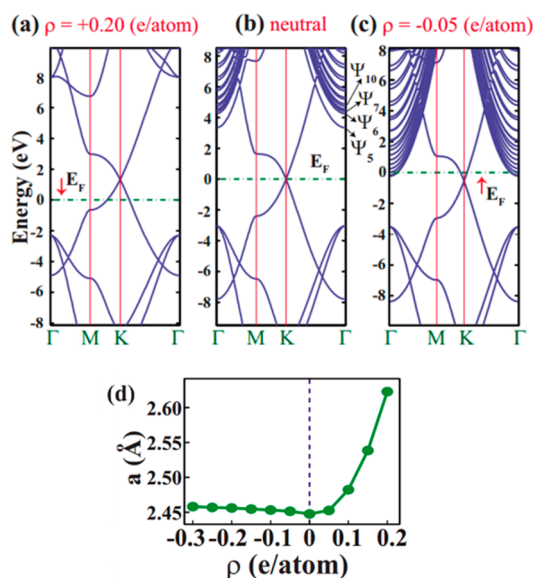


Figure 18. DFT-derived energy band structure of (a) positively charged (+0.20 e/atom), (b) neutral, and (c) negatively charged (−0.05 e/atom) graphene, where excess electrons start to occupy the surface states. Zero of energy is set to Fermi level. (d) DFT calculated variation in lattice constant a of graphene as a function of charge. Reproduced with permission from ref 286. Copyright 2011 AIP Publishing.

fulleride.²⁹⁵ The relative solubility of fullereniums versus neutral fullerenes has not been reported to date; however, fullerenium (and fulleride) synthesis is often performed with fullerenes solvated before and after redox,¹⁷¹ implying that solubility is at least equivalent to the initial fullerene dispersion.

Synthesized salts of the reduced CCNs can spontaneously dissolve in polar aprotic solvents to form solutions of fulleride, graphenide, or nanotubide²⁹⁶ (Figure 20). Unlike the kinetically metastable LPE dispersions of nanotubes and graphenes, these charged solutions are thermodynamically favorable (section 5), illustrated by their spontaneous dissolution, and consist of individualized species, as unambiguously illustrated by neutron scattering for each of C_{60}^{5-} in liquid ammonia^{291,297} (Figure 21a), nanotubide in dimethylformamide²⁹² (DMF, Figure 21, panels b and c), and graphenide in THF¹⁸⁹ (Figure 21, panels d and e). The appropriate solvents are often the same as those used for the LPE of pristine SWCNTs/graphite²⁹⁸ such as DMF²⁹² and dimethyl sulfoxide¹⁹² (DMSO), although questions have been raised about the stability of DMSO with highly reduced CCNs; methylation of the nanomaterial (while depleting charge) may contribute to solubility, at least at high degrees of charging.²⁹⁹ Other aprotic, polar solvents are expected to be suitable if they have similar solubility parameters²⁹⁸ to the reduced carbon nanomaterial and are stable at the relevant redox potentials (dependent on degree of CCN charging). *N,N*-dimethylacetamide (DMAc) is particularly attractive as a solvent for nanotubides, as it can be used as a common medium both to reduce the SWCNTs and dissolve the formed nanotubide in a single step.¹⁴³ The use of an organic charge carrier/group 1 metal (e.g., sodium naphthalide) DMAc solution is well established. However, solid elemental sodium mixed with SWCNTs in DMAc is also reported to yield direct, though kinetically slower, nanotubide dissolution.³⁰⁰

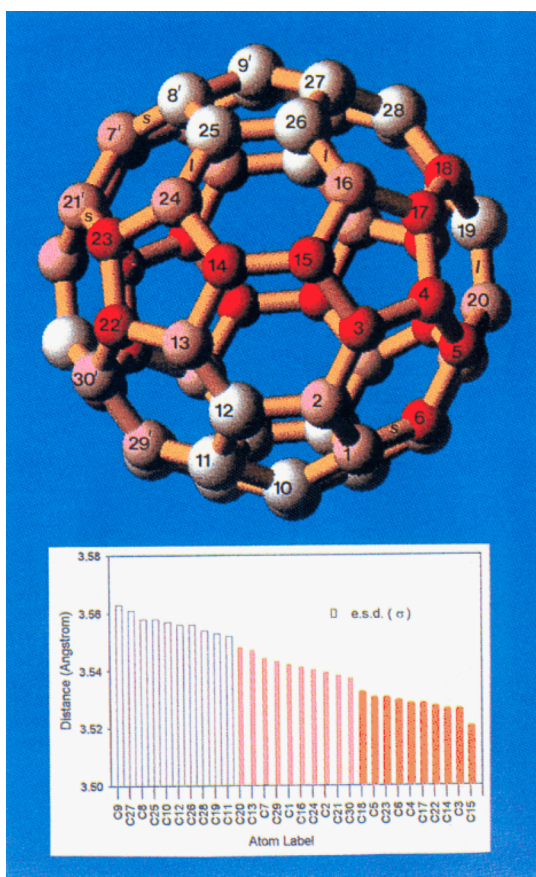


Figure 19. Distortion of C₆₀²⁻ ion. (Top) To-scale C₆₀²⁻ with white/pink/red carbon atoms indicating greater than average/mean/below average distances from the geometric center showing deviation from the parent C₆₀'s ideal spherical structure. (Bottom) Values of center-carbon atom distances. Reproduced from ref 287. Copyright 1994 American Chemical Society.

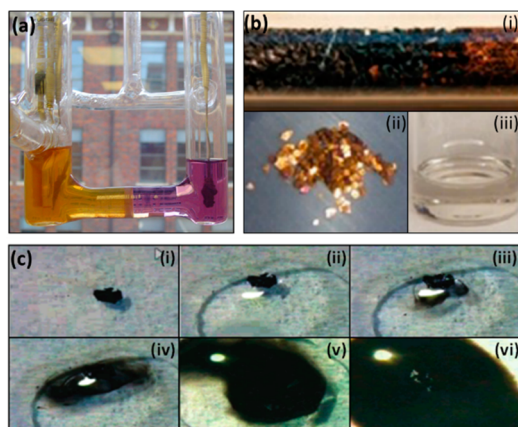


Figure 20. Solutions of reduced CCNs. (a) Electrochemical discharging of a fulleride derivative (orange, left) to fullerene (purple, right), adapted with permission from *C60 Colors*, by Adrian Villalta, licensed under CC BY-SA 2.0. (b) Gas phase intercalation of graphite (i, left) to KC₈ (i, right, and ii) and dissolution in THF (iii). Adapted from ref 290. Copyright 2013 American Chemical Society. (c) Spontaneous dissolution of sodium nanotubide salt in DMSO over time (i–vi). Adapted from ref 192. Copyright 2005 American Chemical Society.

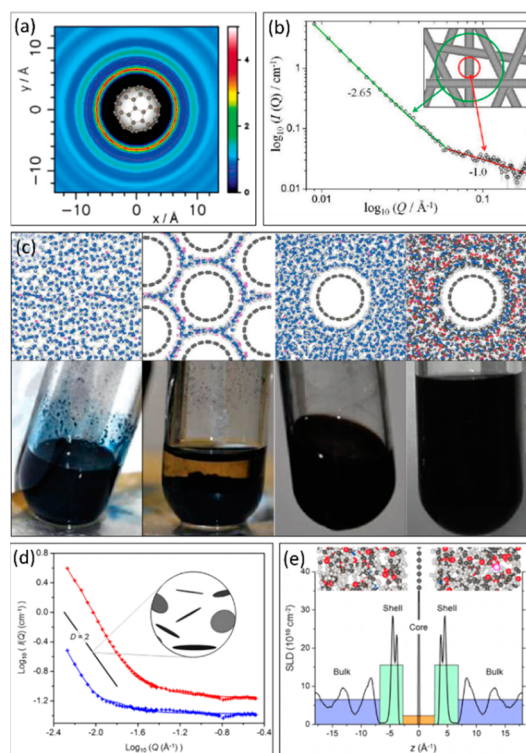


Figure 21. (a) Two-dimensional projection of the solvation of C₆₀⁵⁻ anion by ammonia showing the ensemble average relative density of ammonia molecules around a reference fulleride. The C₆₀⁵⁻ anion is located in the white sphere at the origin. These “giant” solvation shells double the effective radius of the fulleride in solution. Reproduced with permission from ref 291. Copyright 2004 American Chemical Society. (b) Small angle neutron scattering pattern of nanotubide (Na/ND₃) showing regimes of individualized and meshed SWCNTs. Reproduced from ref 292. Copyright 2012 American Chemical Society. (c) Schematic and photographs of Birch reduction and dissolution of SWCNTs, from left to right, Li/NH₃, SWCNTs reduced by Li/NH₃, dissolved nanotubide in NH₃, and nanotubide solution in DMF. (d) Small-angle neutron scattering from 0.1 wt % (red) and 0.01 wt % (blue) graphene platelets in D₈-THF solution. (e) Scattering length density normal to the ab-plane of a single charged graphene platelet. Reproduced from ref 189. Copyright 2012 American Chemical Society.

3.4.1. Charged SWCNT Solutions. The percentage of charged SWCNTs that dissolve varies with several factors including SWCNT type, total SWCNT loading (weight solid SWCNT per volume solvent), total transferred charge, and agitation. While some SWCNT types dissolve with (near) 100% yield in idealized charging conditions (e.g., HiPco SWCNTs), other sources may contain intrinsically insoluble components, such as cross-linked SWCNTs, macroscopic networks of amorphous carbon, and highly entangled SWCNTs. Regardless of SWCNT type, the yield may be limited by saturation of SWCNTs in solution; the maximum concentration is thought to depend on nanotube stiffness, aspect ratio, and intrinsic SWCNT repulsion but typically varies between 1 and 3 mg mL⁻¹; above this concentration, additional SWCNTs will not dissolve as an isotropic solution, lowering the final yield. Certain CCN systems facilitate formation of liquid crystals (LC, section 5.3) with an isotropic/LC transition concentration at similar concentrations to the isotropic saturation limit of non-LC systems; however, the LC concentrations still eventually saturate, with the final

limit varying strongly between CCN systems. The nanotubide charge density influences the yield in a nonlinear manner. Initially, increasing charge increases the yield of the dissolution; however, at high metal stoichiometries (above ca. C_4M), the yield of dissolution decreases. The precise stoichiometry for optimized systems varies between systems, depending on purity (charge sequestration) and polyelectrolyte effects, related to the characteristics of the SWCNTs, the counterions, and solvent medium^{143,301} (section 5). Although certain systems dissolve completely, spontaneously, yields are maximized, or at least accelerated, by modest agitation; simple slow stirring is usually sufficient. Particularly long or entangled SWCNT samples may require extended or more vigorous stirring,⁸⁷ sufficient to break the longer, more susceptible species. In the absence of agitation, partial dissolution (for example, at lower degrees of charging) may be selective due to both thermodynamic and kinetic effects (section 6).

3.4.2. GIC Dissolution. The dissolution of donor-GICs to graphenide is possible with extended stirring;²⁹⁰ however, the efficiency and resulting concentrations are notably lower than for the nanotubide counterparts.¹³⁵ GICs formed from small graphene platelets or with large intercalants have smaller total van der Waals interactions between adjacent graphene sheets and can dissolve spontaneously to monolayers (ca. 200 nm flakes)³⁰³ or to predominantly (>95%) monolayer species at higher yield with very brief and mild sonication.^{42,189} Cryomilling to reduce graphite aspect ratio has been shown to improve solubility of the subsequent GIC.³⁰⁴ The best spontaneous dissolution is typically obtained using a stage-1 GIC with maximum possible imbued charge; however, stage-2 and stage-3 GICs have been shown to facilitate bi- and trilayer graphene exfoliation albeit with sonication.³⁰⁵ It is not yet fully clear why graphenide is more challenging to disperse than nanotubide; however, more efficient packing of the carbon layers may lead to a larger lattice energy for the salts. In addition, the dimensionality will alter charge screening and condensation (section 5). Larger graphite flakes are statistically more likely to contain interlayer bonds (section 2.4), which may limit exfoliation. Lastly, diffusion paths for both solvent and counterions are much greater for graphite than for bundled SWCNTs and may be further constrained by Daumas-Hérolé boundaries¹³⁵ and scroll edges. The addition of crown ether chelate counteranions³⁰⁶ or substitution of larger counterions³⁰⁷ leads to improved dispersibility and concentration of graphenide: it is currently unclear whether the increased effective counterion size of solvent-coordinated cations found in solvated-reductant-derived GICs has a similar effect.

Addition of donor-GICs to water can lead to recovery of monolayer fragments of graphene;²³² this exfoliation has been attributed to the explosive release of hydrogen gas formed between the layers, leading to high shear forces separating the layers; the recovered material is typically found to be highly defective with reduced aspect ratios, due to the aggressive mechanical process and the opportunities for functionalization (section 4.4). A gentler interaction with water leading to association with hydroxide ions is discussed later (section 3.5).

Dissolution of the acceptor-GICs and nanotubium is less studied than their reduced counterparts as the shift in Fermi level is typically of a lower magnitude,²²⁸ due to the available stability windows (section 3.2.2).²³¹ The only known routes to individual graphenium ions are through sonication of presynthesized acceptor GICs (Figure 22)^{302,304} or stirring of

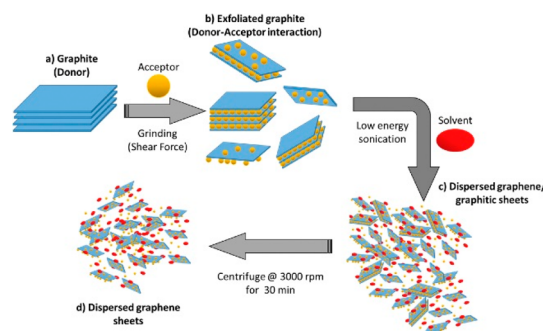


Figure 22. Sonication exfoliation of acceptor-GIC. Reproduced with permission from ref 302. Copyright 2017 Elsevier.

GICs formed from heavily milled, low aspect ratio graphites.³⁰⁴ Even in these cases, the use of strong acids as intercalants makes it unclear whether exfoliation can be attributed to charge transfer to form graphenium ions or associative protonation as established directly with superacids.

3.5. Associative Ion Charging

An alternative route to positively charged carbon nanotubes and graphenes is via associative protonation with superacids,³¹⁰ adopting systems designed for polyaramid processing. Rather than removal of electrons from the delocalized π system, the superacid route involves coating the nanomaterial with associated protons to imbue a positively charged shell^{308,311} (Figure 23). To accomplish the synthesis, the raw nanomaterial (SWCNTs or graphite) is added to the superacid, typically oleum or chlorosulfonic acid, and a solution of the protonated nanomaterial forms spontaneously. The (per-carbon) degree of positive charge may be tuned by using mixtures of superacids, with varying strength (oxidation potential) and quantified through monitoring shift in the Raman spectrum's G mode (section 3.3.3), with a maximum charge of $HC_{12.7}^+$ observed for (purified HiPco) SWCNTs³¹² dissolved in pure $HClSO_3$. Isotropic individualized nanotube solutions up to 0.5 wt % are possible,³¹¹ although the maximum concentration of this isotropic phase is heavily dependent on the nanotube aspect ratio; higher concentrations of SWCNTs in superacid give nematic phases as discussed later (section 5.3). The isotropic phase concentration may be increased through functionalization of the SWCNT sidewall;³¹³ however, access to nematic phases is lost.

Small graphite flakes can be dissolved in superacids, but larger bulk graphite may be left unexfoliated.³¹¹ The yield of this dissolution is dependent on both acid strength and graphite source, likely for similar reasons to those discussed for reductive dissolution (section 3.4). Once the inherently insoluble fraction of the graphitic material has been removed, the remaining flakes can be recovered and redissolved as individual flakes at high concentrations facilitating the formation of liquid crystals. Similarly to SWCNTs, functionalization may be used to increase solubility in the isotropic phase.³¹⁴

Fullerenes degrade in the presence of traditional superacids, including chlorosulfonic acid, although alkyl fullerols $RC_{60}OH$ can be dehydroxylated with triflic acid to form the RC_{60}^+ cation.³¹⁵ However, the parent HC_{60}^+ cation can be created using the hexahalocarboranes ($HCB_{11}H_6X_6$) leading to a localized hydrogen on the C_{60} which can be removed by the presence of water or base to recover the undamaged fullerene.²²⁵ In the cases of superacid-treated graphene¹⁴¹

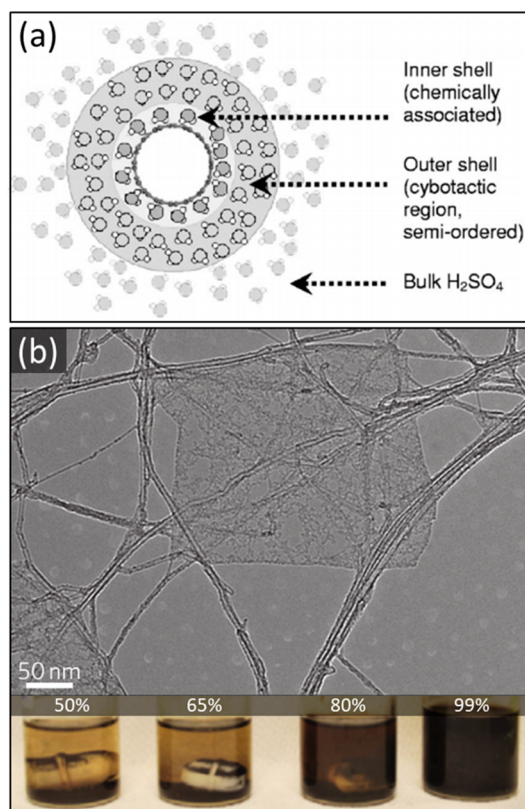


Figure 23. (a) Schematic of solvation shell around SWCNTs in oleum. Reproduced with permission from ref 308. Copyright 2005 The American Physical Society. (b) TEM of graphene monolayer from HClSO_4 dissolution on CNT mesh (top) and digital photographs of graphite stirred in varying concentrations of chlorosulfonic acid (bottom). Reproduced with permission from ref 141. Copyright 2010 Springer Nature.

and nanotubes,³¹⁰ the protons are claimed to be delocalized and reversibly removed by water, as discussed further in section 4.4.

Analogously, an associative anion system has been developed recently, to provide stable aqueous dispersions of graphene with a shell of associated hydroxides. These solutions are formed by air-discharging a graphene/THF solution before immediate addition to degassed water (Figure 24).³¹⁶ The direct addition of graphene to water would be expected to damage the graphitic structure significantly; air discharge minimizes this effect though some functionalization may still occur (section 4.4). The system allows solubility to be maintained through adsorbed hydroxide anions generated from water reduction, forming a negatively charged layer on the graphene;³⁰⁹ through evaporation of the THF, aqueous solutions of graphene can be obtained, and with mild centrifugation, predominantly monolayer graphene solutions may be formed.³¹⁷ Recently, the same group has reported similar associative hydroxylation of SWCNTs. Unlike the superacid associate protonation, the associative hydroxylation does not exfoliate a raw, neutral feedstock. Although routes to directly produce hydroxyl-associated species directly from graphite in a milder manner are under study,³¹⁸ the degree of exfoliation appears to be poor, so far.

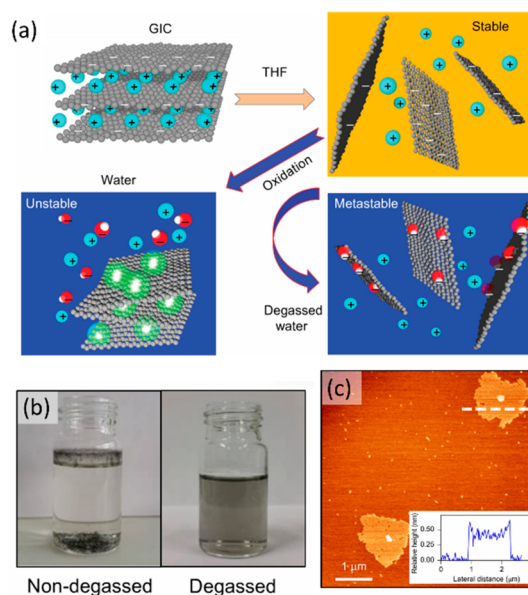


Figure 24. Aqueous associative hydroxide dispersed graphene. (a) Schematic of solution formation, (b) photographs of THF graphene solution after addition of nondegassed (precipitated graphite) and degassed water (aqueous graphene solution), and (c) AFM with height profile of monolayer graphene deposited from aqueous associative hydroxide dispersed graphene solution. Adapted with permission from ref 309. Copyright 2017 Springer Nature.

4. REACTIVITY OF CCNS

4.1. Reactivity of Neutral Nanocarbons

Covalent functionalization of carbon nanomaterials is a vital tool for tuning their behavior, including their solubility, chemical compatibility, and electronic properties. Noncovalent interactions, such as π - π stacking of CNT/pyrene, are sometimes also described as functionalizations; however, while these interactions are undoubtedly useful in many contexts (and have been reviewed previously^{319,320}), here functionalization will only be used to describe the covalent attachment of an external moiety. Functionalization of (uncharged) fullerenes,^{321,322} SWCNTs,^{323,324} and graphene^{325,326} have each been extensively reviewed previously.

The most common types of functionalization rely on heavy oxidation to introduce polar groups, usually through the formation of sp^3 or edge-type defects. For graphite, oxidation may lead to formation of GO, often synthesized through the Hummers' method³²⁷ (KMnO_4 , NaNO_2 , and H_2SO_4), which provides basal plane hydroxyls and 1,2-epoxides and edge epoxidation/carboxylation.³²⁸ For SWCNTs, oxidation can be performed using air, oxygen plasma, or oxidizing acids (most commonly HNO_3), generally to form carboxylic acids among other oxygen-containing species. The acidic route is particularly prevalent for SWCNTs as the conditions also facilitate simultaneous removal of catalyst impurities.³²⁹ The introduced oxygen-containing functional groups can be utilized as an anchor for new, desired functionalities through traditional organic chemical reactions (typically esterification/amidification³²³). However, all these chemical oxidations intrinsically involve extensive damage to the framework, involving etching of carbon to form vacancies¹⁹⁹ which are significantly more detrimental to electronic⁷⁸ and mechanical³⁷ properties than simple sp^3 defects and cannot be repaired through annealing.¹⁹⁹ Fullerenes are more reactive, and hence oxidation is

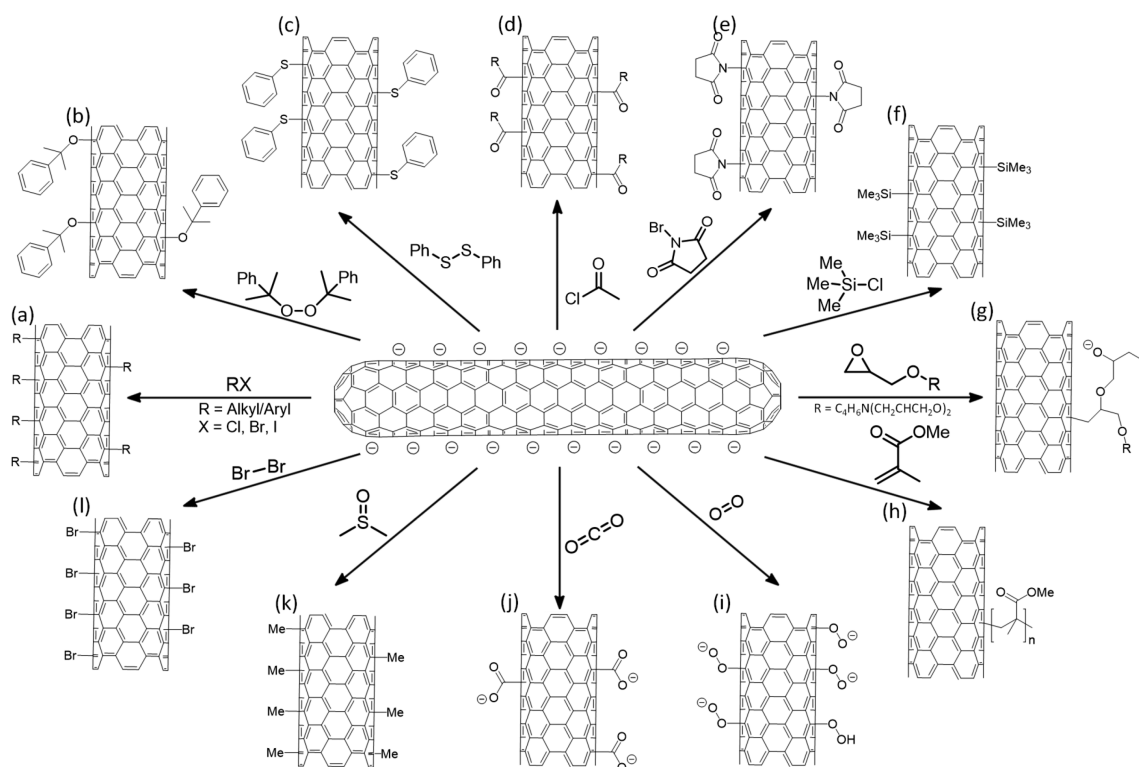


Figure 25. A nonexhaustive selection of reactions of reduced SWCNTs with (a) alkyl/aryl halides,^{301,334} (b) peroxides,^{314,335} (c) disulfides,³³⁶ (d) acyl chlorides,¹⁹⁹ (e) *N*-halosuccinimides,³³⁵ (f) chloroalkylsilanes,^{194,337} (g) epoxides,³³⁸ (h) vinyl monomers,^{339,340} (i) oxygen,^{151,182} (j) carbon dioxide,¹⁹⁹ (k) DMSO,²⁹⁹ and (l) bromine.^{341,342} (*) These reactions have also been demonstrated for graphene.

possible under milder conditions, with (unwanted) epoxidation occurring in the ambient environment (section 2.4); the application of strongly oxidizing acids tends to destroy C₆₀, although oleum can be used to hydroxylate fullerene via sulfonation.³³⁰ The high curvature SWCNT end-caps are similarly susceptible to oxidation and are removed preferentially in oxidizing conditions to create “opened” structures. As an alternative to oxidation, the low reactivity sp² framework of nanotubes and graphenes can be directly attacked by unstable, short-lived reagents such as carbenes, nitrenes, or ylides.^{323,331} These reagents require predispersion of the nanomaterial through potentially damaging ultrasonication to prevent reactions occurring predominantly on bundle/stack exteriors.^{314,332} Related reactions are commonly performed on fullerenes, with their higher curvature and strain increasing reactivity toward radicals. In these molecular systems, the complex variety of substitution patterns can be separated chromatographically. In the other nanocarbons, the locus of functionalization is largely unexplored. In situations where the added reagent has a reduction potential below that of the Fermi level of the uncharged nanocarbon, the neutral nanomaterial is capable of directly acting as a reductant.³³³

4.2. Reductive Functionalization

The reactivities of the fullerene ions are dictated by their molecular orbital chemistries, in sharp contrast to the eDOS-driven properties of SWCNTs/graphene ions which are the focus for this section. The chemistries of the fullerene ions have been covered comprehensively by Reed et al.,¹⁷¹ but in short, fullerides are noted for their exceptional Lewis basicity with reactivity trending strongly with the magnitude of the charge. Reactions typically proceed via SET followed by a radical functionalization owing to the highly delocalized nature

of the electrons in the fulleride, while functionalized fullerides (having lower symmetry and more localized charge) tend to act nucleophilically.³⁴³ Conversely, although the reactivity of fullerene ions depends strongly on the medium, in general they are strong electrophiles/oxidants, particularly efficient at Diels–Alder reactions.^{171,344} For both fullerene and fulleride, the extent of reactivity depends on the extent of charging (as for graphene/nanotube); for example, iodobenzene³⁴⁵ reacts only with C₆₀^{3−} and higher charges and will not react with the mono/bireduced fullerene.

As an alternative route to nanocarbon functionalization, the charge of CCNs can enable reactions of the dissolved species at ambient temperatures and pressures with minimal damage to the sp² framework. Reductive functionalization reactions are usually conducted at room temperature [although reactions in liquid ammonia (<−34 °C) are also well-established], typically through stirring of the reduced CCN solution with the reagent, or solution thereof, which contains a reactive functional group (Figure 25). Functionalization of a nanocarbon electrode during electrochemical charging is also well-established and can facilitate high grafting densities as depleted charge is restored throughout the reaction.³⁴⁶

The most common reagents are organohalides;^{186,314,334} however, the reaction can be performed with peroxides,³³⁵ disulfides,³³⁶ acyl chlorides,³⁴⁷ *N*-halosuccinimides,³³⁵ diazonium salts,¹⁸⁷ chloroalkylsilanes,^{194,337} epoxides,³³⁸ elemental bromine,³⁴¹ diazonium salts,¹⁸⁶ haloformates,¹⁹⁷ ketones with α -electron-withdrawing groups,³⁴⁷ and iodonium salts.³⁴⁸ The reagents used should be anhydrous and degassed to prevent unnecessary discharge and damage (section 4.4).³⁴⁹ Since reagents with labile protons (notably hydroxyls¹⁸²) will lead to protonation, they should generally be avoided, although

reagents containing both labile protons and reactive functional groups will lead to some organic functionalization.³³⁵ Highly charged CCNs can react even with inert molecules; for example, carbon dioxide is reported to react with both nanotubide¹⁹⁹ and electrochemically expanded donor GICs.³⁵⁰ Although the degree of grafting is generally low, without repetition, due to the stability of CO₂, the approach provides an appealing route to carboxylic acid functionalities, accessing chemistries developed for acid-oxidized SWCNT and graphene oxide, without the need to etch carbons from the CCN framework. In general, CCN functionalization is accompanied by precipitation of the nanocarbon, as the charge is removed (section 4.4) over several hours. The reactions are most commonly monitored through statistical Raman spectroscopy (increase in the D/G mode ratio) and thermogravimetric analysis (TGA), ideally coupled with mass spectroscopy. In Raman spectroscopy, quantification is challenging, but models are available to estimate degree of functionalization,^{351,352} defect type,^{353,354} and extent of exfoliation.^{317,355} In TGA, care is needed to ensure that any weight losses related to the reaction conditions³⁵⁶ (reagent/solvent adsorption, reagent ashing, functionalization from uncontrolled discharging, etc.) are not misattributed to functionalization.

Reductive functionalization on CCN solutions offers a significant advantage over reactions performed on LPE exfoliated nanocarbons, as the entire surface is accessible (Figure 26), unlike bundled/stacked or surfactant-coated nanomaterials, in principle leading to higher degree and homogeneity. However, the degree of functionalization is inherently limited by the quantity of charge within the system (vide infra), as well as the reactivity of the reagent. When the degree of functionalization is constrained by accessible surface (e.g., grafting with presynthesized polymers) (Figure 27), reductive functionalization methodologies give higher polymer loadings than classic nonreductive approaches.³⁵⁶

Oxidative functionalization of nanotubium has been demonstrated²²⁸ by reacting the oxidative CCN with amino-functionalized silicon surfaces to pin the nanotube onto the surface, and oxidative potentiostatic functionalization is also known.³⁵⁷ Mildly (electrochemically) oxidized exfoliated graphite has been shown to react with diazonium salts more rapidly during exfoliation than for pre-exfoliated graphene.³⁵⁸ However, the reaction relies on charge transfer from nanocarbon to organic reagent (similar to reductive CCN functionalization, section 4.3), so further increasing the magnitude of oxidative charge may be expected to decrease the reactivity. The development of the chemistry of oxidative CCNs remains an open topic; successful reagents are likely to require loss of a stable cationic leaving group and may have to act as a nucleophile in their initial state. Associatively protonated carbon nanomaterials may be functionalized via diazonium chemistries akin to neutral nanomaterials;³³² however, the number of chemicals available for functionalization is inherently limited, as many materials are destroyed by the superacids used for CCN associative protonation.³³²

4.3. Mechanism of Reductive Functionalization

The functionalization reactions of all the reductive CCNs are currently attributed to a SET mechanism^{343,359,361} (Figure 28) analogous to the reductive functionalization of reduced molecular polyaromatics;³⁶² in the key step, a reagent, typically an organohalide, accepts an electron from the doped conduction band of the carbon nanomaterial. The so-formed

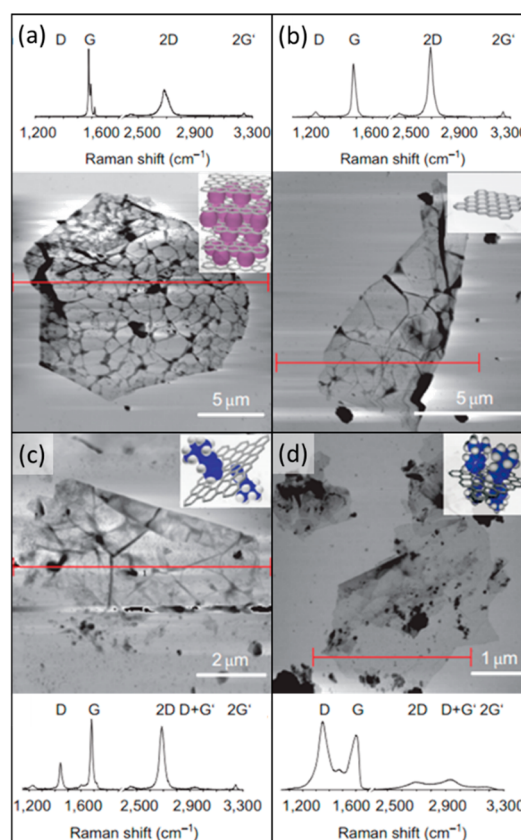


Figure 26. AFM and Raman spectra of the reductive exfoliation and functionalization of graphite. (a) GIC, (b) exfoliated monolayer graphene, and (c and d) mildly and heavily functionalized graphene, respectively, after reaction with 4-*tert*-butylbenzenediazonium tetrafluoroborate. Adapted with permission from ref 187. Copyright 2011 Springer Nature.

radical anion decomposes to form a neutral radical and an anionic leaving group.³⁵⁹ Some fraction of the radicals may self-terminate to generate dimers of the intended grafting moiety, as a side product.^{334,361} However, the radical moiety is predominantly grafted onto the carbon nanomaterial by attacking a double bond in the sp² framework forming an sp³ site, through the same mechanism as diazonium/azide functionalizations, as proposed by Schmidt et al.³⁶³ In accordance with one view, this transfer generates a new SWCNT-bound radical, subsequently capable of transferring to another reagent molecule to form a new organoradical, thus representing propagation step. However, the nature/reactivity of nanotube-bound radicals remains unclear.³⁶⁴ For example, no nanotube radical cross-linking termination is reported, despite such reactions being reported through other SWCNTs radical routes.³⁶⁵ The delocalized conduction band in CCNs may limit conventional localized radical propagation steps, representing an alternative termination.

The SET mechanism implies that the CCN Fermi level (a function of unutilized charge) must be sufficiently high to reduce the added grafting agent.¹⁵¹ As the concentration of electrons in the CCN conduction band diminishes with grafting, the Fermi level drops until it is equal to the reduction potential of the reagent. Hence, by selecting reagents with less negative reduction potentials, the degree of functionalization can be improved, for example, the grafting ratios from alkyl halide functionalization following the trend of increasing with

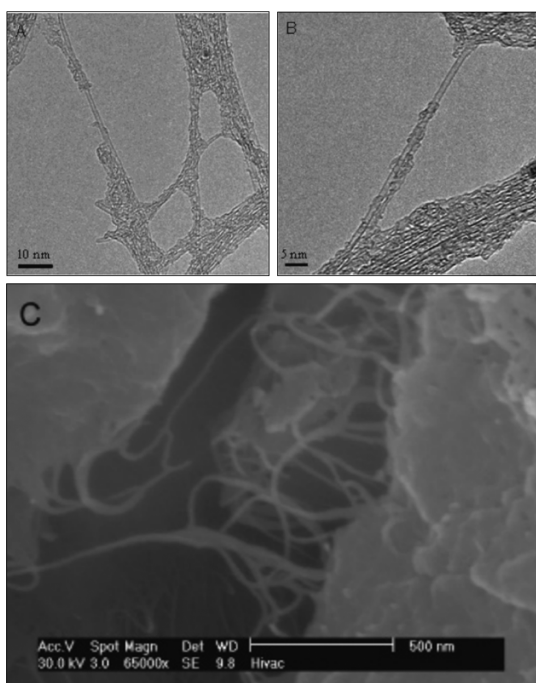


Figure 27. (a and b) TEM and (c) scanning electron microscopy (SEM) of poly(methyl methacrylate) grafted SWCNTs from nanotubide-initiated polymerization. Reproduced from ref 340. Copyright 2006 American Chemical Society.

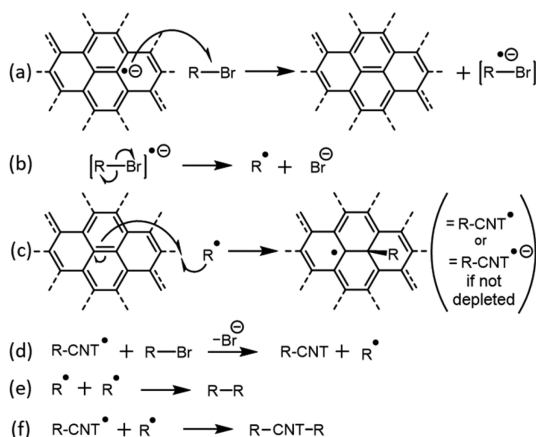


Figure 28. Reaction SET reductive functionalization mechanism (extended from the original suggestion by Voiry et al.³⁵⁹). (a) SET from nanotube to reagent RX, (b) decomposition of RX radical anion to R radical and X anion, (c) propagation step of SWCNT attacking R radical leaving nanotube R-CNT radical, (d) propagation step of R-CNT radical attacking R-Br to reform R radical, (e) termination via R dimer formation, and (f) termination through CNT-R and R radicals combination.

increasing halide size¹⁴³ and thus decreasing reduction potential.³⁶⁶ As the reduction potential of the functionalizing species is typically higher than the Fermi level of the neutral nanomaterial, there is typically residual charge remaining on the nanocarbon after functionalization. By subsequently adding a second reactive species with a lower reduction potential, the residual charge can be used to initiate a second reductive functionalization (Figure 29).¹⁸² This residual charge does not occur for fullerides, as the first functionalization forms a functionalized fulleride (RC_{60}^{n-}) which is typically more

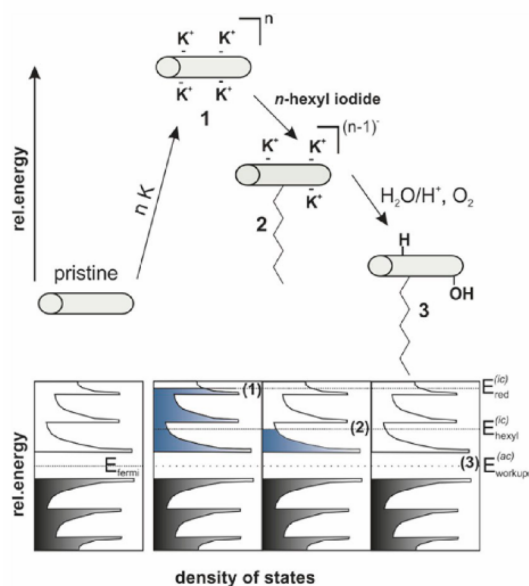


Figure 29. Scheme (top) and illustrative eDOS (bottom) of residual charge mechanism of SWCNT reductive functionalization. From left to right, reduction of SWCNT to nanotubide (1), functionalization to residually charged functionalized nanotubide (2), and final discharging in atmospheric conditions to give functionalized and hydroxylated/protonated SWCNT (3). Reproduced from ref 182. Copyright 2013 American Chemical Society.

reactive than the more highly charged parent fulleride ($\text{C}_{60}^{(n+1)-}$); since functionalized fullerides have lower symmetry and more localized charges, they act as strong nucleophiles which react preferentially until the charge is exhausted.³⁴³ Some reagents with particularly high reduction potentials are known to react with nanotube,^{87,143,367,368} most notably alkyl chlorides (ca. -2.8 to -3.1 V vs SHE,³⁶⁹ greater than sodium, -2.71 V), which are unlikely to undergo direct reduction from the CCN, indicating that the current understanding of the grafting mechanism is incomplete.

The dimensionality of the nanocarbon influences the degree of functionalization; the higher curvature of 1d SWCNTs versus the 2d nanocarbons leads to higher levels of functionalization;³⁷⁰ smaller diameter, more highly strained nanotubides also show greater reactivity.³⁷¹ The degree of exfoliation and hence assessable surface area is also important, as illustrated by the relatively low degrees of functionalization of GICs³⁷² compared to graphenide.¹⁸⁶

In addition to these electronic effects, steric interactions can affect the degree of functionalization; more hindered functionalities lead to lower grafting densities.³⁷³ Even for linear reagents, the grafting ratio depends on length down to very short alkyl chains.¹⁴³ However, the locus of functionalization is not well-understood, and local interactions may well influence the overall degree of grafting. Deng et al.³⁶⁰ proposed that during reductive functionalization, grafting is more favorable near a pre-existing sp^3 site (e.g., defects and previous grafting sites), which can cause banding as functionalization proceeds (Figure 30). Interestingly, this propagation mechanism mirrors that of fluorination occurring adjacent to previously formed sp^3 sites of both graphene³⁷⁴ and nanotubes.³⁷⁵ However, their density functional theory (DFT) calculations indicated that charge localization is only significant for carbons ortho to the sp^3 site, which are easily sterically

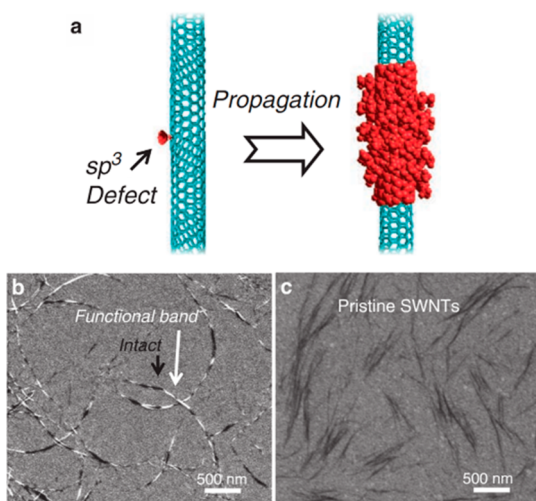


Figure 30. (a) Schematic illustration of reaction propagation initiated at sp^3 defect centers that propagate along tubular direction creating sp^3 bands of functional groups. (b) SEM of functionalized SWCNTs showing functionalized bands as bright regions along the SWCNT and (c) SEM of pristine SWCNTs. Adapted with permission from ref 360. Copyright 2011 Springer Nature.

blocked by even small species, preventing the preferential grafting. Similar trends have been observed during hydrogenation of negatively charged FLGs,¹³⁶ with preferential grafting alpha to the pre-existing defects/edges; however single-layer graphene showed homogeneous coverage.

Larger species, especially polymers, cannot attach closely on the carbon framework due to the large steric bulk of the backbone; the intergrafting distances have been modeled on de Gennes' theory of polymers adhered to surfaces.³⁷⁶ Here, well-spaced polymers coil into a "mushroom" conformation, while more densely grafted polymers have to behave in a "brush" manner, extending away from the surface. The transition between the two states occurs when the locus of functionalization is closer than the (molecular weight dependent) solvated radius of the mushroom state. In a so-called "graft-to" reaction, where presynthesized polymer molecules are attached iteratively onto the graphene/nanotube surface (which may be modeled as random sequential adsorptions), the exclusion of adjacent grafting sites favors the mushroom regime. Conversely, in a "graft-from" reaction, the monomer is added to the end of the growing polymer chains in situ; grafting density then depends on the number of initiation sites on the carbon nanomaterial, which may be sufficiently high (and thus close) to form "brush" polymers.³³⁹ CCNs can initiate anionic graft-from polymerizations directly from the nanocarbon surface without the need to introduce specific initiating groups first. The choice of monomer however is restricted, as for traditional anionic polymerizations, by the need to avoid side reactions and stabilize the negative charge on the growing chain; vinyl^{194,340,377} and epoxide^{338,378} monomers have been used effectively. The polymerizations of vinyl groups (the most studied CCN-initiated graft-from reaction) have been shown to be a living polymerization, allowing block copolymers to be synthesized in situ.³⁷⁹ These graft-from functionalized nanocarbons show contrasting properties compared to graft-to approaches, prepared by attaching monoterminated presynthesized polymers to the

CCN. The graft-from approach has been shown to produce higher grafting ratios and higher solubilities for graphenides.³³⁹

4.4. Discharging CCNs

In many cases, CCNs must be returned to the neutral state for applications in ambient conditions and/or that require the electronic properties of the undoped nanocarbon. Ideal, simple discharging removes the reactive charges while preserving the nanocarbon framework and the associated properties, undamaged; discharging also occurs during deliberate (section 4.2) or inadvertent (vide infra) functionalization. Following deliberate functionalization of nanotube and graphenide, further residual charge typically remains to be removed (section 4.3). In all cases, SWCNT and graphenide solutions typically begin to reaggregate upon discharging.⁶³ Most commonly, CCNs are discharged by exposure to ambient conditions, although a number of other strategies have been explored. Reactions with ambient water may evolve hydrogen, producing alkali metal hydroxide as a byproduct,¹⁵¹ which is easily removed by washing. Similarly, the fullerides and fullereniums discharge upon exposure to oxygen, with the residual charge(s) electronically oxidized/reduced returning the neutral, undamaged fullerene.^{381,382} The singly charged C_{60}^- may discharge slowly in the presence of oxygen, with the kinetics dependent on the counterion and solvent³⁸³ (notably, trace water catalyzes discharge) and, consequently, pseudo-stable C_{60}^- solutions may be created by adding additional reducing agent as a buffer.¹⁷¹ Interestingly, C_{60}^- is stable in the presence of (deoxygenated) water, as its basicity is low, although higher charged fullerenes will protonate and discharge completely as the single charge on the intermediate $H_nC_{60}^-$ is sufficiently nucleophilic for water reactivity, as discussed previously (section 4.3).

In the majority of studies, CCNs discharged in ambient atmosphere/pure oxygen are found to have excellent properties, with negligible or only minor damage reported, as judged by Raman spectroscopy^{122,143} and X-ray photoelectron spectroscopy.¹⁹⁶ However, it has long been known that charged nanocarbons, particularly GICs, can be hydrogenated in the presence of protic reagents, particularly at defect sites. However, the GICs have chemistry more similar to the group 1 metals than reduced molecular polyaromatics (e.g., naphthalide), with addition of water, alcohols, or ammonia leading to hydrogen evolution, while the polyaromatics anions are hydroxylated.^{136,384} More recently, there is evidence that exposure of highly charged graphenide or nanotube to air can introduce a proportion of oxygen-containing functional groups;^{182,309,316} one proposed mechanism proceeds via a superoxide intermediate (Figure 31). Since the effect is not consistently identified, the extent of functionalization may depend on a variety of factors, including discharging conditions, degree of charging (redox potential), and/or initial defect concentration. For more controlled CCN discharge, re-oxidation can be performed via the addition of a chemical with a redox potential below the oxygen reduction potential, which does not degrade to nanocarbon-reactive species upon reduction, such as iodine,³⁸⁰ benzyl nitriles,³⁸⁵ and C_{60} (which produces easily discharged fullerides³⁸⁰). These approaches remove excess charge to produce stable products that can easily be washed from the sample, minimizing possible functionalization reactions. This pure reoxidation of the anionic CCNs relates to their use as reducing agents; in

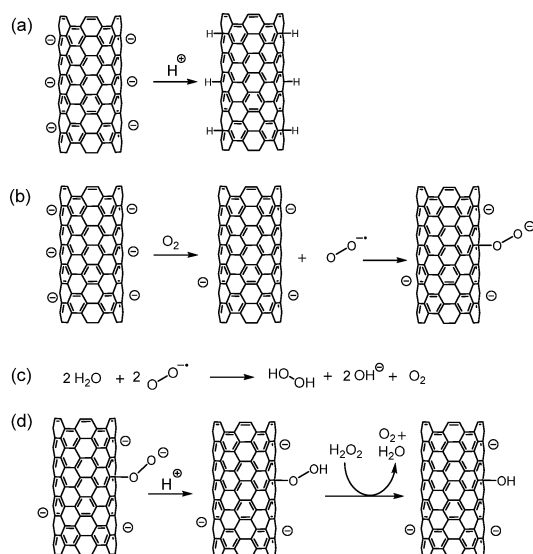


Figure 31. Possible routes to functionalization during the discharging of nanotubide in air proposed by Hof et al.¹⁸² (a) Protonation of nanotubide with protic solvent, (b) reaction of nanotubide with oxygen to form reactive superoxide, (c) generation of peroxide from superoxide in the presence of water, and (d) hydroxylation of nanotubes from superoxide-functionalized SWCNTs.

particular, the stage-1 GIC KC_8 has long been used in organic chemistry³⁸⁶ and is commonly used to this day.^{387–389}

The reduction potential of the GIC can be tuned through its metal/carbon stoichiometry,¹⁵¹ although the most highly reducing KC_8 product is most commonly applied. The continuously variable redox characteristics of nanotubides and graphenides have been more recently exploited to reduce organometallic complexes and metal salts to metallic nanoparticles; the added charge shifts the position of the nanocarbon in the electrochemical series (Figure 32), allowing it to reduce a wider range of metallic precursors. Conversely,

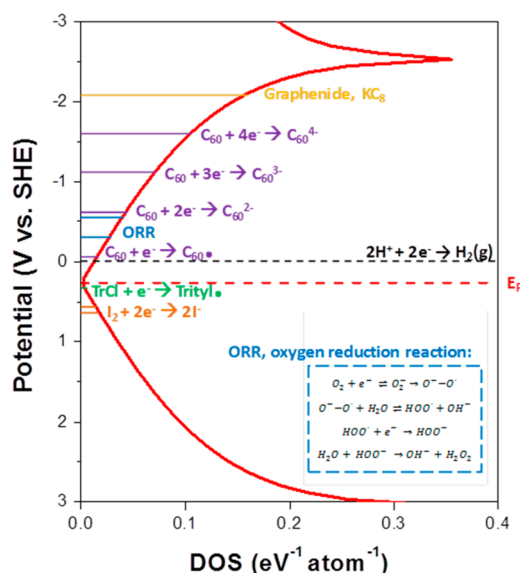


Figure 32. Band structure of graphene with energies of redox couples of materials which can act as discharging agents. Reproduced with permission from ref 380. Copyright 2017 The Royal Society of Chemistry.

the yield of metal nanoparticles can be used to estimate the effective redox potential of the CCN.^{390,391} The fullerides offer a more conventional redox chemistry based on their molecular orbitals and discrete localized reaction sites. Hence, the reaction of alkyl-fulleride with certain organometallic complexes may form covalent metal-fullerene bonds rather than crystalline metallic nanoparticles.³⁹² Analogous covalent bonds between metal atoms and the basal plane of SWCNTs or graphene have not yet been identified. The more conventional coordination of metal atoms at oxygen-containing defects is well-established, and recently, covalent metal–graphene edge bonds have been demonstrated,³⁹³ although neither approach requires a CCN precursor.

Residual charge may also be removed potentiostatically, as illustrated by the stable cyclic voltammetry of CCNs, allowing the Fermi level to be set to any potential including the undoped state; potentiostatic discharging in this manner has been demonstrated for all formally charged CCNs: graphenide,⁴² nanotubide,⁶³ nanotubium,²²⁸ fulleride,⁴⁰ and fullerenium.⁴⁰

Superacid dispersed nanocarbons can be discharged through the addition of water by dilution of the associated protons. While it is claimed that the removal of these protons does not damage the sp^2 structure of the nanomaterial,³¹⁰ residual doping effects remain,³⁹⁴ implying that the underlying structure has been altered, possibly due to oxidation as seen for fullerenes,²²⁵ or that some superacid remains.

5. BEHAVIOR OF CCN SOLUTIONS

5.1. Polyelectrolyte Theory

One approach to modeling solubility of (the nonfullerene) CCNs, particularly nanotubide, is through an adaption of DLVO (Derjaguin–Landau–Verwey–Overbeek) colloid theory.³⁹⁵ In this model, colloids avoid agglomeration due to van der Waals attractions through formation of a classic Stern electrical double layer against the inherently charged colloid surface (Figure 33). The double layer consists of counterions (as point charges) in a surface-bound Helmholtz layer and a diffuse Gouy–Chapman layer, causing a charge field which dissipates at increasing distances from the colloid due to

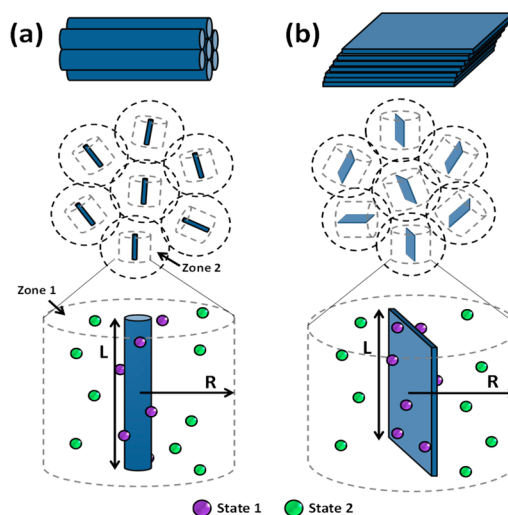


Figure 33. A Schematic representation of Oosawa-Manning two-state model of (a) rigid rods and (b) platelets.

screening from the increasing volume of electrolyte. For an independent species in solution, the distance required to screen the surface charge is characterized by the Debye length (eq 1), which is inversely related to the ionic strength (eq 2) of the electrolyte. When the fields of two colloids in solution overlap (i.e., distance $< 2\lambda_D$ for identical colloids), they electrostatically repel. DVLO theory combines the electrostatic repulsion with the (geometrically dependent) van der Waals attraction to calculate the net interaction between the two particles in solution.

Debye length (λ_D), solvent dielectric constant (ϵ_r), permittivity of free space (ϵ_0), Boltzmann constant (k_B), absolute temperature (T), Avogadro's constant (N_A), elementary charge (e), and electrolyte ionic strength (I).

$$\lambda_D = \sqrt{\frac{\epsilon_r \epsilon_0 k_B T}{2 N_A e^2 I}} \quad (1)$$

Ionic strength (I), concentration of ionic species i (c_i), and charge of ionic species i (z_i). For a monocharged electrolyte solution, ionic strength is equal to the salt concentration (in molecules/m³).

$$I = \frac{1}{2} \sum_i c_i z_i^2 \quad (2)$$

The model can be expanded by incorporating polyelectrolyte counterion condensation as modeled by Ooawa-Manning (OM) theory.³⁹⁶ When the colloid in question is a polyelectrolyte (polymeric species with regular ionic functional groups along the backbone) and is placed in a solvent, it dissociates into a polyion and solvated counterions: the charge on the polyion after dissociation replaces the electrical potential difference from colloid/electrolyte interactions of DVLO theory. If the charge on the backbone is too concentrated, counterions from the electrolyte condense into the Helmholtz layer of the polyelectrolyte to decrease electrostatic repulsions. Such counterion condensation will occur until the distances between unscreened charges (l_{charge}) on the polyion decreases to match the separation of two like-charges in the solvent from purely thermal effects: the so-called Bjerrum length (eq 3). The Bjerrum length can be decreased by increasing temperature or selecting a solvent with a higher dielectric constant. The polyion here is modeled as infinitely thin and linear, with l_{charge} equal to the charges per chain divided by the chain length. Even though charges are physically localized in polyelectrolytes to their dissociated ionic functional groups, charges are modeled as evenly dispersed along the polyion.³⁹⁷

Bjerrum length (l_B), elementary charge (e), solvent dielectric constant (ϵ_r), permittivity of free space (ϵ_0), Boltzmann constant (k_B), and absolute temperature (T).

$$l_B = \frac{e^2}{4\pi\epsilon_r\epsilon_0 k_B T} \quad (3)$$

5.2. Polyelectrolyte Theory for CCNs

The application of DLVO/OM theory to CCNs and their solutions was pioneered by Pénicaud, originally postulated alongside the first spontaneous dissolution of nanotube,¹⁹² with a formal model³⁹⁸ and application to graphene²⁹⁰ demonstrated later. When using these models, the differences

between classic polyelectrolytes and CCNs must be considered.

The one-dimensional character of SWCNTs allows them to be considered as (semi)rigid polyelectrolytes; however, the charge is delocalised over a π cloud, rather than localized on specific groups. The delocalization gives a physical basis for the continuum of possible l_{charge} values proposed in OM theory, allowing counterions to condense at any location along the surface. However, SWCNTs/graphenes do not act as infinitely thin chains (diameter effects are known to be significant for nanotube dissolution^{64,400}) and can instead be treated as surfaces with uniform charge density.¹⁹² Acid-oxidized and some other functionalized nanocarbons, including GO, do have charges limited to dissociating functional groups, more directly akin to classic polyelectrolytes.⁴⁰¹

As a CCN is charged, one electron is added with each added counterion, increasing charge density; eventually as the average backbone charge spacing become closer than the Bjerrum length, screening occurs by condensation. At higher charging ratios, with increasing charge condensation, additional charge increases the ionic strength of the electrolyte, decreasing the Debye length without increasing Coulombic repulsion between the CCNs, leading to agglomeration and precipitation ("salting-out"). This tendency is likely to depend on the effective "lattice energy" of the agglomerated form and hence to be increased for purer, more homogeneous samples, which can pack more efficiently. Due to this effect, in high charging regimes, increasing the charge does not increase solubility, instead first causing plateau and eventually a decrease in CCN concentration³⁹⁸ (Figure 34). The same precipitation can be induced by adding a separate salt to increase ionic strength without altering CCN charge.

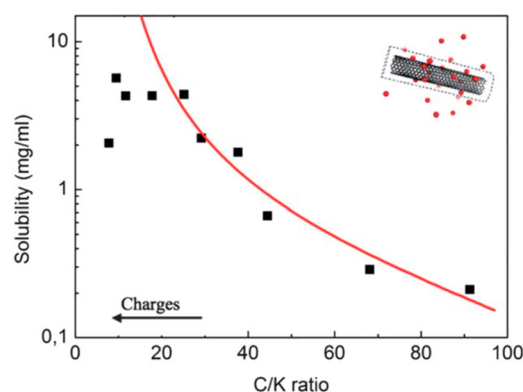


Figure 34. Solubility of nanotube versus charge ratio (black squares experimental data and red line polyelectrolyte model). Adapted with permission from ref 398. Copyright 2011 The Royal Society of Chemistry.

A similar dependence on metal stoichiometry can be observed during reductive functionalization of graphene³⁰¹ and nanotube;^{143,402} during the reaction, charge is depleted, gradually decreasing the electrostatic repulsion of the nanomaterials. Once insufficient to overcome the van der Waals attractive forces, nanomaterials will begin to aggregate, limiting subsequent functionalization to the exterior of the agglomerate. High degrees of charging increase counterion concentration (which remains constant throughout the reaction) and accelerate the aggregation; however, using a low degree of charge limits both the dissolution and reactive charge available,

also reducing the degree of functionalization (section 4.2). Thus, an intermediate stoichiometry is required to balance sufficient charge and excessive salting out. Much of the early literature used very high concentrations of alkali metal, assuming that excess charge would be beneficial; however, these compositions lie far beyond the optimum stoichiometry. When optimizing grafting conditions, subsequent work focused on the metal (or charge) to carbon ratio;^{348,359,403} however, since the salting out is driven by the counterions, their concentration should be the controlling parameter. A consistent intermediate absolute counterion concentration^{143,301} (12.5 mM for Na with SWCNTs, 25 mM for Na with GICs) was found to optimize the grafting ratio at all nanocarbon concentrations. Although the underlying theory requires further study, the different optimums can be tentatively assigned to geometric effects, both in terms of dimensionality and the access to either one or two surfaces. As more highly charged CCNs still facilitate higher degrees of functionalization, the total degree of grafting may be increased by raising the charge stoichiometry while increasing dilution.

There is debate over the thermodynamic driving force for the spontaneous dissolution of nanotubide. Voiry et al.³⁹⁸ proposed that the systems are driven entropically by counterion solvation, balanced by OM condensation, overcoming the energy cost of forming enthalpically unfavorable solvent-nanotubide interactions. This hypothesis attributes the observed preferential dissolution of wider diameter SWCNTs at low charge ratios to the increased external area of the SWCNTs; other groups have attributed this phenomenon to electronic effects (section 6.1). It is likely that the specific free energies will vary between CCN salts (as they do for classic simple ionic salts⁴⁰⁴ and polyelectrolytes⁴⁰⁵), and both enthalpically and entropically driven dissolution may be possible in differing systems; further work is needed to elucidate the underlying physical chemistry.

DVLO and OM theories model counterions as point charges which, while usually appropriate for atomic metal cations, fail to address the steric effects of bulky counterions (Figure 35) which can have a significant role on the system. Chelated counterions (often with crown ethers for group 1 metal) are sterically hindered from condensation to the Helmholtz layer.⁴⁰⁶ By forcing counterions into the diffuse layer (and likely by reducing lattice enthalpy of the corresponding CCN salt), the stability of the dissociated, dissolved salt is favored, allowing higher concentration solutions to be formed with higher net surface charge. A similar effect is seen for both donor-^{399,407} and acceptor-type^{307,408} GICs, with expansion from coating/chelating the intercalated counterions increasing the separation between the layers and facilitating exfoliation.

The validity of DVLO and OM theories to describe nanoparticle (as opposed to micron scale particle) dispersions has recently been called into question.⁴⁰⁹ In particular, it has been noted that local solvent ordering effects become increasingly important for smaller particle dimensions, for which CCNs are limiting examples in 0, 1, and 2 dimensions. Most importantly, in this regime, the solvent can no longer be considered as a uniform density continuum described by a single dielectric constant. For example, the arrangement of the solvating ammonia molecules around fullerides has been measured, in detail, using advanced neutron scattering methods.^{291,297} Notably, the solvent shells were found to be up to four times the density of the bulk solvent; similarly, dense solvation shells have been measured for a range of other

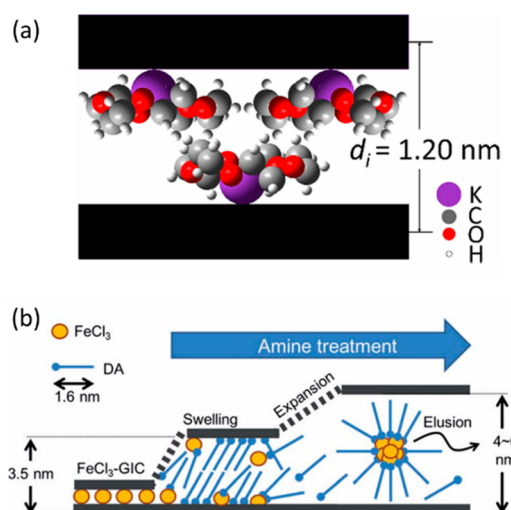


Figure 35. (a) Schematic diagram of the intercalate bilayer arrangement in KC_8 where potassium cations are chelated by 15-crown-5. Reproduced from ref 399. Copyright 2016 American Chemical Society (b) Schematic of increase in GIC interlayer distance upon coating of FeCl_3 intercalant with dodecylamine (DA). Reproduced with permission from ref 307. Copyright 2014 The Royal Society of Chemistry.

nanoparticles in different solvents.⁴¹⁰ Furthermore, for the fulleride dispersions, the polar moment of the solvating ammonia molecules did not point toward the C_{60} anions, rather tangentially with only one H atom per ammonia molecule directed to the fullerides.^{291,297} This counterintuitive arrangement enables the ammonia molecules within the solvation shells to maintain the hydrogen-bonding arrangement found in bulk ammonia.⁴¹¹ Thus, the factors associated with the local solvent ordering, including steric effects, hydrogen bonding, and charge-screening have been shown to be intrinsically interlinked. These observations question the effectiveness of additive models, such as DVLO and OM for understanding CCN solutions, which perhaps are more analogous to solutions of simple salts, for which dissolution is driven by a free energy gain upon solvation/solvent ordering. In such a molecular model, at the highest degrees of charging, the free energy associated with forming the CCN salt lattice becomes greater than the free energy gain upon dissolution, leading to the observed loss of CCN solubility.⁶⁴

5.3. Liquid Crystals

Due to the high aspect ratios of both SWCNTs and graphene, sufficiently high concentrations, in principle, allow the formation of lyotropic (solvent-based) liquid crystal (LC) phases.⁴¹³ While some functionalized fullerenes can form high aspect ratio aggregates and subsequently LC mesophases,^{414,415} spherically symmetric fullerenes do not shown this behavior. Under suitable conditions, anisotropic solutes can form ordered, orientated domains which remain capable of flow (unlike a gel). LC phases provide an attractive route to improve the alignment and packing of nanomaterials, in order to exploit anisotropic properties effectively. LCs of uncharged SWCNTs⁴¹⁶ and graphene⁴¹⁷ dispersions have been reviewed previously. Such systems are very effective for fiber and ordered film production in a wide range of contexts; applications of CCN-derived LCs are covered in section 8.

SWCNTs and graphenes can most simply be treated with Onsager's hard rod and rigid platelet models⁴¹⁸ which predict

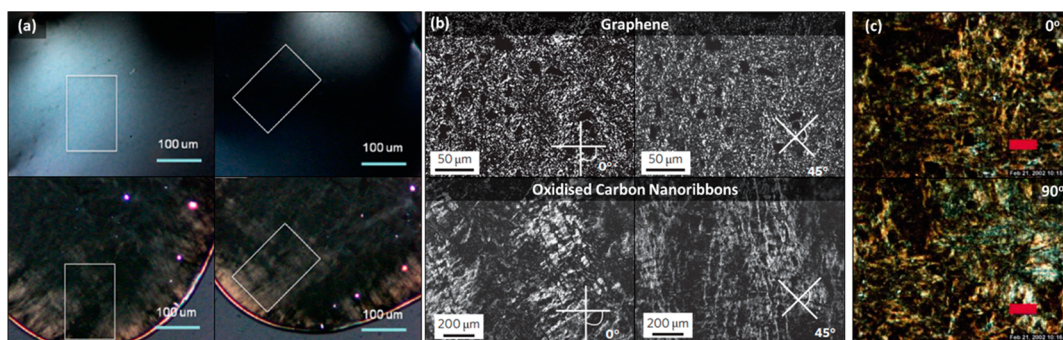


Figure 36. Polarized optical micrographs of LC phases of CCNs. (a) HiPco nanotubide at 3.8 mg/mL (top) and 4.4 mg/mL with 20 mg/mL crown ether (bottom). Polarization rotated to 0° (left) and 45° (right). Reproduced with permission from ref 406. Copyright 2013 American Chemical Society. (b) Graphene (top) and oxidized GNR (bottom) at ca. 2 wt % in chlorosulfonic acid. Adapted with permission from ref 141. Copyright 2010 Springer Nature. (c) SWCNTs (4 wt %) in 102% H₂SO₄, showing brightness change under rotation of polarization. Scale bar 250 μm. Adapted from ref 412. Copyright 2004 American Chemical Society.

that as concentration of an isotropic phase increases, there is a penalty to translational entropy due to volume exclusion. By forming a liquid crystal phase, there is a marked gain to translational entropy at the cost of orientation freedom; a concentration exists where these two factors equate, above which the LC phase forms.⁴¹⁹ The transition from isotropic to liquid crystal typically occurs across a concentration range in which both phases coexist; thus, there are usually two phase transition concentration boundaries: isotropic to biphasic and biphasic to LC.

If nanotubes are treated as monodisperse rigid rods of length L and diameter D , the biphasic regime occurs above a volume fraction of $\phi_{\text{SWCNT}} = 3.3 D/L$, and a pure nematic phase (ordered in one axis) occurs at $\phi_{\text{SWCNT}} > 4.5 D/L$. The diameter should take into account the effective thickness of any stabilizing surfactant or electrostatic repulsion. Typical boundary values for surfactant-dispersed SWCNTs are ca. 3 wt % and ca. 5 wt %, respectively.⁴²⁰ Superacid dispersed SWCNTs exhibit LC transitions at notably lower concentrations (Figure 36), with the discrepancy attributed to the longer nanotube lengths in the unsonicated solution, length polydispersity, and the presence of short-range repulsion and long-range attractions.³¹⁰ In highly polydisperse systems, a larger biphasic window exists with a lower concentration threshold. Within the biphasic regime, thermodynamically, the nematic phase will contain straighter and larger aspect ratio nanotubes,¹⁴⁵ although due to the slower diffusion kinetics of long nanotubes, the nematic phase initially consists of short nanotubes;¹⁴⁵ this length selectivity can allow for separation and reduction in length dispersity, at least in MWCNTs.⁴²¹

The short-range repulsion of charged SWCNTs is critical for LC formation. If there is insufficient charge, agglomeration will limit the solutions to the isotropic phase (Figure 37). As such, increasing the nanomaterial surface charge (through increasing reduction stoichiometry³⁰⁰ or reducing pK_a of a solubilizing superacid³¹²) not only enables the formation of LC phases but also increases the concentration window of the monophasic LC phase. At insufficient pK_a in superacid, a different phase (the so-called “crystal-solvate”⁴²²) forms, with solvent molecules ordered between the aligned SWCNTs, analogously to an intercalation compound. The short-range repulsion can also be increased for reduced CCNs through chelation of the counterion (section 5.2) (Figure 36a).⁴²³ Impurities can reduce the tendency to form liquid crystals; for example, carbonaceous and catalytic impurities in SWCNT samples

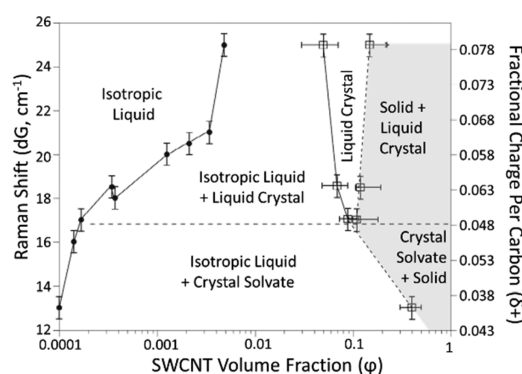


Figure 37. Phase diagram of HiPco SWCNTs in superacid of varying strength (HClSO₃/H₂SO₄ at varying ratios). Adapted with permission from ref 312. Copyright 2009 Springer Nature.

disrupt the ability to form ordered LC domains.⁴²⁰ Similarly, functionalization has been shown to disrupt the packing necessary for LC formation; even when the inherent solubility is increased, the nanomaterials remain in the isotropic phase.³¹³

Other LC phases such as smectic (stacked layers of parallel packed rods) are theorized for SWCNTs, although require higher concentrations and lower dimensional dispersity than currently demonstrated.⁴²⁴ The kinetics of LC phase formation and resulting microstructure are also highly sensitive to aspect ratio, with longer SWCNTs displaying long relaxation times and more anisotropic domains.³¹¹

Graphene dispersions can be modelled as rigid platelets⁴²⁵ of thickness t and diameter D , and treated with Onsager theory,⁴¹⁸ potentially leading to discotic-nematic (aligned faces) or columnar (parallel columns of face-on-face sheets) LC formation at a volume fraction of $\phi_{\text{graphene}} = 4 t/D$. Owing to the monatomic thickness of graphene (combined with often micron scale diameters), the required volume/weight fractions are typically lower than SWCNTs.⁴²⁶ Akin to SWCNTs, graphene polydispersity leads to deviation from the Onsager model predictions and prevents the formation of columnar LC phases common for other rigid platelets, currently limiting graphene LCs to the discotic-nematic phase.

6. SELECTIVITY

6.1. Electronic Selectivity

Carbon nanomaterials are highly heterogeneous in size and shape, intrinsic properties, and quality, all of which influence charging, functionalization, and dissolution processes selectively. In early studies on (neutral) SWCNTs, Raman spectroscopy indicated preferential reaction on m-SWCNTs compared to sc-SWCNTs, attributed to their greater electron affinity. Since the formation of CCNs inherently involves electron transfer, there is an exciting prospect of fractionating carbon nanomaterials according to electronic character. However, progress has been slow; the full picture is complex due to the number of species (both impurities and different types of SWCNTs) and competing physical processes.

It has long been understood that different SWCNT helicities, each of distinct electronic character, should become charged (and potentially therefore, dissolve or functionalize) in sequence (depending on potential). While initial results showed evidence for selectivity,^{292,427} the Raman techniques used were indicative rather than quantitative and highly sensitive to environmental effects. More recent developments have shown that significant differences are only seen for low charge regimes.^{64,400} During reduction, m-SWCNTs indeed charge first, however, between MC₁₀₀ and MC₂₀₀, the sc-SWCNTs also become charged, starting with those with larger diameters (and thus smaller bandgaps); by MC_{~30}, there is no selectivity shown.⁶⁴ In other words, although the eDOSs differ, they also overlap significantly, so that integrated charge is similar at potentials otherwise optimal for dissolution (Figure 38).

Simultaneous functionalization and charging through treatment of neutral nanocarbons with group I organometallics or Grignard reagents occurs through electron transfer from the alkyl (or equivalent) species, immediately followed by grafting of the radical formed. With SWCNTs, electron transfer is more favorable for m-SWCNTs owing to the presence of vacant low-energy states leading to preferential metallic functionalization.⁴²⁷ Small diameter nanotubes also show preferential functionalization in spite of their higher Fermi levels, attributed to their higher sp² strain from curvature.³⁷¹ Electronic⁴²⁸ and diameter selective phenomena⁴²⁹ are widely observed in SWCNT chemistry not just for nanotubide reactions. However, in general, for selective reactions, the SWCNTs should be individualized to maximize the effect; in bundles, the SWCNT with the greatest electron affinity is not necessarily the one most accessible to reagents.

In principle, although not yet explored, polydisperse samples of very small graphenes, or narrow GNRs (where electronic confinement is significant, section 2.2), should be susceptible to analogous selective electronic charging and separation. Similarly, different members of the fullerene family have different redox properties (section 7.1), with the HOMO-LUMO gap tending to decrease with increasing size.

6.2. Geometric Selectivity

In addition to electronic selectivity, it is increasingly clear that there is a geometric selectivity related to kinetic effects. One observation is that for SWCNTs reduced at low charging regimes, the spontaneously dissolved fraction typically contains short/defective SWCNTs and impurities (Figure 39). One hypothesis might be that defective materials charge more readily; however, outside the low-charge regime, the carbon to metal ratio is consistent between the (predominantly

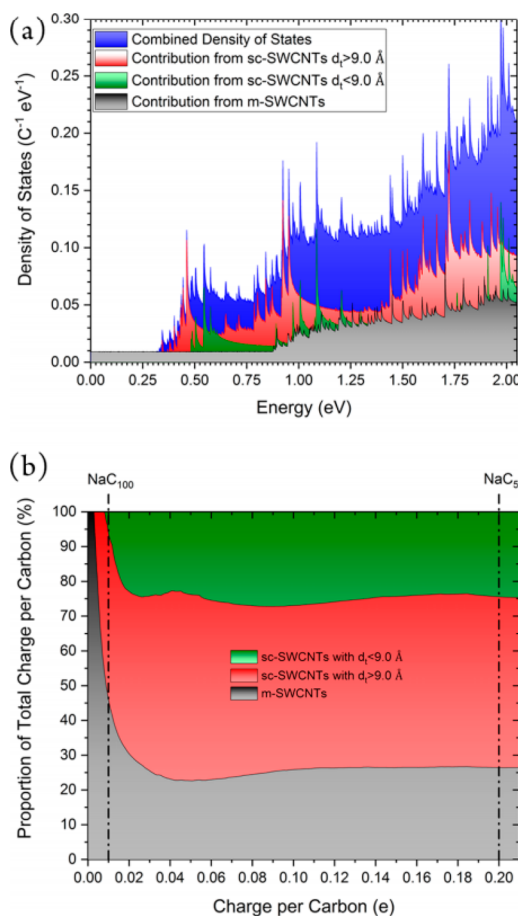


Figure 38. (a) Combined eDOS of HiPco SWCNTs (blue) separated into m-SWCNTs (gray), and small (green) and large (red) diameter sc-SWCNTs; (b) distribution of charge between SWCNT types from (a) as a function of charge per carbon. Adapted with permission from ref 64. Copyright 2017 American Chemical Society.

amorphous carbon) dissolved fraction and the undissolved SWCNTs.¹⁴³ Instead, it is thought that the size disparity between the reduced species leads to a kinetic difference between dissolution rates with smaller species (notably carbonaceous and catalytic impurities) dissolving at a faster rate.^{63,143} By separating the impurity rich solution, the SWCNTs can be purified in a less damaging manner than typical competitive oxidation/combustion purification routes.¹²² An intermediate level of charging is required for reductive purification to prevent dissolution of all species, and agitation must be avoided to maximize the influence of the different diffusion kinetics. The geometric separation is particularly sensitive to SWCNT length: entangled nanotubes may be treated as entangled rigid polymers of a given persistence length. Charged nanotubes initially form a swollen network, through which each individual nanotube must reptate (i.e., wriggle in a snakelike fashion due to Brownian motion) akin to a rigid rodlike polymer in the semi dilute regime.⁴³⁰ The reptation and diffusion rates of SWCNTs show a significant length dependence,¹⁵⁰ allowing short SWCNTs to diffuse substantially faster out of the gel-like bulk into solution.⁶³ For entangled ultralong SWCNTs (>10–100 μm) dissolution may become unfeasibly slow;³³⁹ on the other hand, longer SWCNTs are broken more easily in shear fields.^{148,149} Simple stirring of ultralong nanotubides can lead to sufficient breakage that individualized nanotubide solutions form

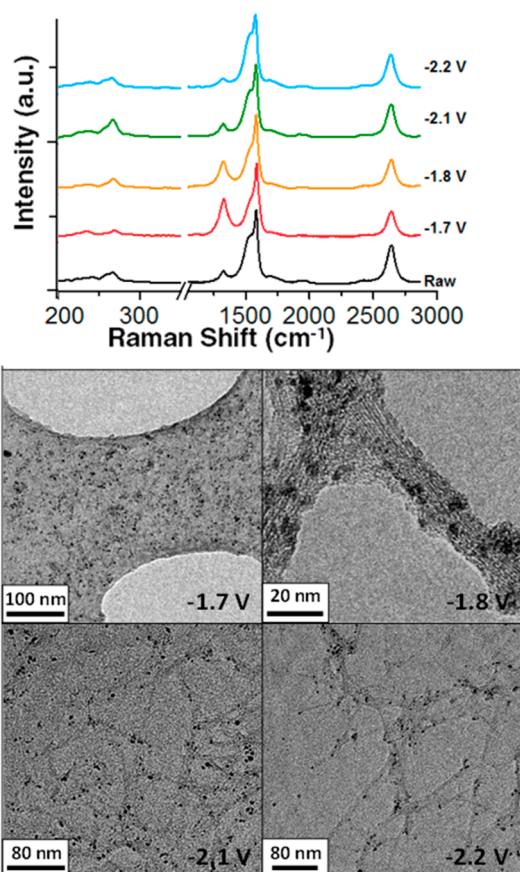


Figure 39. Sequential electrochemical dissolutions of raw HiPco SWCNT powder. (Top) Raman spectra of raw and dissolved SWCNTs at sequential reduction potentials (vs Ag/Ag⁺) showing initial dissolution of defective materials followed by dissolution of graphitic SWCNTs at high potentials. (Bottom) TEM images of selected nanotube fractions showing the preferential dissolution of metallic and carbonaceous debris (−1.6 to −2.0 V) followed by the progressive dissolution of purer individualized SWCNT material (>−2.0 V). Reproduced with permission from ref 228. Copyright 2013 Nature Springer.

conveniently, while still retaining greater lengths than conventional dispersion methods.⁸⁷ Dissolution of ultralong SWCNTs through dissociative protonation has also demonstrated individualization (albeit only at lower concentrations,³¹¹ ca. 50 ppm).

Graphite shows geometric selectivity upon dissolution, with smaller flakes dissolving preferentially through both reductive²⁹⁰ and dissociative protonation¹⁴¹ routes. It is currently unclear whether this selectivity is due to inherent solubility, the kinetics of intercalation, fragmentation during dissolution (akin to breaking of ultralong SWCNTs), or the increased statistical likelihood of larger flakes containing interlayer bonds preventing exfoliation.

7. REDOX CHEMISTRY OF OTHER NANOMATERIALS

7.1. Further Carbon-Based Nanomaterials

In addition to the C₆₀, SWCNT, and graphene systems discussed in depth here, the CCN chemistries can be applied to a large variety of other carbon nanomaterials of all dimensionalities. The higher fullerenes (C₇₀, C₇₆, C₇₈, etc.) have both lower-lying LUMOs and higher HOMOs than C₆₀, which broadly decrease/increase, respectively, with increasing

size, making them susceptible to the same fulleride and fullerene chemistries as buckminsterfullerene itself.¹⁷¹ Uncharged multiwalled fullerenes (aka nano onions) are intrinsically insoluble⁴³³ but have been shown to spontaneously form solutions upon reduction, in addition to facilitating reductive functionalization.⁴³⁴ Multiwalled fullerenes are, however, comparatively unstudied versus other carbon nanomaterials, particularly with regard to their charged forms.

MWCNTs are known to act similarly to SWCNTs in terms of reductive dissolution⁴³⁵ and functionalization.^{349,436} However, in addition to the intertube bundle intercalation found for SWCNTs, intercalation can occur between the walls of MWCNTs. These interwall-intercalated compounds can subsequently unzip through longitudinal splitting to form GNRs^{437,438} with well-defined, straight edges. The negative charge on the GNR is thought to be localized at the newly formed edge and can be used for subsequent reductive functionalization with alkyl halides¹⁸⁵ or anionic polymerizations.⁴³⁹ Application of CCN chemistries to presynthesized GNRs has not been reported to date; however, as studies have indicated that GNR solubility is poor without edge functionalization,⁴⁴⁰ there is clearly scope for investigation. The use of superacids allows MWCNTs (of lengths up to 0.5 mm) to be dissolved at sufficient concentrations to form LC domains.³¹¹ The use of strong acids with MWCNTs may lead to intercalation between the walls^{441,442} which, akin to the reduced MWCNTs, can be used for subsequent unzipping to form ribbons, here through the addition of an oxidizing agent. However, so far, this process appears to be lower in yield and substantially more damaging than the reductive approach, forming graphene oxide nanoribbons;⁴⁴³ these GO nanoribbons may also subsequently be dispersed through associative protonation with chlorosulfonic acid.⁴⁴⁴

Carbon nanofibers (CNFs) consist of (pseudo-)2d nanocarbons of submicron lateral dimensions, stacked in a variety of orientations. While the general behaviors can be described, the electronic character and resulting solvation depend on the constituent material quality and size. CNFs of sufficiently graphitic stacked platelets and full-core stacked nanocones act analogously to graphite: intercalation with excess potassium yields stage-1 stoichiometry with hybridized carbon/potassium states but differing work functions⁴⁴⁵ to graphite-derived KC₈. By adjusting the stoichiometry, other staged compounds can be formed with specific reduction potentials.⁴⁴⁶ Donor-intercalated stacked platelets can be subsequently exfoliated to their constituent graphitic platelets through discharging in protic media⁴⁴⁷ (although predominantly few-layered nanoplatelets are formed and defects are introduced) or stirring in aprotic polar solvents⁴³¹ (Figure 40). Pre-exfoliated few-layer graphene platelets are also easily manipulated by the CCN processing routes.³⁷⁰ Conversely, while hollow-core stacked nanocones have shown exfoliation and functionalization using reductive processes,⁴⁴⁸ the defined, staged intercalated species have not been isolated.

Single-walled nanocones⁴⁴⁹ with lengths ca. 50 nm and diameter ca. 5 nm (often referred to as carbon nanohorns) do not stack like the majority of graphitic nanocarbons and instead are typically found as agglomerates in nanoscale clusters, labeled “dahlias”.⁴⁵⁰ In spite of the structural differences, these dahlias act analogously to the CCNs in terms of reduction routes,⁴⁵¹ spontaneous solubility⁴³² (Figure 41), and subsequent reductive functionalization with alkyl halides,⁴³² albeit with notably lower stoichiometry of charge

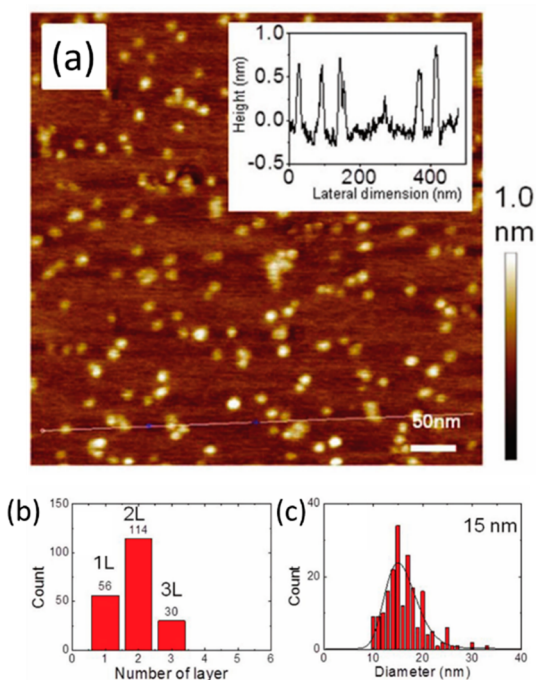


Figure 40. Graphene nanoplatelets exfoliated from CNF. (a) AFM and height profile, (b) number of layers from height distribution, and (c) lateral size distribution using log-normal fit. Adapted with permission from ref 431. Copyright 2016 The Royal Society of Chemistry.

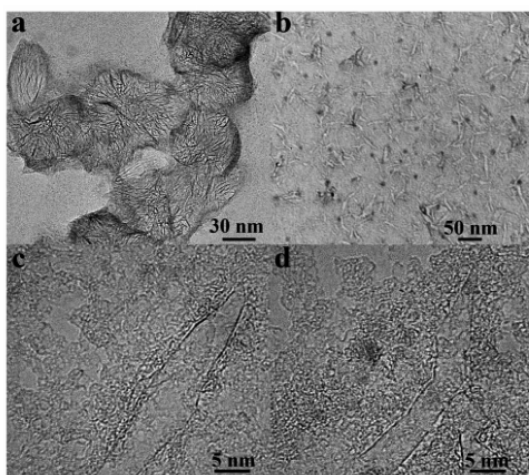


Figure 41. TEM of (a) as received and (b–d) reductively exfoliated single-walled nanocones (nanohorns). Reproduced with permission from ref 432. Copyright 2015 The Royal Society of Chemistry.

transfer at saturation compared to other nanocarbons.⁴⁵¹ Dissolution in superacids to individual, unclustered species has also been demonstrated;⁴⁵² however, the reported residual p-doping is consistent with retained acid or oxidative damage. Reversible oxidative doping is possible with Lewis acids,⁴⁵³ increasing electrical conductivity, as observed for the other carbon nanomaterials, although exfoliation of Lewis acid doped dahlia to individualized nanocones has not been shown.

While some sp^3 -rich carbon materials, notably carbon black,^{370,454} are susceptible to reductive CCN processing, more crystalline and defined materials (e.g., nanodiamond, diamond-like carbon) have not been charged, outside electro-

chemical analyses.^{455,456} Regardless, the comparative ease of functionalizing,^{457,458} and dissolving^{459,460} these materials by established routes, compared to the graphitic nanocarbons, limits the immediate appeal of CCN chemistries.

In addition to extrinsic charging sources, carbon nanomaterials can be doped through heteroatom substitution in the atomic framework, most commonly nitrogen: the synthesis, properties, and applications of heteroatom-doped carbon nanomaterials have been reviewed extensively previously.^{217,461,462} The shift in Fermi energy from this approach is mild in comparison to CCNs and is typically introduced for use in electronic and catalytic applications. Heteroatom doping in graphitic systems is typically limited to a few atom percent; however, other specific phases are known. For example, graphitic sp^2 -hybridized carbon nitrides (gCN) of the general form C_3N_4 can exist as 2d sheets, involving linked heptazine or triazine units, which can form well-defined intralayer pores. Intercalation of these compounds is well-established, including with group 1 metals;^{463,464} however, exfoliation of gCN donor-intercalation compounds has to-date relied on sonication in water, leading to severe damage and poor monolayer levels. Conversely, the smaller (sub-100 nm laterally), more crystalline PTI sheets are comparatively simple to process, spontaneously dissolving without charging as predominantly 8–9 layered species;⁴⁶⁵ very recently, CCN chemistries have been shown to increase exfoliation to predominantly 2–3 layers at >30% yield, and allow functionalisation, under similar conditions to graphenides.⁴⁶⁶

Lastly, although not yet demonstrated, there are new carbon allotropes that are expected to be susceptible to the same (electro)chemical methodologies as the other graphitic carbon nanomaterials. Examples include newly synthesized structures (e.g., the sp/sp^2 polyhexaethynylbenzene “graphdiyne”⁴⁶⁷ and sp^2 ringed, doughnut-like nanotorus⁴⁶⁸) and others that are predicted to be stable but which have not yet been prepared (e.g., the sp^2 haeckelites and schwartzite, and the sp/sp^2 graphyne¹⁸).

7.2. Non-Carbon Nanomaterials

There is potential for the techniques and chemistries of CCNs to be applied to noncarbon nanomaterials. The general principles of nanomaterial charging are quite simple: first, the bulk material should consist of discrete nanomaterials held together by noncovalent interactions. For chemical charging, there must be an accessible LUMO/vacant state(s) at a lower energy than the potential of an available reductant, or a HOMO/occupied state(s) above the oxidation potential of an available oxidant. For electrochemical charging, the relevant HOMO/LUMO levels must lie within an available electrolyte stability window. In addition, the discrete, charged species should exist as a stable state (both intrinsically, and in any solvating medium) when the bond order has been altered by the electronic doping, but the atomic connectivity is retained and covalent reactions with the medium are avoided. The number of electronic states that reside between the Fermi level and maximum charged potential will influence the final charge density, and hence whether the individualized species will overcome inter-nanoparticle attractions leading to dissolution. The choice of counterion may also affect solubility, with $z > 1$ ions such as SO_4^{2-} leading to greater ionic strength in the solutions (eq 2), increasing both charge screening and the lattice energy of the nanoion/counterion salt.

It has been estimated that there are 1825 bulk two-dimensional (2d) crystals similar to graphite that can be exfoliated to single layers.⁴⁷⁰ The transition metal dichalcogenides (TMDs) form one particularly notably family, comprising various combinations of transition metals and chalcogens (S, Se, and Te) with a large variety of composition-dependent properties.^{470–472} Analogous to their carbon counterparts, the TMDs bulk crystals possess strong interlayer van der Waals interactions and may be intercalated (Figure 42) to form TMD

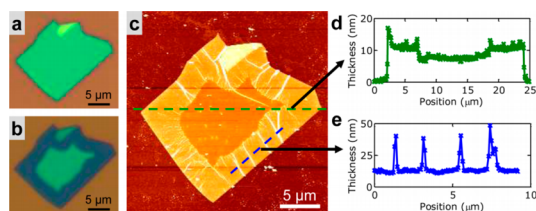


Figure 42. Lithium intercalation of MoS₂ sheets. (a and b) Optical images showing intercalation proceeding from the edge. (c) AFM micrograph with height profiles (d and e) showing increased height in intercalated region and strain-induced sheet wrinkling. Reproduced from ref 469. Copyright 2015 American Chemical Society.

intercalation compounds (TMDICs) via the GIC synthetic routes, including the use of direct metal,⁴⁷³ organometallics,⁴⁷⁴ organic electron carriers, and electrochemistry.⁴⁷⁵ The TMDICs themselves can show interesting properties such as added superconductivity⁴⁷⁶ and pressure dependent electronic character.⁴⁷⁷ A full summary of the TMDICs is outside the scope of this review but are often created with the aim of exfoliation, most commonly through addition to water;^{473,474} however, akin to GIC/water exfoliation, the recovered material is often highly defective. More recently, Birch reduction (metal/ammonia) of TMDs has shown to form TMDICs that are spontaneously soluble in aprotic polar solvents (Figure 43) for a large array of TMDs.³⁰³ A range of other (non-TMD) 2d layers may also be exfoliated from their bulk crystals through reduction and exfoliation, including Bi₂Te₃, V₂O₅, Sb₂Te₃, and GaTe.³⁰³ Alternatively, acceptor-type TMDICs can be formed through the use of Lewis base intercalants, which show exfoliation upon intercalant substitution of iteratively bulkier Lewis bases to separate layers⁴⁷⁸ (similarly to the GICs,⁴² Section 3.4.2). Some TMDs can be synthesized as fullerenes or nanotubes with potentially useful properties (e.g., WS₂ nanotubes show promising mechanical properties) (ca. 16 GPa tensile strength with a ductile failure,⁴⁷⁹ outperforming CNTs in certain composites,⁴⁸⁰ while WS₂ fullerenes are effective solid lubricants⁴⁸¹); however, current processing has been limited to classic shear approaches.⁴⁸² In the future, charge-based processing routes could be applied to other TMD nanotubes/fullerenes.

Boron nitride (BN) nanomaterials are structurally analogous to the carbon nanomaterials forming graphene-like hexagonal lattices (h-BN) and nanotubes (BNNTs). In stark contrast to the carbon nanomaterials (and most TMDs), the band gaps of BN nanomaterials are large⁴⁸³ (5.2 eV for h-BN, 4 eV for BNNTs with diameters ≥ 1.2 nm), leading to electrically insulating materials less susceptible to direct doping. Intercalation of h-BN with potassium⁴⁸⁴ and lithium⁴⁸⁵ is possible; however, charge transfer from the metal to the BN is negligible. The reduction (with sodium naphthalide) and functionalization of BNNTs has recently been reported⁴⁸⁶ and

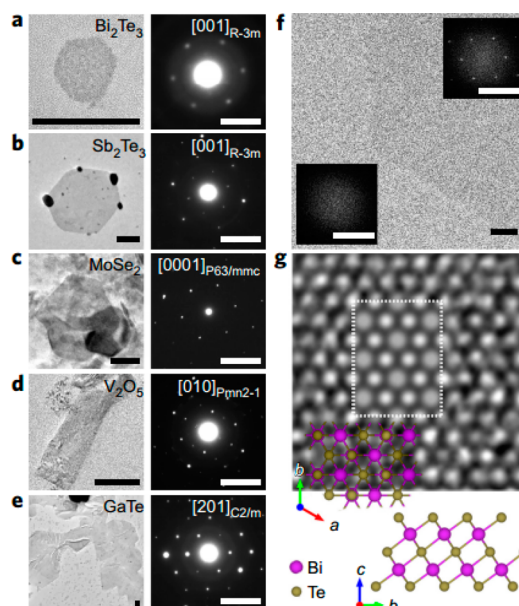


Figure 43. Dissolved TMD nanosheets. (a–e) TEM micrographs of (a) Bi₂Te₃, (b) Sb₂Te₃, (c) MoSe₂, (d) V₂O₅, and (e) GaTe nanosheets, alongside their corresponding diffraction patterns marked with in-plane orientation and space groups for each structure (TEM scale bars, 100 nm; diffraction scale bars, 5 nm^{−1}). (f) The 120° facet of a Bi₂Te₃ single layer (scale bar, 10 nm) which is confirmed with fast Fourier transform data (scale bars 5 nm^{−1}) from inside the hexagon and the carbon support. (g) High-resolution electron micrograph showing the atomic structure in (f) overlaid with image simulation (in dashed rectangle) and the in-plane structural model of Bi (purple) and Te (gold) atoms for a monolayer of Bi₂Te₃. Also shown is the structural model for the single layer perpendicular to the sheets. Adapted with permission from ref 303. Copyright 2017 Nature Springer.

may proceed via localized charges, in contrast to the delocalized charges in the nanocarbon systems. Carbon doping of BNNTs is known to introduce easily accessible bands as a new LUMO,⁴⁸⁷ providing a route to potentially charge separate carbon-doped BNNTs.

Multiwalled BNNTs can be intercalated with potassium between the walls and then longitudinally split to form (predominantly few layer) BN nanoribbons⁴⁵⁷ (Figure 44), similar to MWCNT splitting (section 7.1). However, unlike the MWCNT/GNR synthesis, subsequent edge-functionalization has only been proposed rather than demonstrated.⁴⁸⁸ More recently, associative protonation with chlorosulfonic acid has been shown to dissolve micron-length BNNTs,⁴⁸⁹ preferentially to synthesis side-products, facilitating a simple purification procedure.⁴⁹⁰

8. CURRENT AND EMERGING APPLICATIONS

There is a diverse range of applications for CCNs (Figure 45), most famously, reduced graphitic materials have long been used commercially as anodes in lithium ion batteries;⁴⁹³ however, SWCNT/MWCNT anode replacements are currently attracting attention.^{437,494} It is thought that hierarchical assemblies of CNTs (often vertically grown arrays) may be capable of higher specific charge densities as Li intercalation does not require opening of galleries between graphene sheets. However, the larger surface area may limit the performance through additional electrolyte decomposition. CCNs may also be useful for chemical energy storage; Ca-doped graphene⁴⁹⁵

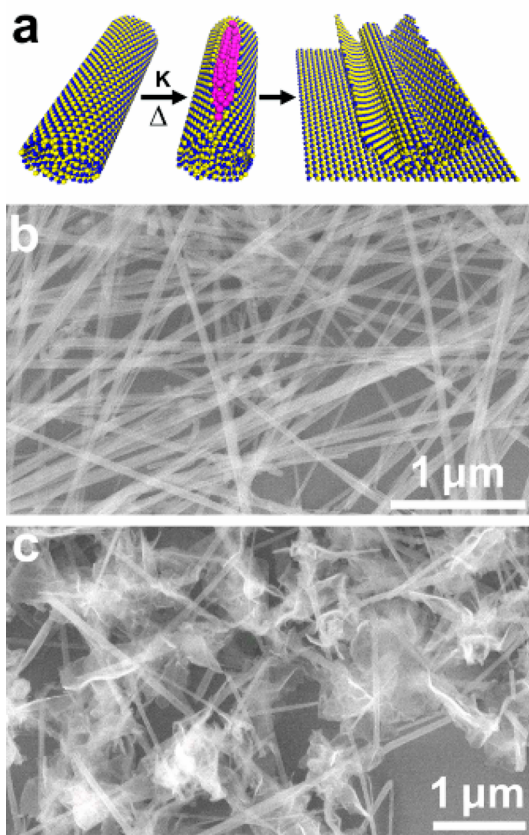


Figure 44. (a) Scheme of the unzipping of BNNTs to form BN nanoribbons, (b) SEM image of pristine BNNTs, and (c) SEM image of BNNRs formed by splitting BNNTs by potassium vapor at 300 °C for 72 h. Reproduced with permission from ref 457. Copyright 2014 American Chemical Society.

(ca. 5 wt %) and Li/K intercalated SWCNT bundles²⁷⁴ (ca. 20 wt %) are reported to offer higher H₂ storage than most current hydrogen absorption solutions,⁴⁹⁶ although the

accuracy of these results are the subject of ongoing debate.^{497,498}

More recently, intercalation of chemical fuels into SWCNT bundles has been used to develop a new form of energy storage termed thermopower wave devices.⁴⁹⁹ Here, the propagating reaction drives a current through the nanostructured carbon support, offering an energy density which can approach that of lithium ion batteries.⁵⁰⁰ Semiconducting SWNTs also offer excellent performance as more conventional thermoelectrics; since the Seebeck coefficient depends on the density of states, tuning the Fermi level to a van Hove singularity, by either chemical or electrochemical doping, can increase performance significantly.⁵⁰¹ The use of hydroxide- and halide-doped SWCNTs counterbalanced by chelated alkali metal ions has been shown to create air-stable n-type thermoelectrics with promising performance⁵⁰² (figure of merit, $ZT > 0.1$). In addition, the combination of oxidative and reductive doping can produce the n- and p-type constituents needed for an effective thermopile.⁵⁰³ As described earlier (section 3.3.2), many of the CCNs show superconductivity, notably GICs¹⁸¹ and fullerenes;²⁵³ however, CCN superconductors are likely of predominantly academic interest only, owing to their air sensitivity and low T_c compared to existing iron and cuprate high-temperature superconductors.⁵⁰⁴

The longstanding use of KC₈ as a reducing agent in organic chemistry (along with other less-reducing GICs) may be improved through use of the more highly tunable nanotube as a reducing agent, with the reduction potential set by carbon/metal stoichiometry, rather than the staging-dependent potential of the GICs.¹⁵¹ The added tunability, in principle, allows selective reactivity of chemicals with a variety of reduction potentials and can be adapted to form supported metal nanoparticles from otherwise unreactive metal salts, giving rise to hierarchical nanomaterials, relevant for example to (electro)catalytic applications.^{390,391}

Carbon nanomaterial processing can be improved by applying CCN chemistries. One advantage is that purification can easily be integrated; in both chemical²⁹² and electro-

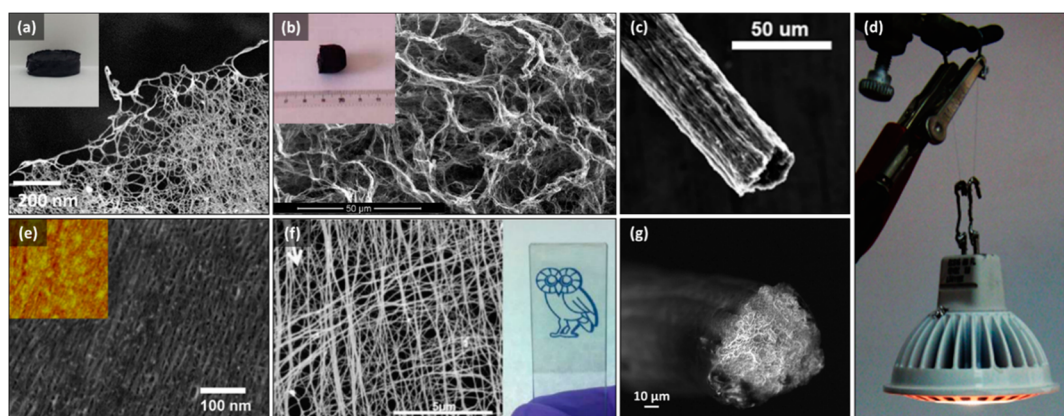


Figure 45. Applications of CCNs. (a and b) SEM and digital pictures of aerogels from nanotube solutions (a) with and (b) without cross-linking from reduction functionalization from nanotube solution. (a) Adapted with permission from ref 402. Copyright 2016 The Royal Society of Chemistry. (b) Reproduced with permission from ref 491. Copyright 2014 Elsevier. (c) SEM of SWCNT yarn spun from nanotube. Reproduced from ref 423. Copyright 2014 American Chemical Society. (d) High strength, high conductivity SWCNT fiber from superacid processing, acting as support and wires for a 46 g LED light. Reproduced with permission from ref 84. Copyright 2013 AAAS. (e) SWCNT film with high alignment from nanotube liquid crystals (SEM and AFM inset). Reproduced from ref 300. Copyright 2015 American Chemical Society. (f) SEM and digital picture of TCF from superacid dispersed SWCNTs. Reproduced with permission from ref 492. Copyright 2012 American Chemical Society. (g) SEM of SWCNT/poly(vinyl chloride) composite fiber fracture cross-section. Reproduced with permission from ref 87. Copyright 2017 The Royal Society of Chemistry.

chemical⁶³ reductions, low charge ratios dissolve undesirable contaminants preferentially, leaving more perfect, longer, purified SWCNTs behind.¹⁴³ When directly compared to all other typical SWCNT purification routes, the reductive purification has been shown to be the best compromise between introduced damage, impurity removal, and yield.¹²² The differing eDOS of SWCNTs may allow enrichment or separation, by helicity or electronic type,^{64,292} although the effects are complex (section 6.1).

The functionalization of carbon nanomaterials is of vital importance to their broader processing and, as discussed extensively earlier (section 4), and can be facilitated with minimal damage by using CCNs as an intermediate. Functionalization can be used to increase solubility in a range of solvents, alter surface energies and structure,³⁷⁰ and compatibility with matrices for composites: CCNs are particularly pertinent for composite materials, allowing strong covalent bonds to form between matrix with the nanomaterial to increase shear stress transfer.^{338,340,368,378,505} As the reductive functionalization can be applied to the entire CCN family, it allows quick and simple access to corresponding families of functionalized carbon nanomaterials, allowing systematic studies of geometry to be performed.³⁷⁰

A variety of carbon constructs have been prepared via CCN routes, including fibers, films, and aerogels (Figure 45 panels a and b). The CCN approaches minimize bundling, damage to the sp^2 framework, and contamination (for example, from surfactants). 3d Assemblies of SWCNTs can be created through freeze-drying of nanotubide solutions to give free-standing, ultralight, highly porous cryogels.⁴⁹¹ The gels are mechanically weak unless a polymer matrix is introduced to the initial solution, although the exposed SWCNT surface is lowered. Alternatively, high concentration nanotubide solutions may be cross-linked with reductive functionalization to form a SWCNT gel which can be freeze-dried to form mechanically robust materials.^{402,506} These porous assemblies can act as supercapacitors,⁴⁰² gas storage scaffolds,⁵⁰⁷ Joule heaters,⁵⁰⁸ fuel cell catalysts,⁵⁰⁹ and the chemistries can be modified to incorporate graphenide to form hybrid nano-carbon constructs.

2d Transparent conductive films (TCFs) can be synthesized from simple dip-coating, spin-coating, spraying, or casting of nanotubide,⁵¹⁰ graphenide,⁵¹¹ or superacid/SWCNT solutions⁴⁹² forming flexible thin films with high strength and low resistances. Values below 100 Ω/sq at 90% transparency⁵¹² place such systems among the best SWCNT TCFs created to date.⁵¹² The liquid crystallinity of high concentration dispersions of both nanotubide/superacid dispersed SWCNTs can be exploited to form aligned films.³⁰⁰ The current properties are approximately the same as typical data for the ubiquitous but brittle and expensive TCF indium tin oxide coated glass. Similar TCFs using charged graphenes have recently been produced, both from graphenide²⁹⁰ and superacid dispersed graphene,¹⁴¹ and are thought to be promising alternatives, although properties have yet to match those from the more mature SWCNT field. Devices incorporating TCFs currently suffer from weak adhesion to the supporting substrate; however, CCNs offer a possible solution, utilizing the inherent reactivity of the CCN to bond to the substrate covalently as a self-assembled monolayer.²²⁸ Electrophoretic deposition of neutral carbon nanomaterials is already a sizable field,⁵¹³ which may be aided by the availability of CCNs,⁶³ which do not rely on surfactants or defects.

Similarly, solutions of reduced, individualized TMD sheets have been electroplated to form films;³⁰³ however, their properties have not yet been measured and compared to alternative TMD assembly routes.

Polymer composites exploiting the exceptional mechanical properties of carbon nanomaterials require good dispersion, strong interfaces with the matrix, and high aspect ratios; alignment is also often useful to maximize anisotropic properties.⁸⁵ Mild charge-based processing has been shown to be an excellent route to high performance materials since there is a high degree of individualization with little damage. The interface properties of subsequent nanocomposites can be improved using the CCN's inherent reactivity, increasing composite strength, and toughness.^{338,378} Alternatively, the matrix can be grown directly from the CCN,³⁴⁰ using graft-from polymerizations (see section 4.3)

Aligned, anisotropic nanocarbons are particularly suited to the formation of high performance fibers. CCN solutions can be used as the precursor solution for continuous coagulation spinning of pure SWCNT fibers by simple injection into water.^{423,514} The resultant materials from superacid SWCNT dispersions have high uniaxial mechanical properties (highly dependent on SWCNT source⁵¹⁵) with tensile strength up to 2.4 GPa, a Young's modulus of 150 GPa, and a strain to failure of 1.7%, all at low density. The high tensile strength of these fibers is aided by the presence of LC domains in the initial dope, which increases the alignment of the SWCNTs during the spinning process. The resulting fiber exhibits high specific electrical and thermal conductivities (up to 4.18 $\text{kS m}^2 \text{kg}^{-1}$ and 451 $\text{mW m}^2 \text{kg}^{-1} \text{K}$, respectively, after iodine doping⁸⁴). Fibers from coagulating nanotubide liquid crystals⁴²³ in water lead to inferior mechanical properties, likely due to damage from uncontrolled discharging. Initial aqueous-spun graphenide³⁰⁶ and graphenide/nanotubide hybrid³⁰⁶ fibers have been recently demonstrated but currently exhibit poorer properties than the best current reduced graphene oxide fibers.^{516,517} The use of a polymer coagulant in lieu of water for nanotubide solutions can lead to a composite fiber, which is more mechanically robust.⁴³⁵ The use of a reactive polymer solution as the coagulant allows a covalent interface to form between matrix and nanotube in situ as the fiber forms, offering increased composite toughness.³³⁹

9. CONCLUSION

CCNs provide invaluable opportunities to aid the processing of otherwise intractable materials, particularly SWCNTs and graphenes. Charging provides a nondamaging route for the preparation and manipulation of individualized nanomaterial solutions while retaining the properties of interest, particularly their high aspect ratio. These CCN solutions can facilitate purification, separation, and (self-)assembly into a variety of hierarchical functional structures. In addition, CCNs provide versatile access to a wide range of derivatization chemistries, with minimal damage. These advantages are increasing relevant, as high quality SWCNTs are becoming available at ever-lower costs and in larger quantities. CCN chemistries allow technologists to take advantage of these high quality materials, especially for mechanical and (opto)electronic applications where individualization of high aspect ratio, high crystallinity nanocarbons are needed. While CCN chemistries typically require controlled atmospheres, they are essentially bulk processes, unlike the intensive ultrasound or ultracentrifugation steps otherwise needed for individualization.

In principle, the CCN approach is ready to implement industrially at whatever scale is relevant to application.

In addition to their practical utility, the CCNs are of interest from an academic perspective. Notably, CCNs exist as a unique class of materials: low dimensionality, macroscopic, high aspect ratio, and discrete molecular species with a continuum DOS. Their properties are a complex balance of redox chemistry, physical electrostatic interactions, and lattice energies. While clear overlaps exist with metal clusters, organic polyelectrolytes, and charged plates, bespoke CCN models are necessary. A fuller understanding of how the eDOS depends on CCN geometry and degree of reduction/oxidation may be the key to revealing selective dissolution and functionalization mechanisms in more detail. In addition, the effects of charge localization, locus of functionalization, and charge condensation should be more thoroughly investigated, taking into account sample heterogeneity, the presence of impurities, and subsequent charge partitioning. With the increasing availability of sorted SWCNTs, which represent a large family of around 1000 distinct molecules²² with characteristic properties and redox behaviors, a rich vein of chemistry will become accessible, drawing on a new class of well-defined polyelectrolyte. More generally, the reductive chemistries may be applied to a wide range additional nanomaterials; while the preliminary studies, noted above, including nanohorns, nano-onions, and TMDs, are promising, the development of charge-based processing will continue to enable new applications and reveal intriguing new phenomena.

AUTHOR INFORMATION

Corresponding Author

*E-mail: m.shaffer@imperial.ac.uk.

ORCID

Mustafa K. Bayazit: 0000-0002-3203-6601

Christopher A. Howard: 0000-0003-2550-0012

Milo S. P. Shaffer: 0000-0001-9384-9043

Notes

The authors declare no competing financial interest.

Biographies

Adam J. Clancy graduated from Cardiff University in 2011 with first-class honours MChem in Chemistry. He completed his Ph.D. under Prof Milo Shaffer at Imperial College London (ICL) in 2015 on the processing of SWCNTs and synthesis of novel hierarchical composites. He was awarded an EPSRC Doctoral Prize Fellowship in 2016 and currently works as a Research Associate in Materials Chemistry at UCL, developing multifunctional nanocomposite coatings.

Mustafa K. Bayazit received his M.Sc. in Chemistry from Abant Izzet Baysal University before earning his Ph.D. at the University of Durham, in 2010. He then worked at ICL as a PDRA before moving to UCL in 2014; his current work involves the processing and applications of 2D nanomaterials and microwave flow systems. He is the recipient of doctoral fellowship awarded by the Scientific and Technological Research Council of Turkey and was awarded the 1st Community Achievement Award by the Centre for Turkey Studies and Development in 2012, and was listed in Marquis Who's Who in the World 2013.

Stephen A. Hodge is a Research Associate in the Nanomaterials and Spectroscopy Group at the Cambridge Graphene Centre, Teaching Fellow in the EPSRC CDT in Graphene Technology and Bye-Fellow

of Murray Edwards College. He has particular interests in the chemistry and physics of nanomaterials, including fullerenes, carbon nanotubes, graphene, and the many other two-dimensional analogues. His current focus is on the scalable production of these enabling materials for mechanical, optical, and electronic applications.

Neal Skipper is Professor of Physics, a founder member of the Condensed Matter and Materials Physics group at University College London and a Principal Investigator in the London Centre for Nanotechnology. He studied B.Sc. in Chemical Physics and a Ph.D. in Physics at Bristol University before working as a PDRA at Oxford University. He was awarded a Sir Henry Jones Research Fellowship which he undertook at the University Pembroke College Cambridge and Department of Chemistry before taking a lectureship at UCL in 1994, earning a professorship in 2006. His current interests revolve around understanding the underlying physics of nanomaterials to improve manipulation and utilization of these exotic structures.

Christopher A. Howard is a Associate Professor in the Department of Physics & Astronomy at University College London, where he had previously obtained his Ph.D. His current research focuses on the manipulation of low dimensional materials via chemical doping that he studies both in the solid state and in liquids. He uses a wide range of in-house experimental methods and spends a lot of time at central facilities, particularly for X-ray and neutron scattering.

Milo S. P. Shaffer is currently Professor of Materials Chemistry at ICL and Co-Director of the London Centre for Nanotechnology. He completed his first degree, Ph.D., and a Trinity College Research Fellowship, at the University of Cambridge before working as a consultant in new materials technology development and exploitation. He has extensive experience of manipulation, functionalization, and characterization of carbon nanotubes and has studied a wide variety of composite systems, including structural matrices and conducting polymers for device applications. Current interests include carbon and hierarchical structure assembly.

ACKNOWLEDGMENTS

The authors would like to thank Siân M. Rankin-Turner for assisting with translation of C. Schafhaeuti, *J. Prakt. Chem.* (1840). SWCNT eDOS data for Figure 4 was downloaded from the website of Prof Shigeo Maruyama, University of Tokyo (www.photon.t.u-tokyo.ac.jp/~maruyama/kataura/kataura.html). The authors would like to acknowledge the EPSRC for funding through The Doctoral Training Partnership New Directions (EP/L001896/1), High Performance Ductile Composite Technology (HiPerDuCT, EP/I02946X/1), and graphene engineering programs (EP/K01658X/1).

LIST OF ABBREVIATIONS

AFM	atomic force microscopy
ARPES	angle-resolved photoemission spectroscopy
BN	boron nitride
BNNT	boron nitride nanotube
CCN	charged carbon nanomaterial
CDW	charge density wave
CNF	carbon nanofiber
CNT	carbon nanotube
CV	cyclic voltammetry
CVD	chemical vapor deposition
DA	dodecylamine
DFT	density functional theory
DLVO	Derjaguin–Landau–Verwey–Overbeek (colloid theory)

DMAC	<i>N,N</i> -dimethylacetamide
DMF	<i>N,N</i> -dimethylformamide
DMSO	dimethyl sulfoxide
eDOS	electronic density of states
gCN	graphitic carbon nitride
GIC	graphite intercalation compound
GNR	graphene nanoribbon
GO	graphene oxide
h-BN	hexagonal boron nitride
HOMO	highest occupied molecular orbital
IL	interlayer
IR	infrared
LC	liquid crystal
LPE	liquid phase exfoliation
LUMO	lowest unoccupied molecular orbital
MO	molecular orbital
m-SWCNT	metallic single-walled carbon nanotube
MWCNT	multi-walled carbon nanotube
OM	Ooawa-Manning (theory)
PTI	polymerised triazine imide
rGO	reduced graphite oxide
sc-SWCNT	semiconducting single-walled carbon nanotube
SEM	scanning electron microscopy
SET	single electron transfer
STM	scanning tunnelling microscopy
SWCNT	single-walled carbon nanotube
TCF	transparent conductive film
TEM	transmission electron microscopy
THF	tetrahydrofuran
TMD	transition metal dichalcogenide
TMDIC	transition metal dichalcogenide intercalation compound
UV	ultra-violet (light)
vHS	van Hove singularity

LIST OF SYMBOLS

A_{charge}	charge area density
c_i	concentration of ionic species i
D	diameter
e	elementary charge
I	electrolyte ionic strength
k_B	Boltzmann constant
L	length
l_B	Bjerrum length
l_{charge}	distance between unscreened charges
N_A	Avogadro's constant
T	absolute temperature
t	thickness
T_c	critical temperature
z_i	charge of ionic species i
ϵ_0	permittivity of free space
ϵ_r	solvent dielectric constant
λ_D	Debye length
ϕ_i	volume fraction of species i
ZT	(thermoelectric) figure of merit

REFERENCES

- (1) Kroto, H. W.; Heath, J. R.; O'Brien, S. C.; Curl, R. F.; Smalley, R. E. C60: Buckminsterfullerene. *Nature* **1985**, *318*, 162–163.
- (2) Zhang, J.; Terrones, M.; Park, C. R.; Mukherjee, R.; Monthieux, M.; Koratkar, N.; Kim, Y. S.; Hurt, R.; Frackowiak, E.; Enoki, T.; et al. Carbon Science in 2016: Status, Challenges and Perspectives. *Carbon* **2016**, *98*, 708–732.

- (3) Baird, T.; Fryer, J.; Grant, B. Structure of Fibrous Carbon. *Nature* **1971**, *233*, 329–330.
- (4) Monthieux, M.; Kuznetsov, V. L. Who Should Be given the Credit for the Discovery of Carbon Nanotubes? *Carbon* **2006**, *44*, 1621–1623.
- (5) Iijima, S.; Ichihashi, T. Single-Shell Carbon Nanotubes of 1-nm Diameter. *Nature* **1993**, *363*, 603–605.
- (6) Bethune, D.; Kiang, C.; De Vries, M.; Gorman, G.; Savoy, R.; Vazquez, J.; Beyers, R. Cobalt-Catalysed Growth of Carbon Nanotubes with Single-Atomic-Layer Walls. *Nature* **1993**, *363*, 605–607.
- (7) Novoselov, K.; Geim, A.; Morozov, S.; Jiang, D.; Zhang, Y.; Dubonos, S.; Grigorieva, I.; Firsov, A. Electric Field Effect in Atomically Thin Carbon Films. *Science* **2004**, *306*, 666–669.
- (8) Awasthi, K.; Srivastava, A.; Srivastava, O. N. Synthesis of Carbon Nanotubes. *J. Nanosci. Nanotechnol.* **2005**, *5*, 1616–1636.
- (9) Li, X.; Colombo, L.; Ruoff, R. S. Synthesis of Graphene Films on Copper Foils by Chemical Vapor Deposition. *Adv. Mater.* **2016**, *28*, 6247–6252.
- (10) Zheng, L. X.; O'Connell, M. J.; Doorn, S. K.; Liao, X. Z.; Zhao, Y. H.; Akhadov, E. A.; Hoffbauer, M. A.; Roop, B. J.; Jia, Q. X.; Dye, R. C.; et al. Ultralong Single-Wall Carbon Nanotubes. *Nat. Mater.* **2004**, *3*, 673–676.
- (11) Jiang, L.; Niu, T.; Lu, X.; Dong, H.; Chen, W.; Liu, Y.; Hu, W.; Zhu, D. Low-Temperature, Bottom-Up Synthesis of Graphene via a Radical-Coupling Reaction. *J. Am. Chem. Soc.* **2013**, *135*, 9050–9054.
- (12) Kumar, M.; Ando, Y. Chemical Vapor Deposition of Carbon Nanotubes: A Review on Growth Mechanism and Mass Production. *J. Nanosci. Nanotechnol.* **2010**, *10*, 3739–3758.
- (13) Chen, L.; Hernandez, Y.; Feng, X.; Müllen, K. From Nanographene and Graphene Nanoribbons to Graphene Sheets: Chemical Synthesis. *Angew. Chem., Int. Ed.* **2012**, *51*, 7640–7654.
- (14) Zhu, Y.; Murali, S.; Cai, W.; Li, X.; Suk, J.; Potts, J. R.; Ruoff, R. S. Graphene and Graphene Oxide: Synthesis, Properties, and Applications. *Adv. Mater.* **2010**, *22*, 3906–3924.
- (15) Zhang, Q.; Huang, J.-Q. Q.; Zhao, M.-Q. Q.; Qian, W.-Z. Z.; Wei, F. Carbon Nanotube Mass Production: Principles and Processes. *ChemSusChem* **2011**, *4*, 864–889.
- (16) Scott, L. T. Methods for the Chemical Synthesis of Fullerenes. *Angew. Chem., Int. Ed.* **2004**, *43*, 4994–5007.
- (17) Suarez-Martinez, I.; Grobert, N.; Ewels, C. P. Nomenclature of sp² Carbon Nanoforms. *Carbon* **2012**, *50*, 741–747.
- (18) Dalhaes, P. *Graphite and Precursors*; Gordon and Breach Science Publishers, 2001.
- (19) Palser, A. H. R. Interlayer Interactions in Graphite and Carbon Nanotubes. *Phys. Chem. Chem. Phys.* **1999**, *1*, 4459–4464.
- (20) Lee, J.-K.; Lee, S.-C.; Ahn, J.-P.; Kim, S.-C.; Wilson, J. I. B.; John, P. The Growth of AA Graphite on (111) Diamond. *J. Chem. Phys.* **2008**, *129*, 234709.
- (21) Miyata, Y.; Kawai, T.; Miyamoto, Y.; Yanagi, K.; Maniwa, Y.; Kataura, H. Chirality-Dependent Combustion of Single-Walled Carbon Nanotubes. *J. Phys. Chem. C* **2007**, *111*, 9671–9677.
- (22) Hodge, S. A.; Bayazit, M. K.; Coleman, K. S.; Shaffer, M. S. P. Unweaving the Rainbow: A Review of the Relationship Between Single-Walled Carbon Nanotube Molecular Structures and Their Chemical Reactivity. *Chem. Soc. Rev.* **2012**, *41*, 4409–4429.
- (23) Thess, A.; Lee, R.; Nikolaev, P.; Dai, H.; Petit, P.; Robert, J.; Xu, C.; Lee, Y. H.; Kim, S. G.; Rinzler, A.; et al. Crystalline Ropes of Metallic Carbon Nanotubes. *Science* **1996**, *273*, 483–487.
- (24) Tang, J.; Qin, L.-C.; Sasaki, T.; Yudasaka, M.; Matsushita, A.; Iijima, S. Compressibility and Polygonization of Single-Walled Carbon Nanotubes under Hydrostatic Pressure. *Phys. Rev. Lett.* **2000**, *85*, 1887–1889.
- (25) Elliott, J. A.; Sandler, J. K.; Windle, A. H.; Young, R. J.; Shaffer, M. S. Collapse of Single-Wall Carbon Nanotubes Is Diameter Dependent. *Phys. Rev. Lett.* **2004**, *92*, 095501.
- (26) Hata, K.; Futaba, D. N.; Mizuno, K.; Namai, T.; Yumura, M.; Iijima, S. Water-Assisted Highly Efficient Synthesis of Impurity-Free Single-Walled Carbon Nanotubes. *Science* **2004**, *306*, 1362–1364.

- (27) Zhang, R.; Zhang, Y.; Zhang, Q.; Xie, H.; Qian, W.; Wei, F. Growth of Half-Meter Long Carbon Nanotubes Based on Schulz–Flory Distribution. *ACS Nano* **2013**, *7*, 6156–6161.
- (28) Kharisova, O. V.; Kharisov, B. I. Variations of Interlayer Spacing in Carbon Nanotubes. *RSC Adv.* **2014**, *4*, 30807–30815.
- (29) Brinkmann, G.; Fowler, P. W.; Manolopoulos, D. E.; Palser, A. H. R. A Census of Nanotube Caps. *Chem. Phys. Lett.* **1999**, *315*, 335–347.
- (30) Qi, Z.; Zhang, H. A Note on the Cyclical Edge-Connectivity of Fullerene Graphs. *J. Math. Chem.* **2008**, *43*, 134–140.
- (31) Konarev, D. V.; Lyubovskaya, R. N. Donor Acceptor Complexes and Radical Ionic Salts Based on Fullerenes. *Russ. Chem. Rev.* **1999**, *68*, 19–38.
- (32) Heiney, P. A. Structure, Dynamics and Ordering Transition of Solid C60. *J. Phys. Chem. Solids* **1992**, *53*, 1333–1352.
- (33) Zhang, X.; Xin, J.; Ding, F. The Edges of Graphene. *Nanoscale* **2013**, *5*, 2556–2569.
- (34) Stone, A. J.; Wales, D. J. Theoretical Studies of Icosahedral C60 and Some Related Species. *Chem. Phys. Lett.* **1986**, *128*, 501–503.
- (35) Park, T.-J.; Banerjee, S.; Hemraj-Benny, T.; Wong, S. S. Purification Strategies and Purity Visualization Techniques for Single-Walled Carbon Nanotubes. *J. Mater. Chem.* **2006**, *16*, 141–154.
- (36) Terrones, H.; Lv, R.; Terrones, M.; Dresselhaus, M. S. The Role of Defects and Doping in 2D Graphene Sheets and 1D Nanoribbons. *Rep. Prog. Phys.* **2012**, *75*, 062501.
- (37) Zandiatashbar, A.; Lee, G.-H.; An, S.; Lee, S.; Mathew, N.; Terrones, M.; Hayashi, T.; Picu, C.; Hone, J.; Koratkar, N. Effect of Defects on the Intrinsic Strength and Stiffness of Graphene. *Nat. Commun.* **2014**, *5*, 3186.
- (38) Cognet, L.; Tsybouski, D. A.; Rocha, J.-D. R.; Doyle, C. D.; Tour, J. M.; Weisman, R. B. Stepwise Quenching of Exciton Fluorescence in Carbon Nanotubes by Single-Molecule Reactions. *Science* **2007**, *316*, 1465–1468.
- (39) Nourbakhsh, A.; Cantoro, M.; Vosch, T.; Pourtois, G.; Clemente, F.; van der Veen, M. H.; Hofkens, J.; Heyns, M. M.; De Gendt, S.; Sels, B. F. Bandgap Opening in Oxygen Plasma-Treated Graphene. *Nanotechnology* **2010**, *21*, 435203.
- (40) Xie, Q.; Perez-Cordero, E.; Echegoyen, L. Electrochemical Detection of C60- and C70-: Enhanced Stability of Fullerides in Solution. *J. Am. Chem. Soc.* **1992**, *114*, 3978–3980.
- (41) Al-Zubaidi, A.; Inoue, T.; Matsushita, T.; Ishii, Y.; Hashimoto, T.; Kawasaki, S. Cyclic Voltammogram Profile of Single-Walled Carbon Nanotube Electric Double-Layer Capacitor Electrode Reveals Dumbbell Shape. *J. Phys. Chem. C* **2012**, *116*, 7681–7686.
- (42) Cooper, A. J.; Wilson, N. R.; Kinloch, I. A.; Dryfe, R. Single Stage Electrochemical Exfoliation Method for the Production of Few-Layer Graphene via Intercalation of Tetraalkylammonium Cations. *Carbon* **2014**, *66*, 340–350.
- (43) Shan, B.; Cho, K. First Principles Study of Work Functions of Single Wall Carbon Nanotubes. *Phys. Rev. Lett.* **2005**, *94*, 236602.
- (44) Dresselhaus, M. S.; Dresselhaus, G.; Jorio, A. Unusual Properties and Structure of Carbon Nanotubes. *Annu. Rev. Mater. Res.* **2004**, *34*, 247–278.
- (45) Bolotin, K. I.; Sikes, K. J.; Jiang, Z.; Klima, M.; Fudenberg, G.; Hone, J.; Kim, P.; Stormer, H. L. Ultrahigh Electron Mobility in Suspended Graphene. *Solid State Commun.* **2008**, *146*, 351–355.
- (46) Martin, J.; Akerman, N.; Ulbricht, G.; Lohmann, T.; Smet, J. v.; Von Klitzing, K.; Yacoby, A. Observation of Electron–Hole Puddles in Graphene Using a Scanning Single-Electron Transistor. *Nat. Phys.* **2008**, *4*, 144–148.
- (47) Shi, Y.; Dong, X.; Chen, P.; Wang, J.; Li, L.-J. Effective Doping of Single-Layer Graphene from Underlying SiO2 Substrates. *Phys. Rev. B: Condens. Matter Mater. Phys.* **2009**, *79*, 115402.
- (48) Dragoman, M.; Dragoman, D.; Tiginyanu, I. Atomically Thin Semiconducting Layers and Nanomembranes: A Review. *Semicond. Sci. Technol.* **2017**, *32*, 033001.
- (49) Saito, R.; Dresselhaus, G.; Dresselhaus, M. S. Trigonal Warping Effect of Carbon Nanotubes. *Phys. Rev. B: Condens. Matter Mater. Phys.* **2000**, *61*, 2981–2990.
- (50) Kataura, H.; Kumazawa, Y.; Maniwa, Y.; Umez, I.; Suzuki, S.; Ohtsuka, Y.; Achiba, Y. Optical Properties of Single Wall Carbon Nanotubes. *Synth. Met.* **1999**, *103*, 2555.
- (51) Krupke, R.; Hennrich, F.; Löhneysen, H. v.; Kappes, M. M. Separation of Metallic from Semiconducting Single-Walled Carbon Nanotubes. *Science* **2003**, *301*, 344–347.
- (52) Lu, W.; Xiong, Y.; Hassanien, A.; Zhao, W.; Zheng, M.; Chen, L. A Scanning Probe Microscopy Based Assay for Single-Walled Carbon Nanotube Metallicity. *Nano Lett.* **2009**, *9*, 1668–1672.
- (53) Dutta, S.; Pati, S. K. Novel Properties of Graphene Nanoribbons: A Review. *J. Mater. Chem.* **2010**, *20*, 8207–8223.
- (54) Abergel, D. S. L.; Apalkov, V.; Berashevich, J.; Ziegler, K.; Chakraborty, T. Properties of Graphene: A Theoretical Perspective. *Adv. Phys.* **2010**, *59*, 261–482.
- (55) Son, Y.-W.; Cohen, M. L.; Louie, S. G. Half-Metallic Graphene Nanoribbons. *Nature* **2006**, *444*, 347–349.
- (56) Okazaki, K.; Nakato, Y.; Murakoshi, K. Absolute Potential of the Fermi Level of Isolated Single-Walled Carbon Nanotubes. *Phys. Rev. B: Condens. Matter Mater. Phys.* **2003**, *68*, 035434.
- (57) Zhao, J.; Han, J.; Lu, J. Work Functions of Pristine and Alkali-Metal Intercalated Carbon Nanotubes and Bundles. *Phys. Rev. B: Condens. Matter Mater. Phys.* **2002**, *65*, 193401.
- (58) Su, W. S.; Leung, T. C.; Chan, C. T. Work Function of Single-Walled and Multiwalled Carbon Nanotubes: First-Principles Study. *Phys. Rev. B: Condens. Matter Mater. Phys.* **2007**, *76*, 235413.
- (59) Yang, F.; Wang, X.; Zhang, D.; Yang, J.; Luo, D.; Xu, Z.; Wei, J.; Wang, J.-Q.; Xu, Z.; Peng, F.; et al. Chirality-Specific Growth of Single-Walled Carbon Nanotubes on Solid Alloy Catalysts. *Nature* **2014**, *510*, 522–524.
- (60) Zhang, F.; Hou, P.-X.; Liu, C.; Cheng, H.-M. Epitaxial Growth of Single-Wall Carbon Nanotubes. *Carbon* **2016**, *102*, 181–197.
- (61) Sun, T.; Zeng, T.; Xia, C.; Li, S.; Wu, H. Purification and Separation of Single-Walled Carbon Nanotubes (SWCNTs). *J. Nanosci. Nanotechnol.* **2012**, *12*, 2955–2963.
- (62) Fagan, J. A.; Hároz, E. H.; Ihly, R.; Gui, H.; Blackburn, J. L.; Simpson, J. R.; Lam, S.; Hight Walker, A. R.; Doorn, S. K.; Zheng, M. Isolation of > 1 nm Diameter Single-Wall Carbon Nanotube Species Using Aqueous Two-Phase Extraction. *ACS Nano* **2015**, *9*, 5377–5390.
- (63) Hodge, S.; Fogden, S.; Howard, C.; Skipper, N.; Shaffer, M. Electrochemical Processing of Discrete Single-Walled Carbon Nanotube Anions. *ACS Nano* **2013**, *7*, 1769–1778.
- (64) Buckley, D. J.; Hodge, S. A.; De Marco, M.; Hu, S.; Anthony, D. B.; Cullen, P. L.; Skipper, N. T.; Shaffer, M. S. P.; Howard, C. A.; McKeigue, K. Trajectory of the Selective Dissolution of Charged Single-Walled Carbon Nanotubes. *J. Phys. Chem. C* **2017**, *121*, 21703–21712.
- (65) Haddon, R. C.; Brus, L. E.; Raghavachari, K. Electronic Structure and Bonding in Icosahedral C60. *Chem. Phys. Lett.* **1986**, *125*, 459–464.
- (66) Deibel, C.; Dyakonov, V. Polymer-Fullerene Bulk Heterojunction Solar Cells. *Rep. Prog. Phys.* **2010**, *73*, 096401.
- (67) Bakry, R.; Vallant, R. M.; Najam-ul-Haq, M.; Rainer, M.; Szabo, Z.; Huck, C. W.; Bonn, G. K. Medicinal Applications of Fullerenes. *Int. J. Nanomed.* **2007**, *2*, 639–649.
- (68) Sun, D.; Reed, C. A. Crystal Engineering a Linear Polymer of C60 Fullerene via Supramolecular Pre-Organization. *Chem. Commun.* **2000**, 2391–2392.
- (69) Thong, A. Z.; Shaffer, M. S.; Horsfield, A. P. HOMO–LUMO Coupling: The Fourth Rule for Highly Effective Molecular Rectifiers. *Nanoscale* **2017**, *9*, 8119–8125.
- (70) Hecht, D. S.; Hu, L.; Irvin, G. Emerging Transparent Electrodes Based on Thin Films of Carbon Nanotubes, Graphene, and Metallic Nanostructures. *Adv. Mater.* **2011**, *23*, 1482–1513.
- (71) Song, Y.; Fang, W.; Brenes, R.; Kong, J. Challenges and Opportunities for Graphene as Transparent Conductors in Optoelectronics. *Nano Today* **2015**, *10*, 681–700.

- (72) Zou, R. J.; Hu, J. Q.; Song, Y. L.; Wang, N.; Chen, H. H.; Wu, J. H.; Sun, Y. G.; Chen, Z. G. Carbon Nanotubes as Field Emitter. *J. Nanosci. Nanotechnol.* **2010**, *10*, 7876–7896.
- (73) Wang, C.; Takei, K.; Takahashi, T.; Javey, A. Carbon Nanotube Electronics – Moving Forward. *Chem. Soc. Rev.* **2013**, *42*, 2592–2609.
- (74) Javey, A.; Guo, J.; Wang, Q.; Lundstrom, M.; Dai, H. Ballistic Carbon Nanotube Field-Effect Transistors. *Nature* **2003**, *424*, 654–657.
- (75) Dillon, A. C. Carbon Nanotubes for Photoconversion and Electrical Energy Storage. *Chem. Rev.* **2010**, *110*, 6856–6872.
- (76) Aguirre, C. M.; Auvray, S.; Pigeon, S.; Izquierdo, R.; Desjardins, P.; Martel, R. Carbon Nanotube Sheets as Electrodes in Organic Light-Emitting Diodes. *Appl. Phys. Lett.* **2006**, *88*, 183104.
- (77) Marmolejo-Tejada, J. M.; Velasco-Medina, J. Review on Graphene Nanoribbon Devices for Logic Applications. *Microelectron. J.* **2016**, *48*, 18–38.
- (78) Niyogi, S.; Bekyarova, E.; Itkis, M.; Zhang, H.; Shepperd, K.; Hicks, J.; Sprinkle, M.; Berger, C.; Lau, C.; deHeer, W.; et al. Spectroscopy of Covalently Functionalized Graphene. *Nano Lett.* **2010**, *10*, 4061–4066.
- (79) Bonaccorso, F.; Sun, Z.; Hasan, T.; Ferrari, A. C. Graphene Photonics and Optoelectronics. *Nat. Photonics* **2010**, *4*, 611–622.
- (80) Sgobba, V.; Guldi, D. M. Carbon Nanotubes - Electronic/Electrochemical Properties and Application for Nanoelectronics and Photonics. *Chem. Soc. Rev.* **2009**, *38*, 165–184.
- (81) Avouris, P.; Freitag, M.; Perebeinos, V. Carbon-Nanotube Photonics and Optoelectronics. *Nat. Photonics* **2008**, *2*, 341–350.
- (82) Boncel, S.; Sundaram, R.; Windle, A.; Kozioł, K. K. Enhancement of the Mechanical Properties of Directly Spun CNT Fibers by Chemical Treatment. *ACS Nano* **2011**, *5*, 9339–9344.
- (83) Kobashi, K.; Nishino, H.; Yamada, T.; Futaba, D. N.; Yumura, M.; Hata, K. Epoxy Composite Sheets With a Large Interfacial Area from a High Surface Area-Supplying Single-Walled Carbon Nanotube Scaffold Filler. *Carbon* **2011**, *49*, 5090–5098.
- (84) Behabtu, N.; Young, C.; Tsentlovich, D.; Kleinerman, O.; Wang, X.; Ma, A.; Bengio, E.; ter Waarbeek, R.; de Jong, J.; Hoogerwerf, R.; et al. Strong, Light, Multifunctional Fibers of Carbon Nanotubes with Ultrahigh Conductivity. *Science* **2013**, *339*, 182–186.
- (85) Coleman, J. N.; Khan, U.; Blau, W. J.; Gun'ko, Y. K. Small but Strong: A Review of the Mechanical Properties of Carbon Nanotube–Polymer Composites. *Carbon* **2006**, *44*, 1624–1652.
- (86) Mittal, G.; Dhand, V.; Rhee, K. Y.; Park, S.-J.; Lee, W. R. A Review on Carbon Nanotubes and Graphene as Fillers in Reinforced Polymer Nanocomposites. *J. Ind. Eng. Chem.* **2015**, *21*, 11–25.
- (87) Clancy, A. J.; Anthony, D. B.; Fisher, S. J.; Leese, H.; Roberts, C. S.; Shaffer, M. S. P. Reductive Dissolution of Supergrowth Carbon Nanotubes for Tougher Nanocomposites by Reactive Coagulation Spinning. *Nanoscale* **2017**, *9*, 8764–8773.
- (88) Mutlay, İ.; Tudoran, L. B. Percolation Behavior of Electrically Conductive Graphene Nanoplatelets/Polymer Nanocomposites: Theory and Experiment. *Fullerenes, Nanotubes, Carbon Nanostruct.* **2014**, *22*, 413–433.
- (89) Li, J.; Ma, P. C.; Chow, W. S.; To, C. K.; Tang, B. Z.; Kim, J. K. Correlations Between Percolation Threshold, Dispersion State, and Aspect Ratio of Carbon Nanotubes. *Adv. Funct. Mater.* **2007**, *17*, 3207–3215.
- (90) Naumov, A. V.; Tsyboulski, D. A.; Bachilo, S. M.; Weisman, R. B. Length-Dependent Optical Properties of Single-Walled Carbon Nanotube Samples. *Chem. Phys.* **2013**, *422*, 255–263.
- (91) Oriňáková, R.; Oriňák, A. Recent Applications of Carbon Nanotubes in Hydrogen Production and Storage. *Fuel* **2011**, *90*, 3123–3140.
- (92) Yang, W.; Ni, M.; Ren, X.; Tian, Y.; Li, N.; Su, Y.; Zhang, X. Graphene in Supercapacitor Applications. *Curr. Opin. Colloid Interface Sci.* **2015**, *20*, 416–428.
- (93) Zhang, L.; Zhao, X. S. Carbon-Based Materials as Supercapacitor Electrodes. *Chem. Soc. Rev.* **2009**, *38*, 2520–2531.
- (94) Lee, K.; Zhang, J.; Wang, H.; Wilkinson, D. P. Progress in the Synthesis of Carbon Nanotube- and Nanofiber-Supported Pt Electrocatalysts for PEM Fuel Cell Catalysis. *J. Appl. Electrochem.* **2006**, *36*, 507–522.
- (95) Kauffman, D. R.; Star, A. Carbon Nanotube Gas and Vapor Sensors. *Angew. Chem., Int. Ed.* **2008**, *47*, 6550–6570.
- (96) Kim, M.; Lee, Y.-S. A Comprehensive Review of Gas Sensors Using Carbon Materials. *J. Nanosci. Nanotechnol.* **2016**, *16*, 4310–4319.
- (97) Amieva, E. J. C.; López-Barroso, J.; Martínez-Hernández, A. L.; Velasco-Santos, C. In *Recent Advances in Graphene Research*; Nayak, P. K., Ed.; InTech: Rijeka, 2016, .
- (98) Ji, M.; Daniels, B.; Shieh, A.; Modarelli, D. A.; Parquette, J. R. Controlling the Length of Self-Assembled Nanotubes by Sonication Followed by Polymer Wrapping. *Chem. Commun.* **2017**, *53*, 12806–12809.
- (99) Pang, J.; Bachmatiuk, A.; Ibrahim, I.; Fu, L.; Placha, D.; Martynkova, G.; Trzebicka, B.; Gemming, T.; Eckert, J.; Rummeli, M. H. CVD Growth of 1D and 2D sp² Carbon Nanomaterials. *J. Mater. Sci.* **2016**, *51*, 640–667.
- (100) Wang, C.; Chen, W.; Han, C.; Wang, G.; Tang, B.; Tang, C.; Wang, Y.; Zou, W.; Zhang, X.-A.; Qin, S.; et al. Growth of Millimeter-Size Single Crystal Graphene on Cu Foils by Circumfluence Chemical Vapor Deposition. *Sci. Rep.* **2015**, *4*, 4537.
- (101) Pirkle, A.; Chan, J.; Venugopal, A.; Hinojos, D.; Magnuson, C. W.; McDonnell, S.; Colombo, L.; Vogel, E. M.; Ruoff, R. S.; Wallace, R. M. The Effect of Chemical Residues on the Physical and Electrical Properties of Chemical Vapor Deposited Graphene Transferred to SiO₂. *Appl. Phys. Lett.* **2011**, *99*, 122108.
- (102) Banszerus, L.; Schmitz, M.; Engels, S.; Dauber, J.; Oellers, M.; Haupt, F.; Watanabe, K.; Taniguchi, T.; Beschoten, B.; Stampfer, C. Ultrahigh-Mobility Graphene Devices from Chemical Vapor Deposition on Reusable Copper. *Sci. Adv.* **2015**, *1*, No. e1500222.
- (103) Yi, M.; Shen, Z. A Review on Mechanical Exfoliation for the Scalable Production of Graphene. *J. Mater. Chem. A* **2015**, *3*, 11700–11715.
- (104) Karagiannidis, P. G.; Hodge, S. A.; Lombardi, L.; Tomarchio, F.; Decorde, N.; Milana, S.; Goykhman, I.; Su, Y.; Mesite, S. V.; Johnstone, D. N.; et al. Microfluidization of Graphite and Formulation of Graphene-Based Conductive Inks. *ACS Nano* **2017**, *11*, 2742–2755.
- (105) Coleman, J. N. Liquid-Phase Exfoliation of Nanotubes and Graphene. *Adv. Funct. Mater.* **2009**, *19*, 3680–3695.
- (106) Kharisov, B. I.; Kharisova, O. V.; Dimas, A. V. The Dispersion, Solubilization and Stabilization in “Solution” of Single-Walled Carbon Nanotubes. *RSC Adv.* **2016**, *6*, 68760–68787.
- (107) Chen, Z.; Kobashi, K.; Rauwald, U.; Booker, R.; Fan, H.; Hwang, W.-F.; Tour, J. M. Soluble Ultra-Short Single-Walled Carbon Nanotubes. *J. Am. Chem. Soc.* **2006**, *128*, 10568–10571.
- (108) Motta, M.; Moiala, M.; Kinloch, I. A.; Windle, A. H. High Performance Fibres from ‘Dog Bone’ Carbon Nanotubes. *Adv. Mater.* **2007**, *19*, 3721–3726.
- (109) Zhang, M.; Fang, S.; Zakhidov, A. A.; Lee, S. B.; Aliev, A. E.; Williams, C. D.; Atkinson, K. R.; Baughman, R. H. Strong, Transparent, Multifunctional, Carbon Nanotube Sheets. *Science* **2005**, *309*, 1215–1219.
- (110) Giordani, S.; Bergin, S. D.; Nicolosi, V.; Lebedkin, S.; Kappes, M. M.; Blau, W. J.; Coleman, J. N. Debundling of Single-Walled Nanotubes by Dilution: Observation of Large Populations of Individual Nanotubes in Amide Solvent Dispersions. *J. Phys. Chem. B* **2006**, *110*, 15708–15718.
- (111) Paton, K. R.; Varrla, E.; Backes, C.; Smith, R. J.; Khan, U.; O'Neill, A.; Boland, C.; Lotya, M.; Istrate, O. M.; King, P.; et al. Scalable Production of Large Quantities of Defect-Free Few-Layer Graphene by Shear Exfoliation in Liquids. *Nat. Mater.* **2014**, *13*, 624–630.
- (112) Lucas, A.; Zakri, C.; Maugey, M.; Pasquali, M.; van der Schoot, P.; Poulin, P. Kinetics of Nanotube and Microfiber Scission under Sonication. *J. Phys. Chem. C* **2009**, *113*, 20599–20605.
- (113) Charlier, C. J. Defects in Carbon Nanotubes. *Acc. Chem. Res.* **2002**, *35*, 1063–1069.

- (114) Vejpravova, J.; Pacakova, B.; Kalbac, M. Magnetic Impurities in Single-Walled Carbon Nanotubes and Graphene: A Review. *Analyst* **2016**, *141*, 2639–2656.
- (115) Ruoff, R.; Tse, D. S.; Malhotra, R.; Lorents, D. C. Solubility of Fullerene (C₆₀) in a Variety of Solvents. *J. Phys. Chem.* **1993**, *97*, 3379–3383.
- (116) Semenov, K. N.; Charykov, N. A. Temperature Dependence of Solubility of Individual Light Fullerenes and Industrial Fullerene Mixture in 1-Chloronaphthalene and 1-Bromonaphthalene. *J. Chem. Eng. Data* **2010**, *55*, 2373–2378.
- (117) Nakamura, E.; Isobe, H. Functionalized Fullerenes in Water. The First 10 Years of Their Chemistry, Biology, and Nanoscience. *Acc. Chem. Res.* **2003**, *36*, 807–815.
- (118) Ying, Q.; Marecek, J.; Chu, B. Slow Aggregation of Buckminsterfullerene (C₆₀) in Benzene Solution. *Chem. Phys. Lett.* **1994**, *219*, 214–218.
- (119) Rakovan, J.; Jaszczak, J. A. Multiple Length Scale Growth Spirals on Metamorphic Graphite {001} Surfaces Studied by Atomic Force Microscopy. *Am. Mineral.* **2002**, *87*, 17–24.
- (120) Liu, Z.; Suenaga, K.; Harris, P. J.; Iijima, S. Open and Closed Edges of Graphene Layers. *Phys. Rev. Lett.* **2009**, *102*, 015501.
- (121) Wang, Shan, H.; Hauge, R. H.; Pasquali, M.; Smalley, R. E. A Highly Selective, One-Pot Purification Method for Single-Walled Carbon Nanotubes. *J. Phys. Chem. B* **2007**, *111*, 1249–1252.
- (122) Clancy, A. J.; White, E. R.; Tay, H.; Yau, H.; Shaffer, M. Systematic Comparison of Conventional and Reductive Single-Walled Carbon Nanotube Purifications. *Carbon* **2016**, *108*, 423–432.
- (123) Hou, P.; Liu, C.; Tong, Y.; Xu, S.; Liu, M.; Cheng, H. Purification of Single-Walled Carbon Nanotubes Synthesized by the Hydrogen Arc-Discharge Method. *J. Mater. Res.* **2001**, *16*, 2526–2529.
- (124) Feng, Y.; Zhang, H.; Hou, Y.; McNicholas, T. P.; Yuan, D.; Yang, S.; Ding, L.; Feng, W.; Liu, J. Room Temperature Purification of Few-Walled Carbon Nanotubes with High Yield. *ACS Nano* **2008**, *2*, 1634–1638.
- (125) Atwood, J. L.; Koutsantonis, G. A.; Raston, C. L. Purification of C₆₀ and C₇₀ by Selective Complexation with Calixarenes. *Nature* **1994**, *368*, 229.
- (126) Komatsu, N.; Kadota, N.; Kimura, T.; Kikuchi, Y.; Arikawa, M. Remarkable Improvement in Efficiency of Filtration Method for Fullerene Purification. *Fullerenes, Nanotubes, Carbon Nanostruct.* **2007**, *15*, 217–226.
- (127) Isaacs, L.; Wehrsig, A.; Diederich, F. Improved Purification of C₆₀ and Formation of σ - and π -Homoaromatic Methano-Bridged Fullerenes by Reaction with Alkyl Diazoacetates. *Helv. Chim. Acta* **1993**, *76*, 1231–1250.
- (128) Liu, H.; Nishide, D.; Tanaka, T.; Kataura, H. Large-Scale Single-Chirality Separation of Single-Wall Carbon Nanotubes by Simple Gel Chromatography. *Nat. Commun.* **2011**, *2*, 309.
- (129) Mesgari, S.; Sundramoorthy, A. K.; Loo, L. S.; Chan-Park, M. B. Gel Electrophoresis Using a Selective Radical for the Separation of Single-Walled Carbon Nanotubes. *Faraday Discuss.* **2014**, *173*, 351–363.
- (130) Tvrdy, K.; Jain, R. M.; Han, R.; Hilmer, A. J.; McNicholas, T. P.; Strano, M. S. A Kinetic Model for the Deterministic Prediction of Gel-Based Single-Chirality Single-Walled Carbon Nanotube Separation. *ACS Nano* **2013**, *7*, 1779–1789.
- (131) Xu, X.; Ray, R.; Gu, Y.; Ploehn, H. J.; Gearheart, L.; Raker, K.; Scrivens, W. A. Electrophoretic Analysis and Purification of Fluorescent Single-Walled Carbon Nanotube Fragments. *J. Am. Chem. Soc.* **2004**, *126*, 12736–12737.
- (132) Williamson, G. K. Electron Microscope Studies of Dislocation Structures in Graphite. *Proc. R. Soc. London, Ser. A* **1960**, *257*, 457–463.
- (133) Hennig, G. R. Screw Dislocations in Graphite. *Science* **1965**, *147*, 733–734.
- (134) Huang, J. Y. HRTEM and EELS Studies of Defects Structure and Amorphous-Like Graphite Induced by Ball-Milling. *Acta Mater.* **1999**, *47*, 1801–1808.
- (135) Dimiev, A. M.; Ceriotti, G.; Behabtu, N.; Zakhidov, D.; Pasquali, M.; Saito, R.; Tour, J. M. Direct Real-Time Monitoring of Stage Transitions in Graphite Intercalation Compounds. *ACS Nano* **2013**, *7*, 2773–2780.
- (136) Zhang, X.; Huang, Y.; Chen, S.; Kim, N. Y.; Kim, W.; Schilter, D.; Biswal, M.; Li, B.; Lee, Z.; Ryu, S.; et al. Birch-Type Hydrogenation of Few-Layer Graphenes: Products and Mechanistic Implications. *J. Am. Chem. Soc.* **2016**, *138*, 14980–14986.
- (137) Murdianti, B. S.; Damron, J. T.; Hilburn, M. E.; Maples, R. D.; Hikkaduwa Koralege, R. S.; Kuriyavar, S. I.; Ausman, K. D. C₆₀ Oxide as a Key Component of Aqueous C₆₀ Colloidal Suspensions. *Environ. Sci. Technol.* **2012**, *46*, 7446–7453.
- (138) Segura, J. L.; Martín, N. [60]Fullerene Dimers. *Chem. Soc. Rev.* **2000**, *29*, 13–25.
- (139) Filleter, T.; Espinosa, H. D. Multi-Scale Mechanical Improvement Produced in Carbon Nanotube Fibers by Irradiation Cross-Linking. *Carbon* **2013**, *56*, 1–11.
- (140) Pal, P. P.; Larionova, T.; Anoshkin, I. V.; Jiang, H.; Nisula, M.; Goryunkov, A. A.; Tolochko, O. V.; Karppinen, M.; Kauppinen, E. I.; Nasibulin, A. G. Dry Functionalization and Doping of Single-Walled Carbon Nanotubes by Ozone. *J. Phys. Chem. C* **2015**, *119*, 27821–27828.
- (141) Behabtu, N.; Lomeda, J.; Green, M.; Higginbotham, A.; Sinitiskii, A.; Kosynkin, D.; Tsentlovich, D.; Parra-Vasquez, A.; Schmidt, J.; Kesselman, E.; et al. Spontaneous High-Concentration Dispersions and Liquid Crystals of Graphene. *Nat. Nanotechnol.* **2010**, *5*, 406–411.
- (142) Nam, H.; Kim, Y.; Yang, S.; Ahn, J.-H. Ball-Milling of Graphite and Multi-Wall Carbon Nanotubes. *J. Nanosci. Nanotechnol.* **2014**, *14*, 9103–9107.
- (143) Clancy, A. J.; Melbourne, J.; Shaffer, M. S. P. A One-Step Route to Solubilised, Purified or Functionalised Single-Walled Carbon Nanotubes. *J. Mater. Chem. A* **2015**, *3*, 16708–16715.
- (144) Ivanovskaya, V.; Köhler, C.; Seifert, G. 3D Metal Nanowires and Clusters Inside Carbon Nanotubes: Structural, Electronic, and Magnetic Properties. *Phys. Rev. B: Condens. Matter Mater. Phys.* **2007**, *75*, 075410.
- (145) Puech, N.; Blanc, C.; Grelet, E.; Zamora-Ledezma, C.; Maugéy, M.; Zakri, C. c.; Anglaret, E.; Poulin, P. Highly Ordered Carbon Nanotube Nematic Liquid Crystals. *J. Phys. Chem. C* **2011**, *115*, 3272–3278.
- (146) Dresselhaus, M. S.; Dresselhaus, G. Intercalation Compounds of Graphite. *Adv. Phys.* **1981**, *30*, 139–326.
- (147) Zhang, W.; Zhang, Z.; Zhang, Y. The Application of Carbon Nanotubes in Target Drug Delivery Systems for Cancer Therapies. *Nanoscale Res. Lett.* **2011**, *6*, 555.
- (148) Pagani, G.; Green, M. J.; Poulin, P.; Pasquali, M. Competing Mechanisms and Scaling Laws for Carbon Nanotube Scission by Ultrasonication. *Proc. Natl. Acad. Sci. U. S. A.* **2012**, *109*, 11599–11604.
- (149) Huang, Y. Y.; Knowles, T. P.; Terentjev, E. M. Strength of Nanotubes, Filaments, and Nanowires From Sonication-Induced Scission. *Adv. Mater.* **2009**, *21*, 3945–3948.
- (150) Fakhri, N.; MacKintosh, F. C.; Lounis, B.; Cognet, L.; Pasquali, M. Brownian Motion of Stiff Filaments in a Crowded Environment. *Science* **2010**, *330*, 1804–1807.
- (151) Hodge, S. A.; Tay, H. H.; Anthony, D. B.; Menzel, R.; Buckley, D. J.; Cullen, P. L.; Skipper, N. T.; Howard, C. A.; Shaffer, M. S. Probing the Charging Mechanisms of Carbon Nanomaterial Polyelectrolytes. *Faraday Discuss.* **2014**, *172*, 311–325.
- (152) Sole, C.; Drewett, N. E.; Hardwick, L. J. In Situ Raman Study of Lithium-Ion Intercalation into Microcrystalline Graphite. *Faraday Discuss.* **2014**, *172*, 223–237.
- (153) Shaffäutl, C. Ueber die Verbindungen des Kohlenstoffes mit Silicium, Eisen und anderen Metallen, welche die verschiedenen Gallungen von Roheisen, Stahl und Schmiedeeisen bilden. *J. Prakt. Chem.* **1840**, *21*, 129–157.
- (154) Brodie, B. C. On the Atomic Weight of Graphite. *Philos. Trans. R. Soc. London* **1859**, *149*, 249–259.

- (155) Fredenhagen, K.; Cadenbach, G. Die Bindung von Kalium durch Kohlenstoff. *Z. Anorg. Allg. Chem.* **1926**, *158*, 249–263.
- (156) Rüdorff, W. Inclusion of Base Metals in Graphite and in Metallic Chalcogenides of the Type MeX₂. *Chimia* **1965**, *19*, 489–499.
- (157) Hérold, A. Recherches sur les Composés D'insertion du Graphite. *Bull. Soc. Chim. Fr.* **1955**, 7–8, 999–1012.
- (158) Solin, S. A.; Zabel, H. The Physics of Ternary Graphite Intercalation Compounds. *Adv. Phys.* **1988**, *37*, 87–254.
- (159) Enoki, T.; Endo, M.; Suzuki, M. *Graphite Intercalation Compounds and Applications*; Oxford University Press, 2003.
- (160) Ge, P.; Foulletier, M. Electrochemical Intercalation of Sodium in Graphite. *Solid State Ionics* **1988**, 28–30, 1172–1175.
- (161) Zadik, R. H.; Takabayashi, Y.; Klupp, G.; Colman, R. H.; Ganin, A. Y.; Potočník, A.; Jeglič, P.; Arçon, D.; Matus, P.; Kamarás, K.; et al. Optimized Unconventional Superconductivity in a Molecular Jahn-Teller Metal. *Sci. Adv.* **2015**, *1*, No. e1500059.
- (162) Margadonna, S.; Brown, C. M.; Lappas, A.; Prassides, K.; Tanigaki, K.; Knudsen, K. D.; Le Bihan, T.; Mézouar, M. Pressure and Temperature Evolution of the Structure of the Superconducting Na₂CsC₆₀ Fulleride. *J. Solid State Chem.* **1999**, *145*, 471–478.
- (163) Himmel, K.; Jansen, M. Synthese und Einkristallstruktur-analyse von Bis (benzyltrimethylammonium) fullerid-Ammoniakat; (BzI₃NMe₃)₂C₆₀·3 NH₃. *Z. Anorg. Allg. Chem.* **1998**, *624*, 1–3.
- (164) Fässler, T. F.; Spiekermann, A.; Spahr, M. E.; Nesper, R. Unprecedented Layered Structure of a Fulleride: Synthesis, Structure, and Magnetic Properties of a Potassium-Containing Salt with a C₆₀–Counterion. *Angew. Chem., Int. Ed. Engl.* **1997**, *36*, 486–488.
- (165) Pichler, T.; Sing, M.; Knupfer, M.; Golden, Fink, J. Potassium Intercalated Bundles of Single-Wall Carbon Nanotubes: Electronic Structure and Optical Properties. *Solid State Commun.* **1999**, *109*, 721–726.
- (166) Grigorian, L.; Williams, K. A.; Fang, S.; Sumanasekera, G. U.; Loper, A. L.; Dickey, E. C.; Pennycook, S. J.; Eklund, P. C. Reversible Intercalation of Charged Iodine Chains into Carbon Nanotube Ropes. *Phys. Rev. Lett.* **1998**, *80*, 5560–5563.
- (167) Liu, X.; Pichler, T.; Knupfer, M.; Fink, J. Electronic and Optical Properties of Alkali-Metal-Intercalated Single-Wall Carbon Nanotubes. *Phys. Rev. B: Condens. Matter Mater. Phys.* **2003**, *67*, 125403.
- (168) Khlobystov, A. N.; Britz, D. A.; Briggs, G. A. D. Molecules in Carbon Nanotubes. *Acc. Chem. Res.* **2005**, *38*, 901–909.
- (169) Kiang, C.-H.; Choi, J.-S.; Tran, T. T.; Bacher, A. D. Molecular Nanowires of 1 nm Diameter from Capillary Filling of Single-Walled Carbon Nanotubes. *J. Phys. Chem. B* **1999**, *103*, 7449–7451.
- (170) Hart, M.; White, E. R.; Chen, J.; McGilvery, C. M.; Pickard, C. J.; Michaelides, A.; Sella, A.; Shaffer, M.; Salzmann, C. G. Encapsulation and Polymerization of White Phosphorus Inside Single-Wall Carbon Nanotubes. *Angew. Chem.* **2017**, *129*, 8256–8260.
- (171) Reed, C. A.; Bolskar, R. D. Discrete Fulleride Anions and Fullerenium Cations. *Chem. Rev.* **2000**, *100*, 1075–1119.
- (172) Himmel, K.; Jansen, M. Synthesis and Single-Crystal Structure Analysis of [Ba (NH₃)₇] C₆₀ NH₃. *Inorg. Chem.* **1998**, *37*, 3437–3439.
- (173) Pennington, C. H.; Stenger, V. A. Nuclear Magnetic Resonance of C₆₀ and Fulleride Superconductors. *Rev. Mod. Phys.* **1996**, *68*, 855–910.
- (174) Margadonna, S.; Pontiroli, D.; Belli, M.; Shiroka, T.; Riccò, M.; Brunelli, M. Li₄C₆₀: A Polymeric Fulleride with a Two-Dimensional Architecture and Mixed Interfullerene Bonding Motifs. *J. Am. Chem. Soc.* **2004**, *126*, 15032–15033.
- (175) Pénicaud, A.; Pérez-Benítez, A.; Escudero, R.; Coulon, C. Single Crystal Synthesis of [(C₆H₅)₄P]₂[C₇₀][I] by Electrocrystallization and Experimental Determination of the g-Value Anisotropy of C₇₀- and C₆₀- at 4.2 K. *Solid State Commun.* **1995**, *96*, 147–150.
- (176) Riccò, M.; Pontiroli, D.; Mazzani, M.; Gianferrari, F.; Pagliari, M.; Goffredi, A.; Brunelli, M.; Zandomenighi, G.; Meier, B. H.; Shiroka, T. Fullerenium Salts: A New Class of C₆₀-Based Compounds. *J. Am. Chem. Soc.* **2010**, *132*, 2064–2068.
- (177) Lu, X.; Feng, L.; Akasaka, T.; Nagase, S. Current Status and Future Developments of Endohedral Metallofullerenes. *Chem. Soc. Rev.* **2012**, *41*, 7723–7760.
- (178) Tellgmann, R.; Krawez, N.; Lin, S. H.; Hertel, I. V.; Campbell, E. E. B. Endohedral Fullerene Production. *Nature* **1996**, *382*, 407–408.
- (179) Aoyagi, S.; Nishibori, E.; Sawa, H.; Sugimoto, K.; Takata, M.; Miyata, Y.; Kitauro, R.; Shinohara, H.; Okada, H.; Sakai, T.; et al. A Layered Ionic Crystal of Polar Li@ C₆₀ Superatoms. *Nat. Chem.* **2010**, *2*, 678–683.
- (180) Lee, R.; Kim, H.; Fischer, J.; Thess, A.; Smalley, R. E. Conductivity Enhancement in Single-Walled Carbon Nanotube Bundles Doped with K and Br. *Nature* **1997**, *388*, 255–257.
- (181) Weller, T. E.; Ellerby, M.; Saxena, S. S.; Smith, R. P.; Skipper, N. T. Superconductivity in the Intercalated Graphite Compounds C₆Yb and C₆Ca. *Nat. Phys.* **2005**, *1*, 39–41.
- (182) Hof, F.; Bosch, S.; Eigler, S.; Hauke, F.; Hirsch, A. New Basic Insight into Reductive Functionalization Sequences of Single Walled Carbon Nanotubes (SWCNTs). *J. Am. Chem. Soc.* **2013**, *135*, 18385–18395.
- (183) Anderson, R. E.; Barron, A. R. Solubilization of Single-Wall Carbon Nanotubes in Organic Solvents Without Sidewall Functionalization. *J. Nanosci. Nanotechnol.* **2007**, *7*, 3436–3440.
- (184) Iye, Y.; Tanuma, S.-i. Superconductivity of Graphite Intercalation Compounds with Alkali-Metal Amalgams. *Phys. Rev. B: Condens. Matter Mater. Phys.* **1982**, *25*, 4583–4592.
- (185) Genorio, B.; Lu, W.; Dimiev, A. M.; Zhu, Y.; Raji, A.-R. O.; Novosel, B.; Alemany, L. B.; Tour, J. M. In Situ Intercalation Replacement and Selective Functionalization of Graphene Nanoribbon Stacks. *ACS Nano* **2012**, *6*, 4231–4240.
- (186) Englert, J.; Knirsch, K.; Dotzer, C.; Butz, B.; Hauke, F.; Spiecker, E.; Hirsch, A. Functionalization of Graphene by Electrophilic Alkylation of Reduced Graphite. *Chem. Commun.* **2012**, *48*, 5025–5027.
- (187) Englert, J.; Dotzer, C.; Yang, G.; Schmid, M.; Papp, C.; Gottfried, J.; Steinrück, H.-P.; Spiecker, E.; Hauke, F.; Hirsch, A. Covalent Bulk Functionalization of Graphene. *Nat. Chem.* **2011**, *3*, 279–286.
- (188) Jeong, G.-H.; Hatakeyama, R.; Hirata, T.; Tohji, K.; Motomiya, K.; Yaguchi, T.; Kawazoe, Y. Formation and Structural Observation of Cesium Encapsulated Single-Walled Carbon Nanotubes. *Chem. Commun.* **2003**, *1*, 152–153.
- (189) Milner, E.; Skipper, N.; Howard, C.; Shaffer, M.; Buckley, D.; Rahnejat, K.; Cullen, P.; Heenan, R.; Lindner, P.; Schweins, R. Structure and Morphology of Charged Graphene Platelets in Solution by Small-Angle Neutron Scattering. *J. Am. Chem. Soc.* **2012**, *134*, 8302–8305.
- (190) Tran, N. E.; Lambrakos, S. G.; Lagowski, J. J. Analysis of Capacitance Characteristics of C-60, C-70, and La@C-82. *J. Mater. Eng. Perform.* **2009**, *18*, 95–101.
- (191) Fullagar, W. K.; Gentle, I. R.; Heath, G. A.; White, J. W. Reversible Alkali-Metal Reduction of C₆₀ in Liquid Ammonia; First Observation of Near-Infrared Spectrum of C₅–C₆₀. *J. Chem. Soc., Chem. Commun.* **1993**, *6*, 525–527.
- (192) Pénicaud, A.; Poulin, P.; Derré, A.; Anglaret, E.; Petit, P. Spontaneous Dissolution of a Single-Wall Carbon Nanotube Salt. *J. Am. Chem. Soc.* **2005**, *127*, 8–9.
- (193) Beguin, F.; Setton, R.; Hamwi, A.; Touzain, P.; Beguin, F.; Setton, R. The Reversible Intercalation of Tetrahydrofuran in Some Graphite-Alkali Metal Lamellar Compounds. *Mater. Sci. Eng.* **1979**, *40*, 167–173.
- (194) García-Gallastegui, A.; Obieta, I.; Bustero, I.; Imbuluzqueta, G.; Arbiol, J.; Miranda, J. I.; Aizpurua, J. M. Reductive Functionalization of Single-Walled Carbon Nanotubes with Lithium Metal Catalyzed by Electron Carrier Additives. *Chem. Mater.* **2008**, *20*, 4433–4438.

- (195) Graupner, R.; Abraham, J.; Wunderlich, D.; Vencelová, A.; Lauffer, P.; Röhr, J.; Hundhausen, M.; Ley, L.; Hirsch, A. Nucleophilic-Alkylation-Reoxidation: A Functionalization Sequence for Single-Wall Carbon Nanotubes. *J. Am. Chem. Soc.* **2006**, *128*, 6683–6689.
- (196) Syrgiannis, Z.; Hauke, F.; Röhr, J.; Hundhausen, M.; Graupner, R.; Elmes, Y.; Hirsch, A. Covalent Sidewall Functionalization of SWNTs by Nucleophilic Addition of Lithium Amides. *Eur. J. Org. Chem.* **2008**, *2008*, 2544–2550.
- (197) Bayazit, M. K.; Coleman, K. S. Ester-Functionalized Single-Walled Carbon Nanotubes via Addition of Haloformates. *J. Mater. Sci.* **2014**, *49*, S190–S198.
- (198) Yuan, C.; Chen, W.; Yan, L. Amino-Grafted Graphene as a Stable and Metal-Free Solid Basic Catalyst. *J. Mater. Chem.* **2012**, *22*, 7456–7460.
- (199) Gebhardt, B.; Hof, F.; Backes, C.; Müller, M.; Plocke, T.; Maultzsch, J.; Thomsen, C.; Hauke, F.; Hirsch, A. Selective Polycarboxylation of Semiconducting Single-Walled Carbon Nanotubes by Reductive Sidewall Functionalization. *J. Am. Chem. Soc.* **2011**, *133*, 19459–19473.
- (200) Fagan, P. J.; Krusic, P. J.; Evans, D. H.; Lerke, S. A.; Johnston, E. Synthesis, Chemistry, and Properties of a Monoalkylated Buckminsterfullerene Derivative, Tert-BuC₆₀ Anion. *J. Am. Chem. Soc.* **1992**, *114*, 9697–9699.
- (201) Hirsch, A.; Soi, A.; Karfunhel, H. R. Titration of C₆₀: A Method for the Synthesis of Organofullerenes. *Angew. Chem., Int. Ed. Engl.* **1992**, *31*, 766–768.
- (202) Atovmyan, E. G.; Grishchuk, A. A.; Fedotova, T. N. Polymerization of [60] Fullerene Activated with Butyllithium. *Russ. Chem. Bull.* **2011**, *60*, 1505–1507.
- (203) Duclaux, L.; Metenier, K.; Salvétat, J. P.; Lauginie, P.; Bonnamy, S.; Beguin, F. Doping of Carbon Nanotubes by Heavy Alkali Metals. *Mol. Cryst. Liq. Cryst. Sci. Technol., Sect. A* **2000**, *340*, 769–774.
- (204) Udod, I. Sodium-Graphite Intercalation Compound of the First Stage: Two-Dimensional Structure and Stability. *Synth. Met.* **1997**, *88*, 127–131.
- (205) Moriwake, H.; Kuwabara, A.; Fisher, C. A. J.; Ikuhara, Y. Why Is Sodium-Intercalated Graphite Unstable? *RSC Adv.* **2017**, *7*, 36550–36554.
- (206) Liu, Y.; Merinov, B. V.; Goddard, W. A. Origin of Low Sodium Capacity in Graphite and Generally Weak Substrate Binding of Na and Mg among Alkali and Alkaline Earth Metals. *Proc. Natl. Acad. Sci. U. S. A.* **2016**, *113*, 3735–3739.
- (207) Cohn, A. P.; Share, K.; Carter, R.; Oakes, L.; Pint, C. L. Ultrafast Solvent-Assisted Sodium Ion Intercalation into Highly Crystalline Few-Layered Graphene. *Nano Lett.* **2016**, *16*, 543–548.
- (208) Pruvost, S.; Hérol, C.; Hérol, A.; Lagrange, P. Co-Intercalation into Graphite of Lithium and Sodium with an Alkaline Earth Metal. *Carbon* **2004**, *42*, 1825–1831.
- (209) Gadi, M. E.; Hérol, A.; Hérol, C.; Marêché, J.-F.; Lagrange, P. Intercalation dans le Graphite du Sodium Associé à des Ions Peroxyde. *J. Solid State Chem.* **1997**, *131*, 282–289.
- (210) Guerard, D.; Lagrange, M.; El Makrini, P.; Hérol, A. Insertion de Métaux Alcalino-Terreux dans le Graphite. *Carbon* **1980**, *18*, 257–264.
- (211) Ferro, Y.; Allouche, A.; Linsmeier, C. Absorption and Diffusion of Beryllium in Graphite, Beryllium Carbide Formation Investigated by Density Functional Theory. *J. Appl. Phys.* **2013**, *113*, 213514.
- (212) Liu, X.; Pichler, T.; Knupfer, M.; Fink, J. Electronic Properties of Barium-Intercalated Single-Wall Carbon Nanotubes. *Phys. Rev. B: Condens. Matter Mater. Phys.* **2004**, *70*, 245435.
- (213) Girifalco, L. A.; Montalbano, T. O. Preparation and Properties of a Barium-Graphite Compound. *J. Mater. Sci.* **1976**, *11*, 1036–1040.
- (214) Graupner, R.; Abraham, J.; Vencelová, A.; Seyller, T.; Hennrich, F.; Kappes, M. M.; Hirsch, A.; Ley, L. Doping of Single Walled Carbon Nanotube Bundles by Bronsted Acids. *Phys. Chem. Chem. Phys.* **2003**, *5*, 5472–5476.
- (215) De Blauwe, K.; Kramberger, C.; Plank, W.; Kataura, H.; Pichler, T. Raman Response of FeCl₃ Intercalated Single-Wall Carbon Nanotubes at High Doping. *Phys. Phys. Status Solidi B* **2009**, *246*, 2732–2736.
- (216) Yoon, S.-M. M.; Kim, U. J.; Benayad, A.; Lee, I. H.; Son, H.; Shin, H.-J. J.; Choi, W. M.; Lee, Y. H.; Jin, Y. W.; Lee, E.-H. H.; et al. Thermal Conversion of Electronic and Electrical Properties of AuCl₃-Doped Single-Walled Carbon Nanotubes. *ACS Nano* **2011**, *5*, 1353–1359.
- (217) Kharlamova, M. V. Advances in Tailoring the Electronic Properties of Single-Walled Carbon Nanotubes. *Prog. Mater. Sci.* **2016**, *77*, 125–211.
- (218) Jhi, S.-H.; Louie, S. G.; Cohen, M. L. Electronic Properties of Bromine-Doped Carbon Nanotubes. *Solid State Commun.* **2002**, *123*, 495–499.
- (219) Erbil, A.; Kortan, A.; Birgeneau, R.; Dresslhaus, M. Intercalate Structure, Melting, and the Commensurate-Incommensurate Transition in Bromine-Intercalated Graphite. *Phys. Rev. B: Condens. Matter Mater. Phys.* **1983**, *28*, 6329.
- (220) Rao, A. M.; Eklund, P. C.; Bandow, S.; Thess, A.; Smalley, R. E. Evidence for Charge Transfer in Doped Carbon Nanotube Bundles from Raman Scattering. *Nature* **1997**, *388*, 257–259.
- (221) Rao, A. M.; Eklund, P.; Bandow, S.; Thess, A.; Smalley, R. E. Evidence for Charge Transfer in Doped Carbon Nanotube Bundles from Raman Scattering. *Nature* **1997**, *388*, 257–259.
- (222) Ebert, L. B. Intercalation Compounds of Graphite. *Annu. Rev. Mater. Sci.* **1976**, *6*, 181–211.
- (223) Kobayashi, M.; Akahama, Y.; Kawamura, H.; Shinohara, H.; Sato, H.; Saito, Y. X-Ray Diffraction Study of Iodine-Doped C₆₀. *Solid State Commun.* **1992**, *81*, 93–95.
- (224) Zhu, Q.; Cox, D. E.; Fischer, J. E.; Kniaz, K.; McGhie, A. R.; Zhou, O. Intercalation of Solid C₆₀ with Iodine. *Nature* **1992**, *355*, 712–714.
- (225) Reed, C.; Kim, K.; Bolskar, R.; Mueller, L. Taming Superacids: Stabilization of the Fullerene Cations HC₆₀⁺ and C₆₀⁺. *Science* **2000**, *289*, 101–104.
- (226) Reed, C. A. Carboranes: A New Class of Weakly Coordinating Anions for Strong Electrophiles, Oxidants, and Superacids. *Acc. Chem. Res.* **1998**, *31*, 133–139.
- (227) Kong, J.; Dai, H. Full and Modulated Chemical Gating of Individual Carbon Nanotubes by Organic Amine Compounds. *J. Phys. Chem. B* **2001**, *105*, 2890–2893.
- (228) Hodge, S.; Bayazit, M.; Tay, H.; Shaffer, M. Giant Cationic Polyelectrolytes Generated via Electrochemical Oxidation of Single-Walled Carbon Nanotubes. *Nat. Commun.* **2013**, *4*, 1989.
- (229) Valota, A. T.; Kinloch, I. A.; Novoselov, K. S.; Casiraghi, C.; Eckmann, A.; Hill, E. W.; Dryfe, R. A. W. Electrochemical Behavior of Monolayer and Bilayer Graphene. *ACS Nano* **2011**, *5*, 8809–8815.
- (230) Share, K.; Cohn, A. P.; Carter, R. E.; Pint, C. L. Mechanism of Potassium Ion Intercalation Staging in Few Layered Graphene from in Situ Raman Spectroscopy. *Nanoscale* **2016**, *8*, 16435–16439.
- (231) Izutsu, K. *Electrochemistry in Nonaqueous Solutions*; Wiley-VCH, 2002.
- (232) Low, C. T. J.; Walsh, F. C.; Chakrabarti, M. H.; Hashim, M. A.; Hussain, M. A. Electrochemical Approaches to the Production of Graphene Flakes and Their Potential Applications. *Carbon* **2013**, *54*, 1–21.
- (233) Bianchi, M.; Rienks, E.; Lizzit, S.; Baraldi, A.; Balog, R.; Hornekær, L.; Hofmann, P. Electron-Phonon Coupling in Potassium-Doped Graphene: Angle-Resolved Photoemission Spectroscopy. *Phys. Rev. B: Condens. Matter Mater. Phys.* **2010**, *81*, 041403.
- (234) Bostwick, A.; Ohta, T.; Seyller, T.; Horn, K.; Rotenberg, E. Quasiparticle Dynamics in Graphene. *Nat. Phys.* **2006**, *3*, 36–40.
- (235) McChesney, J. L.; Bostwick, A.; Ohta, T.; Seyller, T.; Horn, K.; González, J.; Rotenberg, E. Extended van Hove Singularity and Superconducting Instability in Doped Graphene. *Phys. Rev. Lett.* **2010**, *104*, 136803.
- (236) Ye, J.; Craciun, M. F.; Koshino, M.; Russo, S.; Inoue, S.; Yuan, H.; Shimotani, H.; Morpurgo, A. F.; Iwasa, Y. Accessing the Transport

Properties of Graphene and Its Multilayers at High Carrier Density. *Proc. Natl. Acad. Sci. U. S. A.* **2011**, *108*, 13002–13006.

(237) Valla, T.; Camacho, J.; Pan, Z.-H.; Fedorov, A.; Walters, A.; Howard, C.; Ellerby, M. Anisotropic Electron-Phonon Coupling and Dynamical Nesting on the Graphene Sheets in Superconducting CaC₆ Using Angle-Resolved Photoemission Spectroscopy. *Phys. Rev. Lett.* **2009**, *102*, 107007.

(238) Pan, Z.-H.; Camacho, J.; Upton, M.; Fedorov, A.; Howard, C.; Ellerby, M.; Valla, T. Electronic Structure of Superconducting KC₈ and Nonsuperconducting LiC₆ Graphite Intercalation Compounds: Evidence for a Graphene-Sheet-Driven Superconducting State. *Phys. Rev. Lett.* **2011**, *106*, 187002.

(239) Yang, S. L.; Sobota, J. A.; Howard, C. A.; Pickard, C. J.; Hashimoto, M.; Lu, D. H.; Mo, S. K.; Kirchmann, P. S.; Shen, Z. X. Superconducting Graphene Sheets in CaC₆ Enabled by Phonon-Mediated Interband Interactions. *Nat. Commun.* **2014**, *5*, 3493.

(240) Calandra, M.; Mauri, F. Theoretical Explanation of Superconductivity in C₆Ca. *Phys. Rev. Lett.* **2005**, *95*, 237002.

(241) Calandra, M.; Mauri, F. Possibility of Superconductivity in Graphite Intercalated with Alkaline Earths Investigated with Density Functional Theory. *Phys. Rev. B: Condens. Matter Mater. Phys.* **2006**, *74*, 094507.

(242) Howard, C.; Dean, M.; Withers, F. Phonons in Potassium-Doped Graphene: The Effects of Electron-Phonon Interactions, Dimensionality, and Adatom Ordering. *Phys. Rev. B: Condens. Matter Mater. Phys.* **2011**, *84*, 241404.

(243) Rahnejat, K.; Howard, C.; Shuttleworth, N.; Schofield, S.; Iwaya, K.; Hirjibehedin, C.; Renner, C.; Aeppli, G.; Ellerby, M. Charge Density Waves in the Graphene Sheets of the Superconductor CaC₆. *Nat. Commun.* **2011**, *2*, 558.

(244) McRae, E.; Mareché, J. F.; Lelaurain, M.; Furdin, G.; Herold, A. Conductivity Anisotropy in AsF₅-Intercalated Graphite. *J. Phys. Chem. Solids* **1987**, *48*, 957–963.

(245) McRae, E.; Maréché, J. F. c-Axis Conductivity and Conductivity Anisotropy in Graphite Intercalation Compounds. *J. Mater. Res.* **1988**, *3*, 75–86.

(246) Khan, M. F.; Iqbal, M. Z.; Eom, J.; Iqbal, M. W. Improving the Electrical Properties of Graphene Layers by Chemical Doping. *Sci. Technol. Adv. Mater.* **2014**, *15*, 055004.

(247) Shiozawa, H.; Pichler, T.; Kramberger, C.; Rummeli, M.; Batchelor, D.; Liu, Z.; Suenaga, K.; Kataura, H.; Silva, S. R. P. Screening the Missing Electron: Nanochemistry in Action. *Phys. Rev. Lett.* **2009**, *102*, 046804.

(248) Skákalová, V.; Kaiser, A. B.; Dettlaff-Weglikowska, U.; Hrnčariková, K.; Roth, S. Effect of Chemical Treatment on Electrical Conductivity, Infrared Absorption, and Raman Spectra of Single-Walled Carbon Nanotubes. *J. Phys. Chem. B* **2005**, *109*, 7174–7181.

(249) Ludbrook, B. M.; Levy, G.; Nigge, P.; Zonno, M.; Schneider, M.; Dvorak, D. J.; Veenstra, C. N.; Zhdanovich, S.; Wong, D.; Dosanjh, P.; et al. Evidence for Superconductivity in Li-Decorated Monolayer Graphene. *Proc. Natl. Acad. Sci. U. S. A.* **2015**, *112*, 11795–11799.

(250) Chapman, J.; Su, Y.; Howard, C. A.; Kundys, D.; Grigorenko, A. N.; Guinea, F.; Geim, A. K.; Grigorieva, I. V.; Nair, R. R. Superconductivity in Ca-Doped Graphene Laminates. *Sci. Rep.* **2016**, *6*, 23254.

(251) Palstra, T. T. M. Fullerides: Superconductivity at the Limit. *Nat. Mater.* **2008**, *7*, 350–351.

(252) Bao, Z.; Batlogg, B.; Berg, S.; Dodabalapur, A.; Haddon, R. C.; Hwang, H.; Kloc, C.; Meng, H.; Schön, J. H. Retraction. *Science* **2002**, *298*, 961.

(253) Palstra, T. T. M.; Zhou, O.; Iwasa, Y.; Sulewski, P. E.; Fleming, R. M.; Zegarski, B. R. Superconductivity at 40 K in Cesium Doped C₆₀. *Solid State Commun.* **1995**, *93*, 327–330.

(254) Baskaran, G. Impurity Band Mott Insulators: A New Route to High T_c Superconductivity. *Sci. Technol. Adv. Mater.* **2008**, *9*, 044104.

(255) Bhaumik, A.; Sachan, R.; Gupta, S.; Narayan, J. Discovery of High-Temperature Superconductivity (T_c = 55 K) in B-Doped Q-Carbon. *ACS Nano* **2017**, *11*, 11915–11922.

(256) Liang, H.; Ma, X.; Yang, Z.; Wang, P.; Zhang, X.; Ren, Z.; Xue, M.; Chen, G. Emergence of Superconductivity in Doped Glassy-Carbon. *Carbon* **2016**, *99*, 585–590.

(257) Hansson, A.; Stafström, S. Electronic Structure Calculations of Potassium-Intercalated Single-Walled Carbon Nanotubes. *Phys. Rev. B: Condens. Matter Mater. Phys.* **2005**, *72*, 125420.

(258) Izumida, W.; Milz, L.; Marganska, M.; Grifoni, M. Topology and Zero Energy Edge States in Carbon Nanotubes with Superconducting Pairing. *Phys. Rev. B: Condens. Matter Mater. Phys.* **2017**, *96*, 125414.

(259) Wong, C.; Lortz, R.; Buntov, E.; Kasimova, R.; Zatsopin, A. A Theoretical Quest for High Temperature Superconductivity on the Example of Low-Dimensional Carbon Structures. *Sci. Rep.* **2017**, *7*, 15815.

(260) Barnett, R.; Demler, E.; Kaxiras, E. Superconducting and Charge-Density Wave Instabilities in Ultrasmall-Radius Carbon Nanotubes. *Solid State Commun.* **2005**, *135*, 335–339.

(261) Shimizu, R.; Sugawara, K.; Kanetani, K.; Iwaya, K.; Sato, T.; Takahashi, T.; Hitosugi, T. Charge-Density Wave in Ca-Intercalated Bilayer Graphene Induced by Commensurate Lattice Matching. *Phys. Rev. Lett.* **2015**, *114*, 146103.

(262) Dragin, F.; Pénicaud, A.; Iurlo, M.; Marcaccio, M.; Paolucci, F.; Anglaret, E.; Martel, R. Raman Doping Profiles of Polyelectrolyte SWCNTs in Solution. *ACS Nano* **2011**, *5*, 9892–9897.

(263) Pisana, S.; Lazzeri, M.; Casiraghi, C.; Novoselov, K. S.; Geim, A. K.; Ferrari, A. C.; Mauri, F. Breakdown of the Adiabatic Born–Oppenheimer Approximation in Graphene. *Nat. Mater.* **2007**, *6*, 198–201.

(264) Murray, R. W. Nanoelectrochemistry: Metal Nanoparticles, Nanoelectrodes, and Nanopores. *Chem. Rev.* **2008**, *108*, 2688–2720.

(265) Liu, X.; Pichler, T.; Knupfer, M.; Fink, J.; Kataura, H. Electronic Properties of FeCl₃-Intercalated Single-Wall Carbon Nanotubes. *Phys. Rev. B: Condens. Matter Mater. Phys.* **2004**, *70*, 205405.

(266) Heller, I.; Kong, J.; Williams, K. A.; Dekker, C.; Lemay, S. G. Electrochemistry at Single-Walled Carbon Nanotubes: The Role of Band Structure and Quantum Capacitance. *J. Am. Chem. Soc.* **2006**, *128*, 7353–7359.

(267) Senokos, E.; Reguero, V.; Palma, J.; Vilatela, J. J.; Marcilla, R. Macroscopic fibres of CNTs as electrodes for multifunctional electric double layer capacitors: from quantum capacitance to device performance. *Nanoscale* **2016**, *8* (6), 3620–3628.

(268) Ferrari, A. C. Raman Spectroscopy of Graphene and Graphite: Disorder, Electron–Phonon Coupling, Doping and Nonadiabatic Effects. *Solid State Commun.* **2007**, *143*, 47–57.

(269) Mak, K.; Ju, L.; Wang, F.; Heinz, T. F. Optical Spectroscopy of Graphene: From the Far Infrared to the Ultraviolet. *Solid State Commun.* **2012**, *152*, 1341–1349.

(270) Jensen, S. A.; Ulbricht, R.; Narita, A.; Feng, X.; Müllen, K.; Hertel, T.; Turchinovich, D.; Bonn, M. Ultrafast Photoconductivity of Graphene Nanoribbons and Carbon Nanotubes. *Nano Lett.* **2013**, *13*, 5925–5930.

(271) Pichler, T.; Liu, X.; Knupfer, M.; Fink, J. Electronic Properties of Intercalated Single-Wall Carbon Nanotubes and C₆₀ Peapods. *New J. Phys.* **2003**, *5*, 156.

(272) Yang, L. Excitonic Effects on Optical Absorption Spectra of Doped Graphene. *Nano Lett.* **2011**, *11*, 3844–3847.

(273) Heath, G. A.; McGrady, J. E.; Martin, R. L. Characterisation of the UV, Visible and Near-IR Spectra of the Fulleride Anions C₆₀^{1–}, C₆₀^{2–} and C₆₀^{3–}, and Theoretical Analysis of the Spectra of C₆₀¹⁺, C₆₀⁰, C₆₀^{1–}, C₆₀^{2–} and C₆₀^{3–} by Self Consistent Field- α -Scattered-Wave (Scf- α -sw) Calculations. *J. Chem. Soc., Chem. Commun.* **1992**, 1272–1274.

(274) Chen, P.; Wu, X.; Lin, J.; Tan, K. High H₂ Uptake by Alkali-Doped Carbon Nanotubes under Ambient Pressure and Moderate Temperatures. *Science* **1999**, *285*, 91–93.

(275) Sfeir, M. Y.; Misewich, J. A.; Rosenblatt, S.; Wu, Y.; Voisin, C.; Yan, H.; Berciaud, S.; Heinz, T. F.; Chandra, B.; Caldwell, R.; et al. Infrared Spectra of Individual Semiconducting Single-Walled Carbon

- Nanotubes: Testing the Scaling of Transition Energies for Large Diameter Nanotubes. *Phys. Rev. B: Condens. Matter Mater. Phys.* **2010**, *82*, 195424.
- (276) Saitta, A. M.; Lazzeri, M.; Calandra, M.; Mauri, F. Giant Nonadiabatic Effects in Layer Metals: Raman Spectra of Intercalated Graphite Explained. *Phys. Rev. Lett.* **2008**, *100*, 226401.
- (277) Das, A.; Pisana, S.; Chakraborty, B.; Piscanec, S.; Saha, S. K.; Waghmare, U. V.; Novoselov, K. S.; Krishnamurthy, H. R.; Geim, A. K.; Ferrari, A. C.; et al. Monitoring Dopants by Raman Scattering in an Electrochemically Top-Gated Graphene Transistor. *Nat. Nanotechnol.* **2008**, *3*, 210–215.
- (278) Mohiuddin, T. M. G.; Lombardo, A.; Nair, R. R.; Bonetti, A.; Savini, G.; Jalil, R.; Bonini, N.; Basko, D. M.; Galotis, C.; Marzari, N.; et al. Uniaxial Strain in Graphene by Raman Spectroscopy: G Peak Splitting, Gruneisen Parameters, and Sample Orientation. *Phys. Rev. B: Condens. Matter Mater. Phys.* **2009**, *79*, 205433.
- (279) Liu, Z.; Zhang, J.; Gao, B. Raman Spectroscopy of Strained Single-Walled Carbon Nanotubes. *Chem. Commun.* **2009**, 6902–6918.
- (280) Lee, J. E.; Ahn, G.; Shim, J.; Lee, Y. S.; Ryu, S. Optical Separation of Mechanical Strain from Charge Doping in Graphene. *Nat. Commun.* **2012**, *3*, 1024.
- (281) Cronin, S. B.; Swan, A. K.; Ünlü, M. S.; Goldberg, B. B.; Dresselhaus, M. S.; Tinkham, M. Measuring the Uniaxial Strain of Individual Single-Wall Carbon Nanotubes: Resonance Raman Spectra of Atomic-Force-Microscope Modified Single-Wall Nanotubes. *Phys. Rev. Lett.* **2004**, *93*, 167401.
- (282) Casiraghi, C. Doping Dependence of the Raman Peaks Intensity of Graphene Close to the Dirac Point. *Phys. Rev. B: Condens. Matter Mater. Phys.* **2009**, *80*, 233407.
- (283) Kukovecz, A.; Pichler, T.; Pfeiffer, R.; Kuzmany, H. Diameter Selective Charge Transfer in p- and n-Doped Single Wall Carbon Nanotubes Synthesized by the HiPCO Method. *Chem. Commun.* **2002**, *16*, 1730–1731.
- (284) Chacón-Torres, J. C.; Wirtz, L.; Pichler, T. Raman Spectroscopy of Graphite Intercalation Compounds: Charge Transfer, Strain, and Electron–Phonon Coupling in Graphene Layers. *Phys. Status Solidi B* **2014**, *251*, 2337–2355.
- (285) Dean, M. P.; Howard, C. A.; Saxena, S. S.; Ellerby, M. Nonadiabatic Phonons Within the Doped Graphene Layers of X C 6 Compounds. *Phys. Rev. B: Condens. Matter Mater. Phys.* **2010**, *81*, 045405.
- (286) Topsakal, M.; Ciraci, S. Static Charging of Graphene and Graphite Slabs. *Appl. Phys. Lett.* **2011**, *98*, 131908.
- (287) Paul, P.; Xie, Z.; Bau, R.; Boyd, P. D. W.; Reed, C. A. Ordered Structure of a Distorted C60- Fulleride Ion. *J. Am. Chem. Soc.* **1994**, *116*, 4145–4146.
- (288) Sun, G.; Kürti, J.; Kertesz, M.; Baughman, R. H. Dimensional Changes as a Function of Charge Injection in Single-Walled Carbon Nanotubes. *J. Am. Chem. Soc.* **2002**, *124*, 15076–15080.
- (289) Fedurco, M.; Olmstead, M. M.; Fawcett, R. W. Single-Crystal X-Ray Structure of C60.cntdot.6SbPh3. A Well-Ordered Structure of C60 and a New Fullerene Solvent. *Inorg. Chem.* **1995**, *34*, 390–392.
- (290) Pénicaud, A.; Drummond, C. Deconstructing Graphite: Graphenide Solutions. *Acc. Chem. Res.* **2013**, *46*, 129–137.
- (291) Howard, C. A.; Thompson, H.; Wasse, J. C.; Skipper, N. T. Formation of Giant Solvation Shells Around Fulleride Anions in Liquid Ammonia. *J. Am. Chem. Soc.* **2004**, *126*, 13228–13229.
- (292) Fogden, S.; Howard, C. A.; Heenan, R. K.; Skipper, N. T.; Shaffer, M. S. P. Scalable Method for the Reductive Dissolution, Purification, and Separation of Single-Walled Carbon Nanotubes. *ACS Nano* **2012**, *6*, 54–62.
- (293) Howard, C. A.; Wasse, J. C.; Skipper, N. T.; Thompson, H.; Soper, A. K. The Solvation Structure of Fulleride C60S- Anions in Potassium Ammonia Solution. *J. Phys. Chem. C* **2007**, *111*, 5640–5647.
- (294) Howard, C. A.; Skipper, N. T. Computer Simulations of Fulleride Anions in Metal-Ammonia Solutions. *J. Phys. Chem. B* **2009**, *113*, 3324–3332.
- (295) Diener, M. D.; Alford, J. M. Isolation and Properties of Small-Bandgap Fullerenes. *Nature* **1998**, *393*, 668–671.
- (296) Jiang, C.; Saha, A.; Martí, A. Carbon Nanotubides: An Alternative for Dispersion, Functionalization and Composites Fabrication. *Nanoscale* **2015**, *7*, 15037–15045.
- (297) Howard, C. A.; Wasse, J. C.; Skipper, N. T.; Thompson, H.; Soper, A. K. The Solvation Structure of Fulleride C60S-anions in Potassium Ammonia Solution. *J. Phys. Chem. C* **2007**, *111*, 5640–5647.
- (298) Bergin, S. D.; Sun, Z.; Rickard, D.; Streich, P. V.; Hamilton, J. P.; Coleman, J. N. Multicomponent Solubility Parameters for Single-Walled Carbon Nanotube-Solvent Mixtures. *ACS Nano* **2009**, *3*, 2340–2350.
- (299) Guan, J.; Martinez-Rubi, Y.; Dénommée, S.; Ruth, D.; Kingston, C.; Daroszewski, M.; Barnes, M.; Simard, B. About the Solubility of Reduced SWCNT in DMSO. *Nanotechnology* **2009**, *20*, 245701.
- (300) Tune, D. D.; Blanch, A. J.; Shearer, C. J.; Moore, K. E.; Pfohl, M.; Shapter, J. G.; Flavel, B. S. Aligned Carbon Nanotube Thin Films from Liquid Crystal Polyelectrolyte Inks. *ACS Appl. Mater. Interfaces* **2015**, *7*, 25857–25864.
- (301) Morishita, T.; Clancy, A. J.; Shaffer, M. S. P. Optimised Exfoliation Conditions Enhance Isolation and Solubility of Grafted Graphenes from Graphite Intercalation Compounds. *J. Mater. Chem. A* **2014**, *2*, 15022–15028.
- (302) Ghariab, D. H.; Gietman, S.; Malherbe, F.; Moulton, S. E. High Yield, Solid Exfoliation and Liquid Dispersion of Graphite Driven by a Donor-Acceptor Interaction. *Carbon* **2017**, *123*, 695–707.
- (303) Cullen, P. L.; Cox, K. M.; Bin Subhan, M. K.; Picco, L.; Payton, O. D.; Buckley, D. J.; Miller, T. S.; Hodge, S. A.; Skipper, N. T.; Tileli, V.; et al. Ionic Solutions of Two-Dimensional Materials. *Nat. Chem.* **2017**, *9*, 244–249.
- (304) Kovtyukhova, N. I.; Wang, Y.; Berkdemir, A.; Cruz-Silva, R.; Terrones, M.; Crespi, V. H.; Mallouk, T. E. Non-Oxidative Intercalation and Exfoliation of Graphite by Brønsted Acids. *Nat. Chem.* **2014**, *6*, 957–963.
- (305) Shih, C.-J.; Vijayaraghavan, A.; Krishnan, R.; Sharma, R.; Han, J.-H.; Ham, M.-H.; Jin, Z.; Lin, S.; Paulus, G. L.; Reuel, N. F.; et al. Bi- and Trilayer Graphene Solutions. *Nat. Nanotechnol.* **2011**, *6*, 439–445.
- (306) Jiang, C.; Peng, Z.; de los Reyes, C.; Young, C. C.; Tsentalovich, D. E.; Jamali, V.; Ajayan, P. M.; Tour, J. M.; Pasquali, M.; Martí, A. A. Increased Solubility and Fiber Spinning of Graphenide Dispersions Aided by Crown-Ethers. *Chem. Commun.* **2017**, *53*, 1498–1501.
- (307) Ujihara, M.; Mahmoud Ahmed, M. M.; Imae, T.; Yamauchi, Y. Massive-Exfoliation of Magnetic Graphene from Acceptor-Type GIC by Long-Chain Alkyl Amine. *J. Mater. Chem. A* **2014**, *2*, 4244–4250.
- (308) Zhou, W.; Fischer, J. E.; Heiney, P. A.; Fan, H.; Davis, V. A.; Pasquali, M.; Smalley, R. E. Single-Walled Carbon Nanotubes in Supercid: X-Ray and Calorimetric Evidence for Partially Ordered H2SO4. *Phys. Rev. B: Condens. Matter Mater. Phys.* **2005**, *72*, 045440.
- (309) Bepete, G.; Anglaret, E.; Ortolani, L.; Morandi, V.; Huang, K.; Pénicaud, A.; Drummond, C. Surfactant-Free Single-Layer Graphene in Water. *Nat. Chem.* **2017**, *9*, 347–352.
- (310) Ramesh, S.; Ericson, L. M.; Davis, V. A. Dissolution of Pristine Single Walled Carbon Nanotubes in Supercacids by Direct Protonation. *J. Phys. Chem. B* **2004**, *108*, 8794–8798.
- (311) Parra-Vasquez, N. G.; Behabtu, N.; Green, M. J.; Pint, C. L.; Young, C. C.; Schmidt, J.; Kesselman, E.; Goyal, A.; Ajayan, P. M.; Cohen, Y.; et al. Spontaneous Dissolution of Ultralong Single- and Multiwalled Carbon Nanotubes. *ACS Nano* **2010**, *4*, 3969–3978.
- (312) Davis, V. A.; Parra-Vasquez, A. N. G.; Green, M. J.; Rai, P. K.; Behabtu, N.; Prieto, V.; Booker, R. D.; Schmidt, J.; Kesselman, E.; Zhou, W.; et al. True Solutions of Single-Walled Carbon Nanotubes for Assembly into Macroscopic Materials. *Nat. Nanotechnol.* **2009**, *4*, 830–834.
- (313) Rai, P. K.; Parra-Vasquez, A. N. G.; Chattopadhyay, J.; Pinnick, R. A.; Liang, F.; Sadana, A. K.; Hauge, R. H.; Billups, W. E.;

- Pasquali, M. Dispersions of Functionalized Single-Walled Carbon Nanotubes in Strong Acids: Solubility and Rheology. *J. Nanosci. Nanotechnol.* **2007**, *7*, 3378–3385.
- (314) Kelly, K.; Billups, W. Synthesis of Soluble Graphite and Graphene. *Acc. Chem. Res.* **2013**, *46*, 4–13.
- (315) Kitagawa, T.; Takeuchi, K. Monofunctionalized C60 Ions: Their Generation, Stability, and Reactions. *Bull. Chem. Soc. Jpn.* **2001**, *74*, 785–800.
- (316) Bepete, G.; Hof, F.; Huang, K.; Kampioti, K.; Anglaret, E.; Drummond, C.; Pénicaud, A. "Eau de Graphene" from a KC8 Graphite Intercalation Compound Prepared by a Simple Mixing of Graphite and Molten Potassium. *Phys. Phys. Status Solidi RRL* **2016**, *10*, 895–899.
- (317) Bepete, G.; Pénicaud, A.; Drummond, C.; Anglaret, E. Raman Signatures of Single Layer Graphene Dispersed in Degassed Water "Eau de Graphene". *J. Phys. Chem. C* **2016**, *120*, 28204–28214.
- (318) Wang, S.; Wang, C.; Ji, X.; Lin, M. Surfactant- and Sonication-Free Exfoliation Approach to Aqueous Graphene Dispersion. *Mater. Lett.* **2018**, *217*, 67–70.
- (319) Britz, D. A.; Khlbystov, A. N. Noncovalent Interactions of Molecules with Single Walled Carbon Nanotubes. *Chem. Soc. Rev.* **2006**, *35*, 637–659.
- (320) Bilalis, P.; Katsigiannopoulos, D.; Avgeropoulos, A.; Sakellariou, G. Non-Covalent Functionalization of Carbon Nanotubes with Polymers. *RSC Adv.* **2014**, *4*, 2911–2934.
- (321) Diederich, F.; Thilgen, C. Covalent Fullerene Chemistry. *Science* **1996**, *271*, 317–324.
- (322) Thilgen, C.; Diederich, F. Structural Aspects of Fullerene Chemistry - A Journey through Fullerene Chirality. *Chem. Rev.* **2006**, *106*, 5049–5135.
- (323) Singh, P.; Campidelli, S.; Giordani, S.; Bonifazi, D.; Bianco, A.; Prato, M. Organic Functionalisation and Characterisation of Single-Walled Carbon Nanotubes. *Chem. Soc. Rev.* **2009**, *38*, 2214–2230.
- (324) Kim, S. W.; Kim, T.; Kim, Y. S.; Choi, H. S.; Lim, H. J.; Yang, S. J.; Park, C. R. Surface Modifications for the Effective Dispersion of Carbon Nanotubes in Solvents and Polymers. *Carbon* **2012**, *50*, 3–33.
- (325) Kuila, T.; Bose, S.; Mishra, A.; Khanra, P.; Kim, N.; Lee, J. Chemical Functionalization of Graphene and Its Applications. *Prog. Mater. Sci.* **2012**, *57*, 1061–1105.
- (326) Bottari, G.; Herranz, M.; Wibmer, L.; Volland, M.; Rodríguez-Pérez, L.; Guldi, D. M.; Hirsch, A.; Martín, N.; D'Souza, F.; Torres, T. Chemical Functionalization and Characterization of Graphene-Based Materials. *Chem. Soc. Rev.* **2017**, *46*, 4464–4500.
- (327) Hummers, W. S.; Offeman, R. E. Preparation of Graphitic Oxide. *J. Am. Chem. Soc.* **1958**, *80*, 1339–1339.
- (328) Guerrero-Contreras, J.; Caballero-Briones, F. Graphene Oxide Powders with Different Oxidation Degree, Prepared by Synthesis Variations of the Hummers Method. *Mater. Chem. Phys.* **2015**, *153*, 209–220.
- (329) Hu, H.; Zhao, B.; Itkis, M. E.; Haddon, R. C. Nitric Acid Purification of Single-Walled Carbon Nanotubes. *J. Phys. Chem. B* **2003**, *107*, 13838–13842.
- (330) Chen, B.-H.; Canteenwala, T.; Patil, S.; Chiang, L. Y. Rapid Sulfation Kinetics of Fullerene in Oleum-Oxide Mixtures. *Synth. Commun.* **2001**, *31*, 1659–1667.
- (331) Park, J.; Yan, M. Covalent Functionalization of Graphene with Reactive Intermediates. *Acc. Chem. Res.* **2013**, *46*, 181–189.
- (332) Stephenson, J. J.; Hudson, J. L.; Leonard, A. D.; Price, K. B.; Tour, J. M. Repetitive Functionalization of Water-Soluble Single-Walled Carbon Nanotubes. Addition of Acid-Sensitive Addends. *Chem. Mater.* **2007**, *19*, 3491–3498.
- (333) Choi, H.; Shim, M.; Bangsaruntip, S.; Dai, H. Spontaneous Reduction of Metal Ions on the Sidewalls of Carbon Nanotubes. *J. Am. Chem. Soc.* **2002**, *124*, 9058–9059.
- (334) Chattopadhyay, J.; Sadana, A. K.; Liang, F.; Beach, J. M.; Xiao, Y.; Hauge, R. H.; Billups, W. E. Carbon Nanotube Salts. Arylation of Single-Wall Carbon Nanotubes. *Org. Lett.* **2005**, *7*, 4067–4069.
- (335) Mukherjee, A.; Combs, R.; Chattopadhyay, J.; Abmayr, D. W.; Engel, P. S.; Billups, W. E. Attachment of Nitrogen and Oxygen Centered Radicals to Single-Walled Carbon Nanotube Salts. *Chem. Mater.* **2008**, *20*, 7339–7343.
- (336) Syrgiannis, Z.; Parola, L. V.; Hadad, C.; La Parola, V.; Lucio, M.; Vázquez, E.; Prato, M. An Atom-Economical Approach to Functionalized Single Walled Carbon Nanotubes: Reaction with Disulfides. *Angew. Chem., Int. Ed.* **2013**, *52*, 6480–6483.
- (337) Knirsch, K. C.; Hof, F.; Lloret, V.; Mundloch, U.; Hauke, F.; Hirsch, A. Topology Driven Reductive Silylation of Synthetic Carbon Allotropes. *J. Am. Chem. Soc.* **2016**, *138*, 15642–15647.
- (338) Martínez-Rubi, Y.; Ashrafi, B.; Guan, J.; Kingston, C.; Johnston, A.; Simard, B.; Mirjalili, V.; Hubert, P.; Deng, L.; Young, R. Toughening of Epoxy Matrices with Reduced Single-Walled Carbon Nanotubes. *ACS Appl. Mater. Interfaces* **2011**, *3*, 2309–2317.
- (339) Rubio, N.; Au, H.; Leese, H. S.; Hu, S.; Clancy, A. J.; Shaffer, M. S. Grafting from Versus Grafting to Approaches for the Functionalization of Graphene Nanoplatelets with Poly (Methyl Methacrylate). *Macromolecules* **2017**, *50*, 7070–7079.
- (340) Liang, F.; Beach, J. M.; Kobashi, K.; Sadana, A. K.; Vega-Cantu, Y. I.; Tour, J. M.; Billups, W. E. Situ Polymerization Initiated by Single-Walled Carbon Nanotube Salts. *Chem. Mater.* **2006**, *18*, 4764–4767.
- (341) Hof, F.; Hauke, F.; Hirsch, A. Brominated Single Walled Carbon Nanotubes as Versatile Precursors for Covalent Sidewall Functionalization. *Chem. Commun.* **2014**, *50*, 6582–6584.
- (342) Au, H.; Rubio, N.; Shaffer, M. S. Brominated Graphene as a Versatile Precursor for Multifunctional Grafting. *Chem. Sci.* **2018**, *9*, 209–217.
- (343) Fukuzumi, S.; Suenobu, T.; Hirasaka, T.; Arakawa, R.; Kadish, K. M. Formation of C60 Adducts with Two Different Alkyl Groups via Combination of Electron Transfer and SN2 Reactions. *J. Am. Chem. Soc.* **1998**, *120*, 9220–9227.
- (344) Bohme, D. K. Buckminsterfullerene Cations: New Dimensions in Gas-Phase Ion Chemistry. *Mass Spectrom. Rev.* **2009**, *28*, 672–693.
- (345) Mangold, K.-M.; Kutner, W.; Dunsch, L.; Fröhner, J. Derivatization of Fullerenes by Electrosynthesis. *Synth. Met.* **1996**, *77*, 73–76.
- (346) Bahr, J. L.; Yang, J.; Kosynkin, D. V.; Bronikowski, M. J.; Smalley, R. E.; Tour, J. M. Functionalization of Carbon Nanotubes by Electrochemical Reduction of Aryl Diazonium Salts: A Bucky Paper Electrode. *J. Am. Chem. Soc.* **2001**, *123*, 6536–6542.
- (347) Gebhardt, B.; Syrgiannis, Z.; Backes, C.; Graupner, R.; Hauke, F.; Hirsch, A. Carbon Nanotube Sidewall Functionalization with Carbonyl Compounds - Modified Birch Conditions Vs the Organometallic Reduction Approach. *J. Am. Chem. Soc.* **2011**, *133*, 7985–7995.
- (348) Hof, F.; Schäfer, R. A.; Weiss, C.; Hauke, F.; Hirsch, A. Novel λ 3-Iodane-Based Functionalization of Synthetic Carbon Allotropes (SCAs)—Common Concepts and Quantification of the Degree of Addition. *Chem. - Eur. J.* **2014**, *20*, 16644–16651.
- (349) Pekker, S.; Salvétat, P. J.; Jakab, E.; Bonard, M. J.; Forró, L. Hydrogenation of Carbon Nanotubes and Graphite in Liquid Ammonia. *J. Phys. Chem. B* **2001**, *105*, 7938–7943.
- (350) Bjerglund, E.; Kongsfelt, M.; Shimizu, K.; Jensen, B. B.; Koefoed, L.; Ceccato, M.; Skrydstrup, T.; Pedersen, S. U.; Daasbjerg, K. Controlled Electrochemical Carboxylation of Graphene to Create a Versatile Chemical Platform for Further Functionalization. *Langmuir* **2014**, *30*, 6622–6628.
- (351) Englert, J. M.; Vecera, P.; Knirsch, K. C.; Schäfer, R. A.; Hauke, F.; Hirsch, A. Scanning-Raman-Microscopy for the Statistical Analysis of Covalently Functionalized Graphene. *ACS Nano* **2013**, *7*, 5472–5482.
- (352) Hof, F.; Bosch, S.; Englert, J. M.; Hauke, F.; Hirsch, A. Statistical Raman Spectroscopy: A Method for the Characterization of Covalently Functionalized Single-Walled Carbon Nanotubes. *Angew. Chem., Int. Ed.* **2012**, *51*, 11727–11730.

- (353) Eckmann, A.; Felten, A.; Mishchenko, A.; Britnell, L.; Krupke, R.; Novoselov, K. S.; Casiraghi, C. Probing the Nature of Defects in Graphene by Raman Spectroscopy. *Nano Lett.* **2012**, *12*, 3925–3930.
- (354) Dresselhaus, M.; Jorio, A.; Souza Filho, A.; Saito, R. Defect Characterization in Graphene and Carbon Nanotubes Using Raman Spectroscopy. *Philos. Trans. R. Soc., A* **2010**, *368*, 5355–5377.
- (355) Salzmann, C. G.; Chu, B. T.; Tobias, G.; Llewellyn, S. A.; Green, M. L. Quantitative Assessment of Carbon Nanotube Dispersions by Raman Spectroscopy. *Carbon* **2007**, *45*, 907–912.
- (356) Clancy, A. J.; Serginson, J. M.; Greenfield, J. L.; Shaffer, M. S. Systematic Comparison of Single-Walled Carbon Nanotube/Poly-(Vinyl Acetate) Graft-to Reactions. *Polymer* **2017**, *133*, 263–271.
- (357) Wang, Y.; Malhotra, S. V.; Owens, F. J.; Iqbal, Z. Electrochemical Nitration of Single-Wall Carbon Nanotubes. *Chem. Phys. Lett.* **2005**, *407*, 68–72.
- (358) Osason, B. D.; Bélanger, D. Functionalization of Graphene Sheets by the Diazonium Chemistry During Electrochemical Exfoliation of Graphite. *Carbon* **2017**, *111*, 83–93.
- (359) Voiry, D.; Roubeau, O.; Pénicaud, A. Stoichiometric Control of Single Walled Carbon Nanotubes Functionalization. *J. Mater. Chem.* **2010**, *20*, 4385–4391.
- (360) Deng, S.; Zhang, Y.; Brozena, A.; Mayes, M.; Banerjee, P.; Chiou, W.-A.; Rubloff, G.; Schatz, G.; Wang, Y. Confined Propagation of Covalent Chemical Reactions on Single-Walled Carbon Nanotubes. *Nat. Commun.* **2011**, *2*, 382.
- (361) Chattopadhyay, J.; Chakraborty, S.; Mukherjee, A.; Wang, R.; Engel, P. S.; Billups, W. E. SET Mechanism in the Functionalization of Single-Walled Carbon Nanotubes. *J. Phys. Chem. C* **2007**, *111*, 17928–17932.
- (362) Sargent, G.; Lux, G. Reactions of Aromatic Radical Anions. III. Evidence for an Alkyl Radical-Radical Anion Combination Mechanism for Alkylation of Sodium Naphthalenide with Alkyl Halides. *J. Am. Chem. Soc.* **1968**, *90*, 7160–7162.
- (363) Schmidt, G.; Gallon, S.; Esnouf, S.; Bourgoin, J. P.; Chenevier, P. Mechanism of the Coupling of Diazonium to Single-Walled Carbon Nanotubes and Its Consequences. *Chem. - Eur. J.* **2009**, *15*, 2101–2110.
- (364) Menzel, R.; Tran, M. Q.; Menner, A.; Kay, C. W. M.; Bismarck, A.; Shaffer, M. S. P. A Versatile, Solvent-Free Methodology for the Functionalisation of Carbon Nanotubes. *Chem. Sci.* **2010**, *1*, 603–608.
- (365) Gao, Y.; Chen, H.; Ge, J.; Zhao, J.; Li, Q.; Tang, J.; Cui, Y.; Chen, L. Direct Intertube Cross-Linking of Carbon Nanotubes at Room Temperature. *Nano Lett.* **2016**, *16*, 6541–6547.
- (366) Cleary, J. A.; Mubarak, M. S.; Vieira, K. L.; Anderson, M. R.; Peters, D. G. Electrochemical Reduction of Alkyl Halides at Vitreous Carbon Cathodes in Dimethylformamide. *J. Electroanal. Chem. Interfacial Electrochem.* **1986**, *198*, 107–124.
- (367) Coleman, J. N.; Cadek, M.; Blake, R.; Nicolosi, V.; Ryan, K. P.; Belton, C.; Fonseca, A.; Nagy, J. B.; Gun'ko, Y. K.; Blau, W. J. High Performance Nanotube-Reinforced Plastics: Understanding the Mechanism of Strength Increase. *Adv. Funct. Mater.* **2004**, *14*, 791–798.
- (368) Blake, R.; Gun'ko, Y. K.; Coleman, J.; Cadek, M.; Fonseca, A.; Nagy, J. B.; Blau, W. J. A Generic Organometallic Approach Toward Ultra-Strong Carbon Nanotube Polymer Composites. *J. Am. Chem. Soc.* **2004**, *126*, 10226–10227.
- (369) Lambert, F. L.; Ingall, G. B. Voltammetry of Organic Halogen Compounds. IV. The Reduction of Organic Chlorides at the Vitreous (Glassy) Carbon Electrode. *Tetrahedron Lett.* **1974**, *15*, 3231–3234.
- (370) Leese, H. S.; Govada, L.; Saridakis, E.; Khurshid, S.; Menzel, R.; Morishita, T.; Clancy, A. J.; White, E. R.; Chayen, N. E.; Shaffer, M. S. P. Reductively PEGylated Carbon Nanomaterials and Their Use to Nucleate 3D Protein Crystals: A Comparison of Dimensionality. *Chem. Sci.* **2016**, *7*, 2916–2923.
- (371) Gebhardt, B.; Graupner, R.; Hauke, F.; Hirsch, A. A Novel Diameter Selective Functionalization of Swcnts with Lithium Alkynylides. *Eur. J. Org. Chem.* **2010**, *2010*, 1494–1501.
- (372) Chakraborty, S.; Chattopadhyay, J.; Guo, W.; Billups, W. E. Functionalization of Potassium Graphite. *Angew. Chem., Int. Ed.* **2007**, *46*, 4486–4488.
- (373) Maeda, Y.; Kato, T.; Hasegawa, T.; Kako, M.; Akasaka, T.; Lu, J.; Nagase, S. Two-Step Alkylation of Single-Walled Carbon Nanotubes: Substituent Effect on Sidewall Functionalization. *Org. Lett.* **2010**, *12*, 996–999.
- (374) Osuna, S. I.; Torrent-Sucarrat, M.; Sola, M.; Geerlings, P.; Ewels, C. P.; Lier, G. V. Reaction Mechanisms for Graphene and Carbon Nanotube Fluorination. *J. Phys. Chem. C* **2010**, *114*, 3340–3345.
- (375) Van Lier, G.; Ewels, C. P.; Zuliani, F.; De Vita, A.; Charlier, J.-C. Theoretical Analysis of Fluorine Addition to Single-Walled Carbon Nanotubes: Functionalization Routes and Addition Patterns. *J. Phys. Chem. B* **2005**, *109*, 6153–6158.
- (376) de Gennes, P. G. Conformations of Polymers Attached to an Interface. *Macromolecules* **1980**, *13*, 1069–1075.
- (377) Viswanathan, G.; Chakrapani, N.; Yang, H.; Wei, B.; Chung, H.; Cho, K.; Ryu, C. Y.; Ajayan, P. M. Single-Step in Situ Synthesis of Polymer-Grafted Single-Wall Nanotube Composites. *J. Am. Chem. Soc.* **2003**, *125*, 9258–9259.
- (378) Ashrafi, B.; Backman, D.; Johnston, A.; Martinez-Rubi, Y.; Simard, B. Effects of SWCNTs on Mechanical and Thermal Performance of Epoxy at Elevated Temperatures. *J. Mater. Sci.* **2013**, *48*, 7664–7672.
- (379) Chen, S.; Chen, D.; Wu, G. Grafting of Poly(tBA) and PtBA-b-PMMA onto the Surface of SWNTs Using Carbanions as the Initiator. *Macromol. Rapid Commun.* **2006**, *27*, 882–887.
- (380) Hodge, S. A.; Buckley, D. J.; Yau, H.; Skipper, N. T.; Howard, C. A.; Shaffer, M. S. P. Chemical Routes to Discharging Graphenides. *Nanoscale* **2017**, *9*, 3150–3158.
- (381) Wei, X.; Wu, M.; Qi, L.; Xu, Z. Selective Solution-Phase Generation and Oxidation Reaction of C₆₀ n-(n= 1, 2) and Formation of an Aqueous Colloidal Solution of C₆₀. *J. Chem. Soc., Perkin Trans. 2* **1997**, *2*, 1389–1394.
- (382) Zhao, W.; Li, Y.; Chen, L.; Liu, Z.; Huang, Y.; Zhao, Z. Metal Vapor Synthesis of Air-Sensitive Transition Metal Fullerenes: Evidence of IR Spectra. *Solid State Commun.* **1994**, *92*, 313–317.
- (383) Stinchcombe, J.; Penicaud, A.; Bhayrappa, P.; Boyd, P. D.; Reed, C. A. Buckminsterfulleride (1-) Salts: Synthesis, EPR, and the Jahn-Teller Distortion of C₆₀. *J. Am. Chem. Soc.* **1993**, *115*, 5212–5217.
- (384) Ebert, L. B.; Mills, D. R.; Garcia, A. R.; Scanlon, J. C. More on the Reaction of Graphite/Potassium with Water. *Mater. Res. Bull.* **1985**, *20*, 1453–1460.
- (385) Vecera, P.; Holzwarth, J.; Edlhalhammer, K. F.; Mundloch, U.; Peterlik, H.; Hauke, F.; Hirsch, A. Solvent-Driven Electron Trapping and Mass Transport in Reduced Graphites to Access Perfect Graphene. *Nat. Commun.* **2016**, *7*, 12411.
- (386) Rashkov, I.; Panayotov, I.; Shishkova, V. Reduction of Aromatic Compounds by Potassium-Graphite Intercalation Compounds. *Carbon* **1979**, *17*, 103–108.
- (387) Joseph, C.; Kuppuswamy, S.; Lynch, V. M.; Rose, M. J. FeS₂Mo Cluster with Iron-Carbide and Molybdenum-Carbide Bonding Motifs: Structure and Selective Alkyne Reductions. *Inorg. Chem.* **2018**, *57*, 20–23.
- (388) Auerhammer, D.; Arrowsmith, M.; Bissinger, P.; Braunschweig, H.; Dellermann, T.; Kupfer, T.; Lenczyk, C.; Roy, D. K.; Schäfer, M.; Schneider, C. Increasing the Reactivity of Diborenes: Derivatization of NHC-Supported Dithienyldiborenes with Electron-Donor Groups. *Chem. - Eur. J.* **2018**, *24*, 266–273.
- (389) Kroc, M. A.; Prajapati, A.; Wink, D. J.; Anderson, L. L. Cascade Synthesis of 3-Functionalized Indoles from Nitrones and Their Conversion to Cycloheptanone-Fused Indoles. *J. Org. Chem.* **2018**, *83*, 1085–1094.
- (390) Bayazit, M. K.; Hodge, S. A.; Clancy, A. J.; Menzel, R.; Chen, S.; Shaffer, M. S. P. Carbon Nanotube Anions for the Preparation of Gold Nanoparticle-Nanocarbon Hybrids. *Chem. Commun.* **2016**, *52*, 1934–1937.

- (391) Wang, Z.; Shi, Z.; Gu, Z. Synthesis of Single-Walled Carbon Nanotube/Metal Nanoparticle Hybrid Materials from Potassium-Filled Nanotubes. *Carbon* **2010**, *48*, 443–446.
- (392) Halim, M.; Kennedy, R. D.; Suzuki, M.; Khan, S. I.; Diaconescu, P. L.; Rubin, Y. Complexes of Gold (I), Silver (I), and Copper (I) with Pentaaryl [60] Fullerides. *J. Am. Chem. Soc.* **2011**, *133*, 6841–6851.
- (393) Wang, H.; Feng, Q.; Cheng, Y.; Yao, Y.; Wang, Q.; Li, K.; Schwingenschlög, U.; Zhang, X. X.; Yang, W. Atomic Bonding Between Metal and Graphene. *J. Phys. Chem. C* **2013**, *117*, 4632–4638.
- (394) Harris, J. M.; Headrick, R. J.; Semler, M. R.; Fagan, J. A.; Pasquali, M.; Hobbie, E. K. Impact of SWCNT Processing on Nanotube-Silicon Heterojunctions. *Nanoscale* **2016**, *8*, 7969–7977.
- (395) Verway, E. J. W. Theory of the Stability of Lyophobic Colloids. *J. Phys. Colloid Chem.* **1947**, *51*, 631–636.
- (396) Oosawa, F. *Polyelectrolytes*; M. Dekker, 1971.
- (397) Manning, G. S. Limiting Laws and Counterion Condensation in Polyelectrolyte Solutions. *Biophys. Chem.* **1978**, *9*, 65–70.
- (398) Voiry, D.; Drummond, C.; Penicaud, A. Portrait of Carbon Nanotube Salts as Soluble Polyelectrolytes. *Soft Matter* **2011**, *7*, 7998–8001.
- (399) Zhang, H.; Lerner, M. M. Preparation of Graphite Intercalation Compounds Containing Crown Ethers. *Inorg. Chem.* **2016**, *55*, 8281–8284.
- (400) Gebhardt, J.; Bosch, S.; Hof, F.; Hauke, F.; Hirsch, A.; Gorling, A. Selective Reduction of SWCNTs - Concepts and Insights. *J. Mater. Chem. C* **2017**, *5*, 3937–3947.
- (401) Ryu, S.; Lee, B.; Hong, S.; Jin, S.; Park, S.; Hong, S. H.; Lee, H. Salting-Out as a Scalable, In-Series Purification Method of Graphene Oxides from Microsheets to Quantum Dots. *Carbon* **2013**, *63*, 45–53.
- (402) De Marco, M. D. M.; Markoulidis, F.; Menzel, R.; Bawaked, S.; Mokhtar, M.; Al-Thabaiti, S.; Basahel, S.; Shaffer, M. Cross-Linked Single-Walled Carbon Nanotube Aerogel Electrodes via Reductive Coupling Chemistry. *J. Mater. Chem. A* **2016**, *4*, 5385–5389.
- (403) Bahr, J. L.; Tour, J. M. Covalent Chemistry of Single-Wall Carbon Nanotubes. *J. Mater. Chem.* **2002**, *12*, 1952–1958.
- (404) Bromley, L. A. Thermodynamic Properties of Strong Electrolytes in Aqueous Solutions. *AIChE J.* **1973**, *19*, 313–320.
- (405) Crescenzi, V.; Quadrioglio, F.; Delben, F. Calorimetric Investigation of Poly (Methacrylic Acid) and Poly (Acrylic Acid) in Aqueous Solution. *J. Polym. Sci., Part B* **1972**, *10*, 357–368.
- (406) Jiang, C.; Saha, A.; Xiang, C.; Young, C.; Tour, J.; Pasquali, M.; Marti, A. Increased Solubility, Liquid-Crystalline Phase, and Selective Functionalization of Single-Walled Carbon Nanotube Polyelectrolyte Dispersions. *ACS Nano* **2013**, *7*, 4503–4510.
- (407) Maluanguant, T.; Bui, G. T.; Huntington, B. A.; Lerner, M. M. Preparation of a Homologous Series of Graphite Alkylamine Intercalation Compounds Including an Unusual Parallel Bilayer Intercalate Arrangement. *Chem. Mater.* **2011**, *23*, 1091–1095.
- (408) Sirisaksoontorn, W.; Adenuga, A. A.; Remcho, V. T.; Lerner, M. M. Preparation and Characterization of a Tetrabutylammonium Graphite Intercalation Compound. *J. Am. Chem. Soc.* **2011**, *133*, 12436–12438.
- (409) Silvera Batista, C. A.; Larson, R. G.; Kotov, N. A. Nonadditivity of Nanoparticle Interactions. *Science* **2015**, *350*, 1242477.
- (410) Zobel, M.; Neder, R. B.; Kimber, S. A. Universal Solvent Restructuring Induced by Colloidal Nanoparticles. *Science* **2015**, *347*, 292–294.
- (411) Thompson, H.; Wasse, J. C.; Skipper, N. T.; Hayama, S.; Bowron, D. T.; Soper, A. K. Structural Studies of Ammonia and Metallic Lithium—Ammonia Solutions. *J. Am. Chem. Soc.* **2003**, *125*, 2572–2581.
- (412) Davis, V.; Ericson, L.; Parra-Vasquez, A.; Fan, H.; Wang, Y.; Smalley, R.; Pasquali, M.; Prieto, V.; Longoria, J. A.; Ramesh, S.; et al. Phase Behavior and Rheology of SWNTs in Superacids. *Macromolecules* **2004**, *37*, 154–160.
- (413) Zhang, S.; Kumar, S. Carbon Nanotubes as Liquid Crystals. *Small* **2008**, *4*, 1270–1283.
- (414) Zhang, X.; Hsu, C. H.; Ren, X.; Gu, Y.; Song, B.; Sun, H. J.; Yang, S.; Chen, E.; Tu, Y.; Li, X.; et al. Supramolecular [60]Fullerene Liquid Crystals Formed By Self-Organized Two-Dimensional Crystals. *Angew. Chem., Int. Ed.* **2015**, *54*, 114–117.
- (415) Sawamura, M.; Kawai, K.; Matsuo, Y.; Kanie, K.; Kato, T.; Nakamura, E. Stacking of Conical Molecules with a Fullerene Apex into Polar Columns in Crystals and Liquid Crystals. *Nature* **2002**, *419*, 702–705.
- (416) Yadav, S. P.; Singh, S. Carbon Nanotube Dispersion in Nematic Liquid Crystals: An Overview. *Prog. Mater. Sci.* **2016**, *80*, 38–76.
- (417) Liu, Y.; Xu, Z.; Gao, W.; Cheng, Z.; Gao, C. Graphene and Other 2D Colloids: Liquid Crystals and Macroscopic Fibers. *Adv. Mater.* **2017**, *29*, 1606794.
- (418) Onsager, L. The Effects of Shape on the Interaction of Colloidal Particles. *Ann. N. Y. Acad. Sci.* **1949**, *51*, 627–659.
- (419) Onsager, L. The Effects of Shape on the Interaction of Colloid Particles. *Ann. N. Y. Acad. Sci.* **1949**, *51*, 627–659.
- (420) Zakri, C.; Blanc, C.; Grelet, E.; Zamora-Ledezma, C.; Puech, N.; Anglaret, E.; Poulin, P. Liquid Crystals of Carbon Nanotubes and Graphene. *Philos. Trans. R. Soc., A* **2013**, *371*, 20120499.
- (421) Song, W.; Kinloch, I. A.; Windle, A. H. Nematic Liquid Crystallinity of Multiwall Carbon Nanotubes. *Science* **2003**, *302*, 1363–1363.
- (422) Papkov, S. P. In *Liquid Crystal Polymers I*; Springer, 1984.
- (423) Jiang, C.; Saha, A.; Young, C. C.; Hashim, D. P.; Ramirez, C. E.; Ajayan, P. M.; Pasquali, M.; Marti, A. A. Macroscopic Nanotube Fibers Spun from Single-Walled Carbon Nanotube Polyelectrolytes. *ACS Nano* **2014**, *8*, 9107–9112.
- (424) Zakri, C. Carbon Nanotubes and Liquid Crystalline Phases. *Liq. Cryst. Today* **2007**, *16*, 1–11.
- (425) Xu, Z.; Gao, C. Aqueous Liquid Crystals of Graphene Oxide. *ACS Nano* **2011**, *5*, 2908–2915.
- (426) Shen, T.-Z.; Hong, S.-H.; Song, J.-K. Electro-Optical Switching of Graphene Oxide Liquid Crystals with an Extremely Large Kerr Coefficient. *Nat. Mater.* **2014**, *13*, 394–399.
- (427) Wunderlich, D.; Hauke, F.; Hirsch, A. Preferred Functionalization of Metallic and Small-Diameter Single-Walled Carbon Nanotubes by Nucleophilic Addition of Organolithium and -Magnesium Compounds Followed by Reoxidation. *Chem. - Eur. J.* **2008**, *14*, 1607–1614.
- (428) Usrey, M. L.; Lippmann, E. S.; Strano, M. S. Evidence for a Two-Step Mechanism in Electronically Selective Single-Walled Carbon Nanotube Reactions. *J. Am. Chem. Soc.* **2005**, *127*, 16129–16135.
- (429) Banerjee, S.; Wong, S. S. Demonstration of Diameter-Selective Reactivity in the Sidewall Ozonation of SWNTs by Resonance Raman Spectroscopy. *Nano Lett.* **2004**, *4*, 1445–1450.
- (430) Doi, M. Rotational Relaxation Time of Rigid Rod-Like Macromolecule in Concentrated Solution. *J. Phys.* **1975**, *36*, 607–611.
- (431) Huang, K.; Delpont, G.; Orcin-Chaix, L.; Drummond, C.; Lauret, J.-S.; Penicaud, A. Single Layer Nano Graphene Platelets Derived from Graphite Nanofibres. *Nanoscale* **2016**, *8*, 8810–8818.
- (432) Voiry, D.; Pagona, G.; Del Canto, E.; Ortolani, L.; Morandi, V.; Noé, L.; Monthieux, M.; Tagmatarchis, N.; Penicaud, A. Reductive Dismantling and Functionalization of Carbon Nanohorns. *Chem. Commun.* **2015**, *51*, 5017–5019.
- (433) Camisasca, A.; Giordani, S. Carbon Nano-Onions in Biomedical Applications: Promising Theranostic Agents. *Inorg. Chim. Acta* **2017**, *468*, 67–76.
- (434) Molina-Ontoria, A.; Chaur, M. N.; Plonska-Brzezinska, M. E.; Echegoyen, L. Preparation and Characterization of Soluble Carbon Nano-Onions by Covalent Functionalization, Employing a Na-K Alloy. *Chem. Commun.* **2013**, *49*, 2406–2408.
- (435) Penicaud, A.; Valat, L.; Derre, A.; Poulin, P.; Zakri, C.; Roubeau, O.; Maugéy, M.; Miaudet, P.; Anglaret, E.; Petit, P.; et al. Mild Dissolution of Carbon Nanotubes: Composite Carbon Nano-

tube Fibres from Polyelectrolyte Solutions. *Compos. Sci. Technol.* **2007**, *67*, 795–797.

(436) Voiry, D.; Vallés, C.; Roubeau, O.; Pénicaud, A. Dissolution and Alkylation of Industrially Produced Multi-Walled Carbon Nanotubes. *Carbon* **2011**, *49*, 170–175.

(437) Goriparti, S.; Miele, E.; De Angelis, F.; Di Fabrizio, E.; Proietti Zaccaria, R.; Capiglia, C. Review on Recent Progress of Nanostructured Anode Materials for Li-Ion Batteries. *J. Power Sources* **2014**, *257*, 421–443.

(438) Cano-Márquez, A. G.; Rodríguez-Macías, F. J.; Campos-Delgado, J.; Espinosa-González, C. G.; Tristán-López, F.; Ramírez-González, D.; Cullen, D. A.; Smith, D. J.; Terrones, M.; Vega-Cantú, Y. I. Ex-MWNTs: Graphene Sheets and Ribbons Produced by Lithium Intercalation and Exfoliation of Carbon Nanotubes. *Nano Lett.* **2009**, *9*, 1527–1533.

(439) Nadiv, R.; Shtein, M.; Buzaglo, M.; Peretz-Damari, S.; Kovalchuk, A.; Wang, T.; Tour, J. M.; Regev, O. Graphene Nanoribbon – Polymer Composites: The Critical Role of Edge Functionalization. *Carbon* **2016**, *99*, 444–450.

(440) Dössel, L.; Gherghel, L.; Feng, X.; Müllen, K. Graphene Nanoribbons by Chemists: Nanometer-Sized, Soluble, and Defect-Free. *Angew. Chem., Int. Ed.* **2011**, *50*, 2540–2543.

(441) Mahmoud, W. E.; Al-Hazmi, F. S.; Al-Harbi, G. H. Wall by Wall Controllable Unzipping of MWCNTs via Intercalation with Oxalic Acid to Produce Multilayers Graphene Oxide Ribbon. *Chem. Eng. J.* **2015**, *281*, 192–198.

(442) Kosynkin, D. V.; Higginbotham, A. L.; Sinitskii, A.; Lomeda, J. R.; Dimiev, A.; Price, B. K.; Tour, J. M. Longitudinal Unzipping of Carbon Nanotubes to Form Graphene Nanoribbons. *Nature* **2009**, *458*, 872–876.

(443) Higginbotham, A. L.; Kosynkin, D. V.; Sinitskii, A.; Sun, Z.; Tour, J. M. Lower-Defect Graphene Oxide Nanoribbons from Multiwalled Carbon Nanotubes. *ACS Nano* **2010**, *4*, 2059–2069.

(444) Xiang, C.; Behabtu, N.; Liu, Y.; Chae, H. G.; Young, C. C.; Genorio, B.; Tsentalovich, D. E.; Zhang, C.; Kosynkin, D. V.; Lomeda, J. R.; et al. Graphene Nanoribbons as an Advanced Precursor for Making Carbon Fiber. *ACS Nano* **2013**, *7*, 1628–1637.

(445) Robinson, V. S.; Fisher, T. S.; Michel, J. A.; Lukehart, C. M. Work Function Reduction of Graphitic Nanofibers by Potassium Intercalation. *Appl. Phys. Lett.* **2005**, *87*, 061501.

(446) Michel, J. A.; Robinson, V. S.; Yang, L.; Sambandam, S.; Lu, W.; Westover, T.; Fisher, T. S.; Lukehart, C. M. Synthesis and Characterization of Potassium Metal/Graphitic Carbon Nanofiber Intercalates. *J. Nanosci. Nanotechnol.* **2008**, *8*, 1942–1950.

(447) Viculis, L. M.; Mack, J. J.; Mayer, O. M.; Hahn, T. H.; Kaner, R. B. Intercalation and Exfoliation Routes to Graphite Nanoplatelets. *J. Mater. Chem.* **2005**, *15*, 974–978.

(448) Saito, K.; Ohtani, M.; Fukuzumi, S. Electron-Transfer Reduction of Cup-Stacked Carbon Nanotubes Affording Cup-Shaped Carbons with Controlled Diameter and Size. *J. Am. Chem. Soc.* **2006**, *128*, 14216–14217.

(449) Zhu, S.; Xu, G. Single-Walled Carbon Nanohorns and Their Applications. *Nanoscale* **2010**, *2*, 2538–2549.

(450) Karousis, N.; Suarez-Martinez, I.; Ewels, C. P.; Tagmatarchis, N. Structure, Properties, Functionalization, and Applications of Carbon Nanohorns. *Chem. Rev.* **2016**, *116*, 4850–4883.

(451) Bandow, S.; Rao, A. M.; Sumanasekera, G. U.; Eklund, P. C.; Kokai, F.; Takahashi, K.; Yudasaka, M.; Iijima, S. Evidence for Anomalous Small Charge Transfer in Doped Single-Wall Carbon Nanohorn Aggregates with Li, K and Br. *Appl. Phys. A: Mater. Sci. Process.* **2000**, *71*, 561–564.

(452) Stergiou, A.; Liu, Z.; Xu, B.; Kaneko, T.; Ewels, C. P.; Suenaga, K.; Zhang, M.; Yudasaka, M.; Tagmatarchis, N. Individualized p-Doped Carbon Nanohorns. *Angew. Chem.* **2016**, *128*, 10624–10628.

(453) Khoerunnisa, F.; Fujimori, T.; Itoh, T.; Kanoh, H.; Ohba, T.; Yudasaka, M.; Iijima, S.; Kaneko, K. Electronically Modified Single Wall Carbon Nanohorns with Iodine Adsorption. *Chem. Phys. Lett.* **2011**, *501*, 485–490.

(454) Platzter, N. Action du potassium sur les charbons non graphités. *Comptes Rendus Acad. Sci.* **1957**, 1925–1928.

(455) Zang, J. B.; Wang, Y. H.; Zhao, S. Z.; Bian, L. Y.; Lu, J. Electrochemical Properties of Nanodiamond Powder Electrodes. *Diamond Relat. Mater.* **2007**, *16*, 16–20.

(456) Portet, C.; Yushin, G.; Gogotsi, Y. Electrochemical Performance of Carbon Onions, Nanodiamonds, Carbon Black and Multiwalled Nanotubes in Electrical Double Layer Capacitors. *Carbon* **2007**, *45*, 2511–2518.

(457) Sinitskii, A.; Erickson, K. J.; Lu, W.; Gibb, A. L.; Zhi, C.; Bando, Y.; Golberg, D.; Zettl, A.; Tour, J. M. High-Yield Synthesis of Boron Nitride Nanoribbons via Longitudinal Splitting of Boron Nitride Nanotubes by Potassium Vapor. *ACS Nano* **2014**, *8*, 9867–9873.

(458) Liu, Y.; Gu, Z.; Margrave, J. L.; Khabashesku, V. N. Functionalization of Nanoscale Diamond Powder: Fluoro-, Alkyl-, Amino-, and Amino Acid-Nanodiamond Derivatives. *Chem. Mater.* **2004**, *16*, 3924–3930.

(459) Kuznetsov, O.; Sun, Y.; Thaner, R.; Bratt, A.; Shenoy, V.; Wong, M. S.; Jones, J.; Billups, W. E. Water-Soluble Nanodiamond. *Langmuir* **2012**, *28*, S243–S248.

(460) Nsib, F.; Ayed, N.; Chevalier, Y. Selection of Dispersants for the Dispersion of Carbon Black in Organic Medium. *Prog. Org. Coat.* **2006**, *55*, 303–310.

(461) Wang, H.; Maiyalagan, T.; Wang, X. Review on Recent Progress in Nitrogen-Doped Graphene: Synthesis, Characterization, and Its Potential Applications. *ACS Catal.* **2012**, *2*, 781–794.

(462) Yu, S.-S.; Zheng, W.-T. Effect of N/B Doping on the Electronic and Field Emission Properties for Carbon Nanotubes, Carbon Nanocones, and Graphene Nanoribbons. *Nanoscale* **2010**, *2*, 1069–1082.

(463) Bojdys, M. J.; Severin, N.; Rabe, J. P.; Cooper, A. I.; Thomas, A.; Antonietti, M. Exfoliation of Crystalline 2D Carbon Nitride: Thin Sheets, Scrolls and Bundles via Mechanical and Chemical Routes. *Macromol. Rapid Commun.* **2013**, *34*, 850–854.

(464) Yin, Y.; Han, J.; Zhang, X.; Zhang, Y.; Zhou, J.; Muir, D.; Sutarto, R.; Zhang, Z.; Liu, S.; Song, B. Facile Synthesis of Few-Layer-Thick Carbon Nitride Nanosheets by Liquid Ammonia-Assisted Lithiation Method and Their Photocatalytic Redox Properties. *RSC Adv.* **2014**, *4*, 32690–32697.

(465) Miller, T. S.; Suter, T. M.; Telford, A. M.; Picco, L.; Payton, O. D.; Russell-Pavier, F.; Cullen, P. L.; Sella, A.; Shaffer, M. S. P.; Nelson, J.; et al. Single Crystal, Luminescent Carbon Nitride Nanosheets Formed by Spontaneous Dissolution. *Nano Lett.* **2017**, *17*, 5891–5896.

(466) Jia, J.; White, E. R.; Clancy, A. J.; Rubio, N.; Suter, T.; Miller, T. S.; McColl, K.; McMillan, P. F.; Brazdova, V.; Cora, F.; Howard, C. A.; Law, R. V.; Mattevi, C.; Shaffer, M. S. P. Fast Exfoliation and Functionalisation of 2D Crystalline Carbon Nitride by Framework Charging. *Angew. Chem.* **2018**, DOI: 10.1002/anie.201800875.

(467) Jia, Z.; Li, Y.; Zuo, Z.; Liu, H.; Huang, C.; Li, Y. Synthesis and Properties of 2D Carbon Graphdiyne. *Acc. Chem. Res.* **2017**, *50*, 2470–2478.

(468) Sano, M.; Kamino, A.; Okamura, J.; Shinkai, S. Ring Closure of Carbon Nanotubes. *Science* **2001**, *293*, 1299–1301.

(469) Xiong, F.; Wang, H.; Liu, X.; Sun, J.; Brongersma, M.; Pop, E.; Cui, Y. Li Intercalation in MoS₂: In Situ Observation of Its Dynamics and Tuning Optical and Electrical Properties. *Nano Lett.* **2015**, *15*, 6777–6784.

(470) Mounet, N.; Gibertini, M.; Schwaller, P.; Campi, D.; Merkys, A.; Marrazzo, A.; Sohler, T.; Castelli, I. E.; Cepellotti, A.; Pizzi, G.; et al. Two-Dimensional Materials from High-Throughput Computational Exfoliation of Experimentally Known Compounds. *Nat. Nanotechnol.* **2018**, *13*, 246–252.

(471) Wang, Q. H.; Kalantar-Zadeh, K.; Kis, A.; Coleman, J. N.; Strano, M. S. Electronics and Optoelectronics of Two-Dimensional Transition Metal Dichalcogenides. *Nat. Nanotechnol.* **2012**, *7*, 699–712.

- (472) Zhang, G.; Zhang, Y.-W. Thermoelectric Properties of Two-Dimensional Transition Metal Dichalcogenides. *J. Mater. Chem. C* **2017**, *5*, 7684–7698.
- (473) Joensen, P.; Frindt, R. F.; Morrison, S. R. Single-Layer MoS₂. *Mater. Res. Bull.* **1986**, *21*, 457–461.
- (474) Miremad, B. K.; Morrison, S. R. The Intercalation and Exfoliation of Tungsten Disulfide. *J. Appl. Phys.* **1988**, *63*, 4970–4974.
- (475) Wypych, F.; Sollmann, K.; Schöllhorn, R. Metastable Layered Chalcogenides 1T-MoS₂, 2M-Ws₂ and 1T-Mo₁₂W₁₂S₂: Electrochemical Study on Their Intercalation Reactions. *Mater. Res. Bull.* **1992**, *27*, 545–553.
- (476) Somoano, R. B.; Rembaum, A. Superconductivity in Intercalated Molybdenum Disulfide. *Phys. Rev. Lett.* **1971**, *27*, 402–404.
- (477) Nayak, A. P.; Yuan, Z.; Cao, B.; Liu, J.; Wu, J.; Moran, S. T.; Li, T.; Akinwande, D.; Jin, C.; Lin, J.-F. Pressure-Modulated Conductivity, Carrier Density, and Mobility of Multilayered Tungsten Disulfide. *ACS Nano* **2015**, *9*, 9117–9123.
- (478) Jeong, S.; Yoo, D.; Ahn, M.; Miró, P.; Heine, T.; Cheon, J. Tandem Intercalation Strategy for Single-Layer Nanosheets as an Effective Alternative to Conventional Exfoliation Processes. *Nat. Commun.* **2015**, *6*, 5763.
- (479) Kaplan-Ashiri, I.; Cohen, S. R.; Gartsman, K.; Ivanovskaya, V.; Heine, T.; Seifert, G.; Wiesel, I.; Wagner, H. D.; Tenne, R. On the Mechanical Behavior of WS₂ Nanotubes under Axial Tension and Compression. *Proc. Natl. Acad. Sci. U. S. A.* **2006**, *103*, 523–528.
- (480) Lalwani, G.; Henslee, A.; Farshid, B.; Parmar, P.; Lin, L.; Qin, Y.-X.; Kasper, F.; Mikos, A.; Sitharaman, B. Tungsten Disulfide Nanotubes Reinforced Biodegradable Polymers for Bone Tissue Engineering. *Acta Biomater.* **2013**, *9*, 8365–8373.
- (481) Rapoport, L.; Fleischer, N.; Tenne, R. Fullerene-like WS₂ Nanoparticles: Superior Lubricants for Harsh Conditions. *Adv. Mater.* **2003**, *15*, 651–655.
- (482) Kumar, S.; Borriello, C.; Nenna, G.; Rosentsveig, R.; Di Luccio, T. Dispersion of WS₂ Nanotubes and Nanoparticles into Conducting Polymer Matrices for Application as LED Materials. *Eur. Phys. J. B* **2012**, *85*, 1–7.
- (483) Bauerhenne, B.; Zijlstra, E.; Kalitsov, A.; Garcia, M. Mechanical Properties of Boron-Nitride Nanotubes after Intense Femtosecond-Laser Excitation. *Nanotechnology* **2014**, *25*, 145701.
- (484) Doll, G. L.; Speck, J. S.; Dresselhaus, G.; Dresselhaus, M. S.; Nakamura, K.; Tanuma, I. S. Intercalation of Hexagonal Boron Nitride with Potassium. *J. Appl. Phys.* **1989**, *66*, 2554–2558.
- (485) Kim, J.; Yamasue, E.; Ichitsubo, T.; Okumura, H.; Ishihara, K. N. Electrochemical Lithium Intercalation Behavior of Pristine and Milled Hexagonal Boron Nitride. *J. Electroanal. Chem.* **2017**, *799*, 263–269.
- (486) Shin, H.; Guan, J.; Zgierski, M. Z.; Kim, K. S.; Kingston, C. T.; Simard, B. Covalent Functionalization of Boron Nitride Nanotubes via Reduction Chemistry. *ACS Nano* **2015**, *9*, 12573–12582.
- (487) Terrones, M.; Romo-Herrera, J. M.; Cruz-Silva, E.; López-Urías, F.; Muñoz-Sandoval, E.; Velázquez-Salazar, J. J.; Terrones, H.; Bando, Y.; Golberg, D. Pure and Doped Boron Nitride Nanotubes. *Mater. Today* **2007**, *10*, 30–38.
- (488) Erickson, K. J.; Gibb, A. L.; Sinitskii, A.; Rousseas, M.; Alem, N.; Tour, J. M.; Zettl, A. K. Longitudinal Splitting of Boron Nitride Nanotubes for the Facile Synthesis of High Quality Boron Nitride Nanoribbons. *Nano Lett.* **2011**, *11*, 3221–3226.
- (489) Kleiner, O.; Adnan, M.; Marincel, D. M.; Ma, A. W.; Bengio, E. A.; Park, C.; Chu, S.-H.; Pasquali, M.; Talmon, Y. Dissolution and Characterization of Boron Nitride Nanotubes in Supercritical. *Langmuir* **2017**, *33*, 14340–14346.
- (490) Adnan, M.; Marincel, D. M.; Kleiner, O.; Chu, S.-H.; Park, C.; Hocker, S. J.; Fay, C.; Arepalli, S.; Talmon, Y.; Pasquali, M. Extraction of Boron Nitride Nanotubes and Fabrication of Macroscopic Articles Using Chlorosulfonic Acid. *Nano Lett.* **2018**, *18*, 1615–1619.
- (491) Pénicaud, A.; Dragin, F.; Pécastaings, G.; He, M.; Anglaret, E. Concentrated Solutions of Individualized Single Walled Carbon Nanotubes. *Carbon* **2014**, *67*, 360–367.
- (492) Mirri, F.; Ma, A. W. K.; Hsu, T. T.; Behabtu, N.; Eichmann, S. L.; Young, C. C.; Tsentalovich, D. E.; Pasquali, M. High-Performance Carbon Nanotube Transparent Conductive Films by Scalable Dip Coating. *ACS Nano* **2012**, *6*, 9737–9744.
- (493) Marom, R.; Amalraj, S. F.; Leifer, N.; Jacob, D.; Aurbach, D. A Review of Advanced and Practical Lithium Battery Materials. *J. Mater. Chem.* **2011**, *21*, 9938–9954.
- (494) Kaskhedikar, N. A.; Maier, J. Lithium Storage in Carbon Nanostructures. *Adv. Mater.* **2009**, *21*, 2664–2680.
- (495) Lee, H.; Ihm, J.; Cohen, M. L.; Louie, S. G. Calcium-Decorated Graphene-Based Nanostructures for Hydrogen Storage. *Nano Lett.* **2010**, *10*, 793–798.
- (496) Yu, X.; Tang, Z.; Sun, D.; Ouyang, L.; Zhu, M. Recent Advances and Remaining Challenges of Nanostructured Materials for Hydrogen Storage Applications. *Prog. Mater. Sci.* **2017**, *88*, 1–48.
- (497) Gopalsamy, K.; Subramanian, V. Hydrogen Storage Capacity of Alkali and Alkaline Earth Metal Ions Doped Carbon Based Materials: A DFT Study. *Int. J. Hydrogen Energy* **2014**, *39*, 2549–2559.
- (498) Ferre-Vilaplana, A. Storage of Hydrogen Adsorbed on Alkali Metal Doped Single-Layer All-Carbon Materials. *J. Phys. Chem. C* **2008**, *112*, 3998–4004.
- (499) Mahajan, S. G.; Liu, A. T.; Cottrill, A. L.; Kunai, Y.; Bender, D.; Castillo, J.; Gibbs, S. L.; Strano, M. S. Sustainable Power Sources Based on High Efficiency Thermopower Wave Devices. *Energy Environ. Sci.* **2016**, *9*, 1290–1298.
- (500) Liu, A. T.; Kunai, Y.; Liu, P.; Kaplan, A.; Cottrill, A. L.; Smith-Dell, J. S.; Strano, M. S. Electrical Energy Generation via Reversible Chemical Doping on Carbon Nanotube Fibers. *Adv. Mater.* **2016**, *28*, 9752–9757.
- (501) Yanagi, K.; Kanda, S.; Oshima, Y.; Kitamura, Y.; Kawai, H.; Yamamoto, T.; Takenobu, T.; Nakai, Y.; Maniwa, Y. Tuning of the Thermoelectric Properties of One-Dimensional Material Networks by Electric Double Layer Techniques Using Ionic Liquids. *Nano Lett.* **2014**, *14*, 6437–6442.
- (502) Nonoguchi, Y.; Nakano, M.; Murayama, T.; Hagino, H.; Hama, S.; Miyazaki, K.; Matsubara, R.; Nakamura, M.; Kawai, T. Simple Salt-Coordinated n-Type Nanocarbon Materials Stable in Air. *Adv. Funct. Mater.* **2016**, *26*, 3021–3028.
- (503) Oshima, Y.; Kitamura, Y.; Maniwa, Y.; Yanagi, K. Fabrication of Thermoelectric Devices Using Precisely Fermi Level-Tuned Semiconducting Single-Wall Carbon Nanotubes. *Appl. Phys. Lett.* **2015**, *107*, 043106.
- (504) Paglione, J.; Greene, R. L. High-Temperature Superconductivity in Iron-Based Materials. *Nat. Phys.* **2010**, *6*, 645–658.
- (505) Blake, R.; Coleman, J. N.; Byrne, M. T.; McCarthy, J. E.; Perova, T. S.; Blau, W. J.; Fonseca, A.; Nagy, J. B.; Gun'ko, Y. K. Reinforcement of Poly(Vinyl Chloride) and Polystyrene Using Chlorinated Polypropylene Grafted Carbon Nanotubes. *J. Mater. Chem.* **2006**, *16*, 4206–4213.
- (506) Schirowski, M.; Abellán, G.; Nuin, E.; Pampel, J.; Dolle, C.; Wedler, V.; Fellingner, T. P.; Spiecker, E.; Hauke, F.; Hirsch, A. Fundamental Insights into the Reductive Covalent Cross-Linking of Single-Walled Carbon Nanotubes. *J. Am. Chem. Soc.* **2018**, *140*, 3352–3360.
- (507) Aricò, A. S.; Bruce, P.; Scrosati, B.; Tarascon, J.-M.; Van Schalkwijk, W. Nanostructured Materials for Advanced Energy Conversion and Storage Devices. *Nat. Mater.* **2005**, *4*, 366–377.
- (508) Menzel, R.; Barg, S.; Miranda, M.; Anthony, D. B.; Bawaked, S. M.; Mokhtar, M.; Al-Thabaiti, S. A.; Basahel, S. N.; Saiz, E.; Shaffer, M. S. Joule Heating Characteristics of Emulsion-Templated Graphene Aerogels. *Adv. Funct. Mater.* **2015**, *25*, 28–35.
- (509) Antolini, E. Carbon Supports for Low-Temperature Fuel Cell Catalysts. *Appl. Catal., B* **2009**, *88*, 1–24.
- (510) Catheline, A.; Paolucci, F.; Valenti, G.; Poulin, P.; Pénicaud, A. Transparent Electrodes Made from Carbon Nanotube Polyelec-

trolytes and Application to Acidic Environments. *J. Mater. Res.* **2015**, *30*, 2009–2017.

(511) Wang, Y.; Huang, K.; Derré, A.; Puech, P.; Rouzière, S.; Launois, P.; Castro, C.; Monthieux, M.; Pénicaut, A. Conductive Graphene Coatings Synthesized from Graphenide Solutions. *Carbon* **2017**, *121*, 217–225.

(512) Yu, L.; Shearer, C.; Shapter, J. Recent Development of Carbon Nanotube Transparent Conductive Films. *Chem. Rev.* **2016**, *116*, 13413–13453.

(513) Diba, M.; Fam, D.; Boccaccini, A. R.; Shaffer, M. Electrophoretic Deposition of Graphene-Related Materials: A Review of the Fundamentals. *Prog. Mater. Sci.* **2016**, *82*, 83–117.

(514) Ericson, L.; Fan, H.; Peng, H.; Davis, V.; Zhou, W.; Sulpizio, J.; Wang, Y.; Booker, R.; Vavro, J.; Guthy, C.; et al. Macroscopic, Neat, Single-Walled Carbon Nanotube Fibers. *Science* **2004**, *305*, 1447–1450.

(515) Tsentalovich, D. E.; Headrick, R. J.; Mirri, F.; Hao, J.; Behabtu, N.; Young, C. C.; Pasquali, M. Influence of Carbon Nanotube Characteristics on Macroscopic Fiber Properties. *ACS Appl. Mater. Interfaces* **2017**, *9*, 36189–36198.

(516) Liu, Y.; Xu, Z.; Zhan, J.; Li, P.; Gao, C. Superb Electrically Conductive Graphene Fibers via Doping Strategy. *Adv. Mater.* **2016**, *28*, 7941–7947.

(517) Xin, G.; Yao, T.; Sun, H.; Scott, S.; Shao, D.; Wang, G.; Lian, J. Highly Thermally Conductive and Mechanically Strong Graphene Fibers. *Science* **2015**, *349*, 1083–1087.